

DISS. ETH NO. 24817

MULTI-FREQUENCY POLARIMETRIC SAR TOMOGRAPHY
FOR THE 3-D CHARACTERIZATION AND MONITORING
OF AGRICULTURAL CROPS

A thesis submitted to attain the degree of
DOCTOR OF SCIENCES of ETH ZURICH
(Dr. sc. ETH Zurich)

presented by

HANNAH JOERG

Dipl. Tech.-Math., Technische Universitaet Muenchen (TUM)

born on 27.06.1987

citizen of Germany

accepted on the recommendation of

Prof. Dr. Irena Hajnsek, examiner

Prof. Dr. Laurent Ferro-Famil, co-examiner

Prof. Dr. Alberto Moreira, co-examiner

Prof. Dr. Harry Vereecken, co-examiner

2018

Dedicated to my parents.

*The correct analogy for the mind
is not a vessel that needs filling,
but wood that needs igniting – no more –
and then it motivates one towards originality
and instills the desire for truth.*

Plutarch

Abstract

Monitoring the temporal variation of soil and plant parameters of agricultural crops is of high interest. Since Synthetic Aperture Radar (SAR) measurements are sensitive to dielectric and geometric properties of the observed scattering scenario, they provide key observables for monitoring the temporal variation of biophysical parameters. However, the scattering mechanisms occurring in agricultural vegetation in dependency of biophysical parameters are highly complex and simultaneous dynamics of the soil and the vegetation are difficult to differentiate.

By utilizing several horizontally separated SAR acquisitions, SAR Tomography, as demonstrated for forest volumes, is a powerful tool able to estimate vertical profiles of the backscattered power and to resolve and interpret scattering mechanisms along height. The fact that tomographic SAR techniques are, in principle, independent of scattering models makes their application very promising towards a better understanding of the highly dimensional scattering scenarios of agricultural vegetation. Challenges are however the high vertical resolution required in order to be sensitive to the low plant heights, and the possibly present anisotropic propagation effects of the vegetation volume limiting the application of state-of-the-art tomographic ground and volume separation algorithms.

The Crop Experiment (CROPEX) campaign in 2014, which plays a key role in this PhD thesis, fills the gap in the availability of fully polarimetric multi-frequency and tomographic SAR data over agricultural crops providing high vertical resolution capability and covering different dates of the phenological cycle. The main objective of the campaign is to foster the physical understanding of the influence that changes in soil and plant parameters have on the ground and volume scattering component as a function of crop type, polarization and frequency.

The interpretation of changes on the ground and in the volume from vertical backscatter profiles is limited and can only be quantified by separating the ground and volume scattering components. Without posing model assumptions to the vegetation volume, this separation becomes ill-posed. In the thesis, this is addressed by applying a separation algorithm which overcomes this ambiguity by integrating the a priori knowledge of the ground height as a given parameter and is able to provide robust estimates of the multi-baseline volume coherences and the ground and volume powers. The biggest novelty of this work is the quantitative analysis of the distinct ground and volume powers for agricultural scattering scenarios, particularly taking into account their temporal variation as a function of varying soil and plant parameters. The temporal variation of the estimated powers provides an unambiguous quantification of scattering changes on the ground and in the vegetation. Since the center of mass of the vertical backscatter profiles correspond - at least at the first order - to the interferometric phase center that can be estimated by means of only two acquired tracks, its

analysis gives an understanding of the potential of a reduced observation scenario. In conjunction with in-situ measured soil and plant parameters, the sensitivity of the tomographic parameters across different frequencies, X-, C- and L-band, to dielectric (e.g. dynamics of the water content) and geometric (e.g. alignments of plant components) changes is demonstrated.

The experimental results in this thesis underline the importance of the three-dimensional information. With the separation in height, the conclusions drawn on the changes of the incoherent scattering signature provide a basis for future research including the coherent ground and volume signatures. Scattering models based on the coherent polarimetric signature might provide promising opportunities towards the inversion of biophysical parameters.

Kurzfassung

Die Erfassung der zeitlichen Variation von Boden- und Pflanzenparametern landwirtschaftlicher Nutzpflanzen ist von großer Relevanz. Zur Erfassung dieser Dynamiken, ist die Verwendung von SAR (Radar mit Synthetischer Apertur) Messungen, aufgrund ihrer Sensitivität für dielektrische und geometrische Eigenschaften des beobachteten Streuungsszenarios, sehr vielversprechend. Allerdings sind die in der landwirtschaftlichen Vegetation auftretenden Streumechanismen, und deren Abhängigkeit von biophysikalischen Parametern, hochkomplex und darüber hinaus ist die gleichzeitige Dynamik des Bodens und der Vegetation schwierig zu differenzieren.

SAR Tomographie ist in der Lage, unter Verwendung mehrerer SAR Aufnahmen aus horizontal separierten Perspektiven, vertikale Rückstreuprofile des beobachteten Streuszenarios zu berechnen. Wie bereits für Waldszenarien demonstriert, ermöglicht dies die vertikale Auflösung von Streumechanismen und deren Interpretation. Da SAR Tomographie an sich unabhängig von Streumodellen ist, ist die Anwendung tomographischer Methoden für landwirtschaftliche Vegetation hinsichtlich eines besseren Verständnisses der hochdimensionalen Streuszenarien sehr vielversprechend. Herausforderungen sind neben der hohen vertikalen Auflösung, die durch die niedrigen Pflanzenhöhen erforderlich wird, anisotrope Propagationseffekte des Vegetationsvolumens, die die Anwendung etablierter tomographischer Verfahren zur Separierung von Boden und Volumen einschränken.

Die „Crop Experiment“ (CROPEX) Messkampagne aus dem Jahr 2014 spielt eine zentrale Rolle in dieser Dissertation. Die im Rahmen der CROPEX 2014 Kampagne aufgenommenen SAR Daten beheben den Mangel an polarimetrischen, tomographisch hochauflösenden SAR Daten in verschiedenen Frequenzbändern über landwirtschaftlichen Gebieten und erfassen verschiedene Zeitpunkte der Pflanzenphänologie. Ziel ist die Vertiefung des physikalischen Verständnisses der Auswirkung von Veränderungen in Boden- und Pflanzenparametern auf die Boden- und Volumenstreuung in Abhängigkeit von Pflanzensorte, Polarisation und Frequenzband.

Die Interpretation von Veränderungen der Rückstreubeiträge am Boden und im Volumen ist anhand der vertikalen Rückstreuprofile nur bedingt möglich. Eine quantitative Messung dieser Veränderungen kann allerdings durch eine Trennung der Boden- und Volumenstreukomponenten erreicht werden. Wenn kein Streumodell für das Vegetationsvolumen angenommen wird, stellt die Trennung der beiden Streukomponenten ein schlecht gestelltes Problem dar. Der in dieser Dissertation ausgewählte Algorithmus verwendet die Information der topographischen Höhe des Bodens, was zu einer eindeutigen Lösbarkeit des Problems führt. Somit ist der Algorithmus in der Lage robuste Schätzungen der Volumenkohärenzen für die verschiedenen Basislinien sowie der Rückstreubeiträge am Boden und im Volumen zu liefern. Die zeitliche Variation der aus dieser Separierung gewonnenen Streuparameter erlaubt somit eine eindeutige Quantifizierung von

Veränderungen in Boden- und Volumenrückstreuung. Insbesondere mit dieser Quantifizierung der vertikal separierten Streubeiträge und durch die temporale Komponente liefert die Dissertation neuartige Beiträge bezüglich der Interpretation des Streuszenarios von landwirtschaftlicher Vegetation. Des Weiteren wird mit der Analyse des Schwerpunkts der vertikalen Rückstreuprofile, welcher im Wesentlichen dem interferometrischen Streuzentrum entspricht und aus zwei SAR Aufnahmen gewonnen werden kann, ein Einblick gegeben, inwiefern die Aufnahmekonstellation reduziert werden könnte. Unter Verwendung von in-situ gemessenen biophysikalischen Boden- und Pflanzenparametern wird die Sensitivität der tomographischen Parameter im X-, C- und L-Band für dielektrische (z.B. Veränderungen im Pflanzenwassergehalt) und geometrische (z.B. Ausrichtung einzelner Pflanzenkomponenten) Veränderungen aufgezeigt.

Die experimentellen Ergebnisse in dieser Arbeit unterstreichen die Bedeutung der dreidimensionalen Information. Die auf Basis der vertikal separierten inkohärenten Rückstreubeiträge gewonnenen Erkenntnisse bilden eine Grundlage für zukünftige Forschungsaktivitäten hinsichtlich der Bestimmung der kohärenten Boden- und Volumenstreusignaturen. Elektromagnetische Streumodelle, die auf der kohärenten polarimetrischen Signatur basieren, könnten vielversprechende Erkenntnisse zur Inversion biophysikalischer Parameter aus SAR Daten liefern.

Acknowledgements

This dissertation is the outcome of the research I have been given the opportunity to conduct at the Microwaves and Radar Institute at the German Aerospace Center (DLR) during the last years. Along this journey, I have learnt a lot not only technically but also about myself. In this process, I was and am accompanied by great people to whom I would like to dedicate some words.

I would like to thank Alberto Moreira and Gerhard Krieger for the possibility to work, learn and participate in the very interdisciplinary research atmosphere of the Department and the Institute. Thank you to Laurent Ferro-Famil for agreeing to be a co-examiner of this thesis, your interest in my work and your time for discussions at conferences. I would like to acknowledge also Harry Vereecken for accepting the invitation to be a co-examiner of my work.

I am very grateful to Irena for giving me the opportunity to work on my topic and for supervising this thesis. Knowing that you trust and support me allowed me to grow and gain confidence with my work.

I owe a very special thank you to Matteo for introducing me to the world of SAR Tomography, for motivating me to see things from different perspectives (“not like a mathematician”), for encouraging me in difficult moments (“I can see the light at the end of the tunnel now”) and for all the time you have spent reading and correcting my manuscripts with greatest dedication. I really appreciate you being my colleague and my friend in these last years and many more to come.

I learnt a lot from Kostas about the way to evaluate and question results and would like to thank you for all the discussions, the editing of my manuscripts and the motivation to always go a step further – in my work and in running. All my present and former colleagues of the PolInSAR and SAR Information Retrieval working groups are responsible that I have always felt welcome and comfortable during every day work. Thank you to Sibylle, Marivi, Alberto, Victor, Michelangelo, Georg, Thomas B., Jun Su (for having always an open door for late night discussions on polarimetry) and Sandra (for your support in stressful times). Special thanks go to Giuseppe (yes also thank you for all the cookies you had to sacrifice to me), Maria and Astor for adopting me (back then) when you were still PhD students. Thank you for introducing me to the PhD students’ life, for making conferences, coffee breaks and every day work just this particular little bit nicer and for becoming and being my friends.

The thesis would not be the same without Ralf always doing his best to fulfil my wishes for the F-SAR acquisitions. Thanks also to the F-SAR processing team Rolf, Martin, Jens and Marc for delivering the data always “yesterday”. Particular thanks to Marc for your relentless help with the processing, the interest in my work and your enthusiasm for calibration. However, in the frame of

the CROPEX 2014 campaign, I was not only supported from the “air” but also on the ground during many trips to the Wallerfing test site. Thank you to Philip for sharing your experience, the tools and also your students. Further, Thomas W. and Moritz contributed with their work during their internships and their good company. I would like to thank Manuele and Virginia for travelling mostly on short notice from Zurich to help in the ground parameter collection. In enjoyed our discussions about the data set and our results whether it was in the field, on the phone or at conferences.

Outside DLR, my friends and family have always been a pillar I could rely on. I do not take this for granted and am very grateful to all of you for being there and for sharing the ups and downs of the last years. I am particularly grateful for and to my parents Sieglinde and Wolfgang. Without you, your unconditional support and believe in me, I would not be who and where I am today.

Contents

- 1 Introduction1**
 - 1.1 Synthetic Aperture Radar for Crop Monitoring 1
 - 1.2 SAR Tomography 4
 - 1.3 SAR Tomography and Agricultural Vegetation 5
 - 1.4 Scope and Organization of the Thesis 5
 - 1.5 References 8

- 2 On the Separation of Ground and Volume Scattering Using Multi-Baseline SAR Data13**
 - 2.1 Introduction..... 14
 - 2.2 Data Model and Problem Formulation 15
 - 2.3 Separation Methodologies 16
 - 2.3.1 Estimation of the Volume Coherences 16
 - 2.3.2 Power Estimation..... 17
 - 2.4 Numerical Results 19
 - 2.4.1 Simulated MB Data 19
 - 2.4.2 Estimated Volume Coherences 19
 - 2.4.3 Estimation Performance 19
 - 2.5 Conclusions 22
 - 2.6 References 23

- 3 3-D Scattering Characterization of Agricultural Crops at C-band using SAR Tomography.....25**
 - 3.1 Introduction 26
 - 3.2 The CROPEX 2014 Campaign 28
 - 3.2.1 Test Site and Ground Measurements 28
 - 3.2.2 Multi-Baseline SAR Acquisitions 30
 - 3.3 Multi-Baseline Data Analysis 32
 - 3.4 Ground and Volume Separation..... 36
 - 3.4.1 Data Model 36

3.4.2	Estimation of Volume Signal.....	37
3.4.3	Power Estimation.....	38
3.5	Results.....	39
3.5.1	Volume-Only Multi-Baseline Analysis.....	39
3.5.2	Ground and Volume Scattering Powers.....	40
3.5.3	Significance of Anisotropic Propagation Effects.....	43
3.6	Discussion and Conclusions.....	44
3.7	References.....	46
4	Sensitivity of SAR Tomography to the Phenological Cycle of Agricultural Crops at X-, C- and L-band.....	51
4.1	Introduction.....	52
4.2	Data Time Series.....	53
4.2.1	Corn.....	55
4.2.2	Barley.....	55
4.2.3	Wheat.....	56
4.3	Tomographic Algorithms and Parameters.....	56
4.3.1	Acquisition Parameters.....	57
4.3.2	SAR Tomography.....	58
4.3.3	Separation of Ground and Volume.....	61
4.3.4	Discussion of TomoSAR Parameters.....	62
4.4	Sensitivity to Phenological Transitions at Different Frequencies.....	64
4.4.1	Corn.....	65
4.4.2	Barley.....	67
4.4.3	Wheat.....	68
4.4.4	Discussion.....	70
4.5	Conclusions.....	71
4.6	References.....	72
5	Conclusions.....	77
5.1	Main Findings.....	77
5.2	Outlook.....	80
5.3	References.....	82
	Curriculum Vitae.....	83

Chapter 1

Introduction

The motivation of the work concluded in this thesis is given by, first, the state-of-the-art in terms of techniques for monitoring agricultural crops with Synthetic Aperture Radar (SAR). Secondly, the open issues and challenges are identified which motivate the application of SAR Tomography enabling to resolve the scattering scenario in height. The principle of SAR Tomography and the recent developments in this field are described. The challenges of applying SAR Tomography to agricultural vegetation are discussed leading to the final formulation of the scope and the research objectives of this work.

1.1 Synthetic Aperture Radar for Crop Monitoring

“*SAR remote sensing*” has great potential for monitoring agricultural vegetation. Mounted on an air- or spaceborne platform with a side-looking geometry, SAR provides a high-resolution imaging capability covering large swaths in short and high repeat time. SAR, as an active microwave sensor, can acquire data independent of daylight and (almost) at all weather conditions. This allows a time-continuous observation which is crucial for agricultural crops due to their fast temporal variability across the phenological cycle. Further, due to the sensitivity of the electromagnetic wave to dielectric and geometric properties of the scatterers SAR measurements are influenced by several plant and soil parameters, including plant height, fraction of vegetation cover, vegetation water content (VWC), plant structure, biomass, soil moisture and soil roughness [1,2]. Thus SAR remote sensing has undoubted potential for monitoring the temporal evolution of agricultural vegetation [3-6]. Particularly in view of developing monitoring applications with current and future spaceborne SAR missions, like TanDEM-X [7], Radarsat-2 [8], Sentinel-1 [9] and Tandem-L [10], an understanding of the impact of spatial and temporal variations of soil and plant parameters on SAR measurements is crucial.

Early research reports comprehensive ground based indoor and outdoor experiments with particular focus on the impact of dielectric constants of the soil and single plant components on scattering and attenuation of the electromagnetic wave [1,2]. A simple model for the backscattered power of a vegetation volume over soil is given by the water cloud model [11]. However, it assumes a uniform water distribution inside the plants which might not always be the case [4].

These studies further underline the importance of sensor properties such as incidence angle and frequency, and the polarization of the electromagnetic wave. The frequency drives the sensitivity to different plant components in the size of the order of the wavelength and the choice of polarization the sensitivity to the geometric alignment of those plant components. The use of not only one

polarimetric channel but a combination of two (dual polarimetric systems) or four (fully polarimetric systems) polarimetric channels provides complementary information and hence an increased dimensionality of the observation space. Particularly, polarimetric parameters estimated from coherent **“polarimetric SAR”** (PolSAR) are beneficial in this regard.

The temporal variation of SAR backscatter at different polarizations and their correlation coefficients have been correlated to changes in biophysical parameters, for instance in [12-14]. The generalization of such findings to different study areas even for the same crop type is however limited. An electromagnetic scattering model developed in [15] calculates the coherent polarimetric backscatter as a function of different plant components and their dielectrics. On one hand, this can support the obtained findings from correlations and foster the understanding of the impact of dielectric and geometric plant properties on the backscattering [15,16]. But on the other hand, the high dimensionality of parameters poses limitations on actual quantitative multi-parametric inversion.

The increased observation space of PolSAR has further been successfully exploited for crop classification [17-20], estimation of the plant phenology over time [21] or coherent change detection [22]. The most limiting aspect of these applications is the fact that scattering contributions from the underlying soil and the vegetation are mixed in the scattering signature and are thus difficult to distinguish, particularly when they change simultaneously over time. This can lead to misinterpretation of changes in the vegetation as changes in the underlying soil and vice versa. One possibility to address this issue and at the same time to avoid highly parametric models is to apply polarimetric decompositions, model based and non-model based.

“Polarimetric model based decomposition” techniques fit a set of modelled scattering components to the covariance or coherency matrix. First formulated in [23], an established version is the three-component decomposition with surface, dihedral and volume scattering component. The technique has been widely applied for removing the volume component from the polarimetric data in order to estimate soil moisture from the ground component. In order to reduce the number of unknowns, a dominance criterion is usually applied to neglect either surface or dihedral scattering on the ground [23-25]. However, appropriate electromagnetic modelling for the single components is complicated. For the surface component comprehensive research was done to account for depolarizing effects induced by surface roughness [26]. The most challenging aspect is the modelling of the volume component which depends on many parameters [25].

In this context, the analysis of polarimetric parameters over time can give insight on the ongoing scattering mechanisms particularly in the volume [27]. Especially, the **“non-model based decomposition”** proposed by [28] yields a set of parameters for analyzing and identifying different scattering mechanisms by utilizing the eigendecomposition of the covariance matrix. The polarimetric scattering entropy H and the mean alpha angle can be interpreted regarding number, dominance and kind of observed scattering mechanisms. By weighting the eigenvalues, the scattering entropy indicates the randomness of the scattering, i.e. the number of dominant scattering mechanisms. The individual alpha angles and their mean value are retrieved from the eigenvectors and associated to the type of scattering mechanism. To give an example, entropy and mean alpha at X-, C- and L-band are displayed over corn, wheat and barley fields in Figs. 1 and 2 estimated from airborne fully polarimetric SAR data [29] for dates between May and July. On the corn fields, the

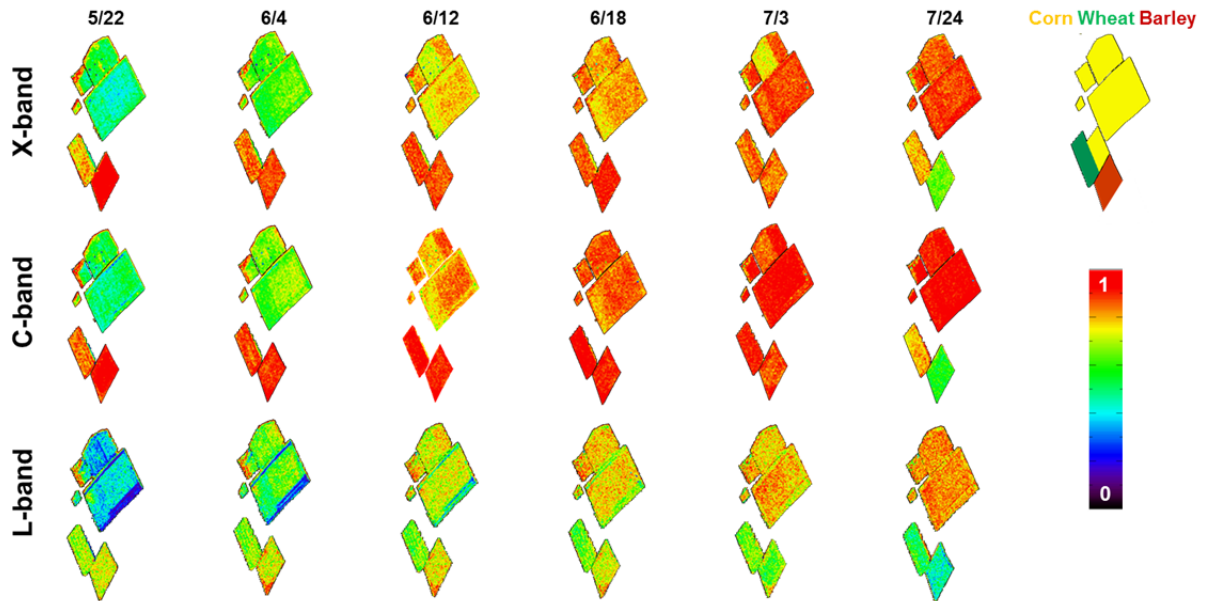


Fig. 1: Polarimetric entropy on different dates for X-, C- and L-band.

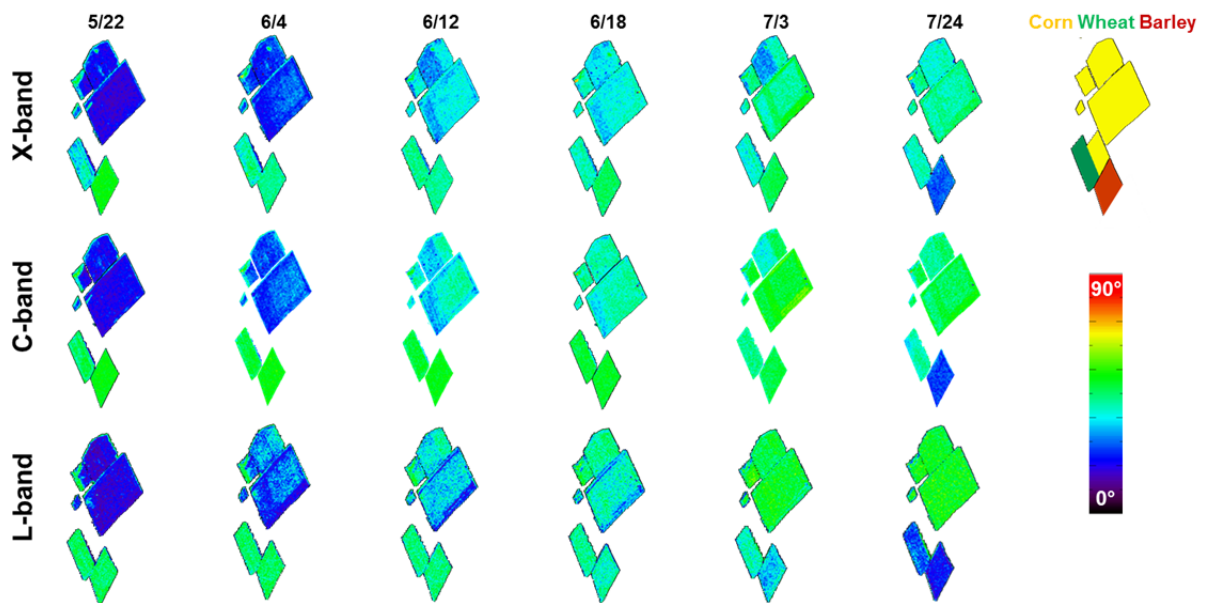


Fig. 2: Polarimetric mean alpha angle on different dates for X-, C- and L-band.

vegetation cover increases over time and the wheat and barley fields are already vegetated and the second part of their phenological cycle is monitored. It is obvious that for vegetated fields, the entropy is close to one, particularly at the high frequencies, but for the corn also at L-band. This is due to the complex structure of the vegetation together with high polarimetric decorrelation. The saturation of the polarimetric entropy limits the physical interpretation of the occurring scattering mechanisms. The mean alpha angle is low for bare fields or low vegetation cover indicating surface scattering. For advanced vegetation, it increases and saturates at values close to 45° . Here, the high entropy level reduces the effective observation space, i.e. the scattering mechanisms cannot be

distinctively analyzed. This example illustrates the high dimensionality of the problem which limits the interpretation of the scattering signature but more importantly, the ability to separate between soil and plant dynamics from a limited observation space.

The introduction of interferometry enables to overcome the saturation of entropy since the degree of interferometric decorrelation can be controlled by the size of the baseline and thus allows the separation of scattering mechanisms in height [30]. **“Polarimetric SAR Interferometry”** (Pol-InSAR) exploits the variation of the interferometric coherence between two (or more) spatially separated tracks for different polarizations [31]. First established for forest applications, the Random-Volume-Over-Ground (RVoG) scattering model [31] assumes a volume layer, modeled as a cloud of particles with no preferred orientation, on top of a ground layer with polarization-dependent scattering properties. The interferometric volume coherence can be obtained by minimizing the ground-to-volume power ratio in the polarimetric space and can be expressed as a function of plant height and the extinction coefficient on the basis of a fixed function describing the backscattered power along height, e.g. exponential [32]. When applying Pol-InSAR techniques to agricultural crops, the Oriented-Volume-over-Ground (OVoG) model was introduced [6,33] in order to account for possible anisotropic propagation effects inside the vegetation volume, i.e. considering polarization dependency also for the volume layer. The OVoG approach allows the robust estimation of the agricultural crop height by using single- or multi-baseline fully polarimetric acquisitions across different frequencies [33-35]. Besides this, Pol-InSAR model inversions yield the ground-to-volume ratio and the extinction at the different polarizations which can give insight on the scattering scenario and are related to biophysical parameters [34,36]. Nevertheless, the observation space with one baseline is still limited and therefore requires an a priori assumption on the shape of the vertical backscattered power function.

1.2 SAR Tomography

“SAR Tomography” enables the non-model based estimation of the backscattered power distribution in height. The acquisition of the same scene from several spatially separated tracks, i.e. in a multi-baseline (MB) configuration, effects a variation of amplitude and phase between the images at the different tracks expressed by the MB coherences. Tomographic SAR techniques perform a spectral estimation on these MB coherences to estimate the 3-D backscattered power. The vertical resolution is inversely proportional to the maximum separation between the tracks. Airborne SAR Tomography was first demonstrated over forests in [37] and the application of different spectral estimators can be found in [38-40]. SAR Tomography was found useful for detecting under-foliage objects [41] or assessing temporal decorrelation [42].

Even though the estimation and a (qualitative) analysis of the 3-D scattering signature are rather established, the ability to identify and quantify the contributing scattering mechanisms (particularly in relation to bio- and geophysical properties) from the 3-D backscatter is limited by vertical tomographic resolution even when applying super-resolution methodologies. For urban applications, i.e. point-like scatterers, MB SAR data was employed to resolve layover of super-imposed scattering contributions in height [43]. In contrast, vegetation scenarios are affected by volume decorrelation and are thus commonly modeled as two-layer media, the sum of a ground and a volume layer. This enables for instance the estimation of the ground topography under a

vegetation layer [44]. With fully polarimetric MB data, a separation of the layers, i.e. an estimation of the MB volume coherences and the ground and volume powers, is facilitated by applying the RVoG model [45,46]. The parameters estimated in this way help to interpret scattering scenarios, as was shown for forest scenarios at L- and P-band [46,47].

1.3 SAR Tomography and Agricultural Vegetation

The ability of SAR tomography to estimate the distribution of the 3-D backscattered power in a non-model based way can help to address the open questions on the characterization of scattering mechanisms in agricultural crops posed in Chapter 1.1. First demonstrations in this context have been done based on indoor and outdoor ground-based experiments as reported in [48-51]. The studies analyzed the 3-D backscatter of corn and wheat as a function of polarization, incidence angle and frequency, drawing first conclusions on the differences of the contributing scattering mechanisms along height. However, the data sets did not cover temporal variation of the agricultural crops and thus no investigation of soil and vegetation changes was possible. Additionally, regarding ground and volume separation the RVoG model assumption of a polarization-independent volume layer may not hold for agricultural crops [33,34]. Additionally, there is a lack of airborne polarimetric MB SAR data over agricultural crops. The main reason is the required high vertical resolution, i.e. the large spatial baselines, in order to be sensitive to the low plant heights.

1.4 Scope and Organization of the Thesis

The main objective is to apply tomographic SAR techniques to agriculturally vegetated fields and to investigate its potential towards a better understanding of the influence of varying soil and plant parameters on the three-dimensional scattering signature. To this purpose, the Crop Experiment (CROPEX) campaign in 2014 was initiated and conducted by DLR to fill the gap of airborne polarimetric MB SAR data over agricultural crops. The campaign is an essential part of the thesis as it includes the design of the acquisitions, its conduction and the evaluation of the acquired MB SAR data.

In Chapter 2, the thesis addresses the difficulty of separating ground and volume scattering components from the MB SAR data without assuming scattering models for the vegetation. Then, Chapter 3 discusses the configuration and the design of the MB SAR acquisitions and presents for the first time a quantitative tomographic analysis at C-band. The possibility of relating the temporal variation of the quantified ground and volume scattering components estimated by the separation algorithm identified in Chapter 2 to the changes in soil and plant parameters is evaluated. Chapter 4 exploits the capability of tomographic parameters for characterizing the 3-D scattering signature of agricultural crops, addressed in Chapter 3, to evaluate the sensitivity of tomographic parameters on specific phenological transitions as a function of frequency. The detailed formulations of the research questions for each of the Chapters are summarized below.

Chapter 2 “On the Separation of Ground and Volume Scattering Using Multi-Baseline SAR Data” In this Chapter, two algorithms for separating ground and volume scattering are compared

regarding their performance for estimating at the same time the MB volume coherences and the ground and volume scattering powers from MB SAR data based on numerical simulations.

This research is motivated by the fact that the separation of ground and volume scattering is essential for the analysis of scattering properties such as the ground-to-volume power ratio or the characteristics of the volume component. However, as stated in previous works [33,34], agricultural vegetation can be affected by anisotropic propagation effects. Then, no closed form expression for the volume only coherences exists, in contrast to the RVoG case [45,46]. The general formulation of a two-layer model with a Dirac- δ like ground under a generic volume component leads to an ill-posed separation problem [52].

In order to address this issue, two algorithms that employ a priori information of the ground topography for the estimation of the MB volume coherences are compared. The algorithms based on an adaptive maximum likelihood method (AML) and a matrix filtering (MF) approach have already been proposed in [52] and [38], but their performances have never been analyzed with respect to their ability to provide a coherent volume component that, in turn, can be further used for parameter inversion. In this context:

- The performance of the separation algorithms is evaluated quantitatively based on the resulting ground and volume powers using the estimated volume coherences. The objective is to analyze trends for different scattering scenarios and to investigate the role of the vertical resolution in the separation approach.
- Since the knowledge of the ground topography is required for both separation approaches, the influence of errors in the assumed a priori information on the estimation performance is investigated.
- Residual phase calibration errors are data non-idealities impacting any tomographic SAR analysis. Thus, the performance is analyzed for a varying disturbance of the phase of the MB SAR data.

Chapter 3 “3-D Scattering Characterization of Agricultural Crops at C-band using SAR Tomography” This Chapter focuses on the interpretation and characterization of the 3-D backscattering distribution at different polarizations along the phenological cycle at C-band and to relate them to changes in soil and plant parameters.

The objective is to exploit the time series of polarimetric MB SAR data acquired by DLR’s airborne sensor F-SAR over the agricultural Wallerfing test site in the frame of the CROPEX 2014 campaign covering the phenological cycle in conjunction with the simultaneously collected ground measurements of soil and plant parameters. Besides analyzing the vertical backscatter profiles, the matrix filter, following the analysis in Chapter 2, is applied to cancel the ground component from the MB SAR data yielding the volume-only MB coherences. Thus, the ground and volume power can be estimated separately. The analysis at C-band includes the discussion of the following aspects.

- The tradeoffs and challenges in the design of the MB SAR acquisitions for the CROPEX 2014 campaign are discussed regarding the large baselines required to be sensitive to the

low plant heights. The vertical tomographic profiles estimated from the MB SAR data are analyzed for the different polarizations and dates especially regarding the influence of temporal changes in soil and vegetation.

- After separating ground and volume the temporal variation of their powers is analyzed in conjunction with changes of soil and plant parameters for corn, wheat and barley.
- The temporal variation of the center of mass of the vertical profiles is evaluated and compared to the findings from the analysis of the separated powers. This can provide an understanding of the potential of a reduced observation scenario that does not allow a tomographic reflectivity reconstruction since the center of mass corresponds - at least at the first order - to the interferometric phase center that can be estimated by means of only two acquired tracks.
- Finally, the significance of anisotropic orientation effects of the vegetation of the different crop types is assessed.

Chapter 4 “Sensitivity of SAR Tomography to the Phenological Cycle of Agricultural Crops at X-, C- and L-band” This Chapter discusses the sensitivity of X-, C- and L-band to specific phenological transitions by using parameters estimated from the MB SAR data.

As shown in Chapter 3, the filtering approach allows the estimation of the MB volume interferometric coherences and the ground and volume powers. This enables the distinct analysis of the center of mass, and ground and volume power changes in time related to the changes in the plants along the phenological cycle.

The suitability of a certain frequency might vary for different crop types and also within the phenological cycle of a single crop type. In order to address this, characteristic phenological transitions related to dielectric (e.g. dynamics of the water content) and geometric (e.g. alignments of plant components) changes have been identified for corn, wheat and barley in the time period of the CROPEX 2014 campaign. The Chapter discusses the sensitivity of the tomographic parameters used in Chapter 3 to such transitions regarding communalities and complementarities of X-, C- and L-band frequencies. The analyses have been focused on:

- Both electromagnetic backscattering and attenuation are expected to be influenced by the amount of water contained in the vegetation to different degrees at the different frequencies. Thus, the changes of the volume power with VWC and wet biomass are analyzed.
- Since the ground power under vegetation is affected by attenuation through the vegetation volume, the effect of vegetation changes on the variation of ground power is analyzed together with soil moisture dynamics.
- The added value of the center of mass of the 3-D backscatter as an interferometric variable is investigated for each of the analyzed transitions.
- Insights on the benefit of the availability of different polarimetric channels are given.

1.5 References

- [1] F. T. Ulaby, and R. P. Jedlicka, “Microwave Dielectric Properties of Plant Materials”, *IEEE Trans. Geosci. Remote Sensing*, vol. GE-22, no. 4, pp. 406-414, Jul. 1984.
- [2] F. T. Ulaby, and E. A. Wilson, “Microwave Attenuation Properties of Vegetation Canopies”, *IEEE Trans. Geosci. Remote Sensing*, vol. GE-23, no. 5, pp. 746–753, Sept 1985.
- [3] H. McNairn, and B. Brisco, “The Application of C-band Polarimetric SAR for Agriculture: A Review”, *Can. J. Remote Sens.*, vol. 30, no. 3, pp. 525-542, Ju. 2004.
- [4] S. C. Steele-Dunne, H. McNairn, A. Monsivais-Huertero, J. Judge, P. W. Liu, K. P. Papathanassiou, “Radar Remote Sensing of Agricultural Canopies: A Review”, *IEEE J. Sel. Top. Appl. Earth Obs. Remote Sens.*, vol. 10, no. 5, pp. 2249-2273, May 2017.
- [5] H. Vereecken, L. Weihermüller, F. Jonard, and C. Montzka, “Characterization of Crop Canopies and Water Stress Related Phenomena using Microwave Remote Sensing Methods: A Review”, *Vadose Zone J.*, vol. 11, no. 2, May 2012.
- [6] J. M. Lopez-Sanchez, and J. D. Ballester-Berman, “Potentials of Polarimetric SAR Interferometry for Agriculture Monitoring”, *Radio Sci.*, vol. 44, no. 2, pp. 141-177, Mar. 2009.
- [7] G. Krieger, A. Moreira, H. Fiedler, I. Hajnsek, M. Werner, M. Younis, and M. Zink, “Tandem-X: A satellite formation for high-resolution SAR interferometry”, *IEEE Trans. Geosci. Remote Sens.*, vol. 45, no. 11, pp. 3317–3341, Nov 2007.
- [8] L. C. Morena, K V James, and J. Beck, “An introduction to the RADARSAT-2 mission”, *Canadian Journal of Remote Sensing*, vol. 30, no. 3, Jun 2004
- [9] R. Torres et al., “GMES Sentinel-1 mission”, *Remote Sensing of Env.*, vol. 120, pp. 9–24, May 2012.
- [10] A. Moreira, G. Krieger, I. Hajnsek, K. Papathanassiou, M. Younis, P. Lopez-Dekker, S. Huber, M. Villano, M. Pardini, M. Eineder, and F. De Zan, “Tandem-L: A highly innovative bistatic SAR mission for global observation of dynamic processes on the Earth's surface”, *IEEE Geosc. and Remote Sensing Magazine*, vol. 3, no. 2, pp. 8-23, 2015.
- [11] E. P. W. Attema, and F. T. Ulaby, “Vegetation modeled as a water cloud”, *Radio Science*, vol. 13, no. 2, pp. 357-364, Mar. 1978.
- [12] P. Ferrazzoli, S. Paloscia, P. Pampaloni, G. Schiavon, S. Sigismondi and D. Solimini, “The potential of multifrequency polarimetric SAR in assessing agricultural and arboreous biomass”, *IEEE Trans. Geosci. Remote Sens.*, vol. 35, no. 1, pp. 5-17, Jan. 1997.
- [13] G. Wiseman, H. McNairn, S. Homayouni and J. Shang, “RADARSAT-2 Polarimetric SAR Response to Crop Biomass for Agricultural Production Monitoring”, *IEEE J. Sel. Top. Appl. Earth Obs. Remote Sens.*, vol. 7, no. 11, pp. 4461-4471, Nov. 2014.

- [14] S. Paloscia, “A summary of experimental results to assess the contribution of SAR for mapping vegetation biomass and soil moisture”, *Can. Journal of Remote Sensing*, vol. 28, no. 2, pp. 246-261, Jun. 2002.
- [15] M. Bracaglia, P. Ferrazzoli, L. Guerriero, “A fully polarimetric multiple scattering model for crops”, *Remote Sensing of Env.*, vol. 54, no. 3, pp. 170-179, Dec. 1995.
- [16] A. Della Vecchia, P. Ferrazzoli, L. Guerriero, L. Ninivaggi, T. Strozzi, and U. Wegmuller, “Observing and Modeling Multifrequency Scattering of Maize During the Whole Growth Cycle”, *IEEE Trans. Geosci. Remote Sens.*, vol. 46, no. 11, pp. 3709-3718, Nov. 2008.
- [17] P. Ferrazzoli, L. Guerriero, and G. Schiavon, “Experimental and model investigation on radar classification capability”, *IEEE Trans. Geosci. Remote Sens.*, vol. 37, no. 2, pp. 960-968, Mar. 1999.
- [18] H. McNairn, J. Shang, X. Jiao, X., and C. Champagne, “The Contribution of ALOS PALSAR Multipolarization and Polarimetric Data to Crop Classification”, *IEEE Trans. Geosci. Remote Sens.*, vol. 47, no. 12, pp. 3981-3992, Dec. 2009.
- [19] D. H. Hoekman, M. A. Vissers, and T. N. Tran, “Unsupervised Full-Polarimetric SAR Data Segmentation as a Tool for Classification of Agricultural Areas”, *IEEE J. Sel. Top. Appl. Earth Obs. Remote Sens.*, vol. 4, no. 2, pp. 402-411, Jun. 2011.
- [20] H. Skriver, “Crop Classification by Multitemporal C- and L-Band Single- and Dual-Polarization and Fully Polarimetric SAR”, *IEEE Trans. Geosci. Remote Sens.*, vol. 50, no. 6, pp. 2138-2149, Jun. 2012.
- [21] L. Mascolo, J. M. Lopez-Sanchez, F. Vicente-Guijalba, F. Nunziata, M. Migliaccio, and G. Mazarella, “A Complete Procedure for Crop Phenology Estimation with PolSAR Data Based on the Complex Wishart Classifier”, *IEEE Trans. Geosci. Remote Sens.*, vol. 54, no. 11, pp. 6505-6515, Nov. 2016.
- [22] A. Alonso-Gonzalez, H. Joerg, K. Papathanassiou, and I. Hajnsek, “Change analysis and interpretation in polarimetric time series over agricultural fields at C-band”, *Proc. EUSAR*, vol. 11, Jun. 2016.
- [23] A. Freeman, and S. L. Durden, “A three-component scattering model for polarimetric SAR data”, *IEEE Trans. Geosci. Remote Sens.*, vol. 36, no. 3, pp. 963-973, May 1998.
- [24] I. Hajnsek, T. Jagdhuber, H. Schon, and K. P. Papathanassiou, “Potential of Estimating Soil Moisture Under Vegetation Cover by Means of PolSAR”, *IEEE Trans. Geosci. Remote Sens.*, vol. 47, no. 2, pp. 442-454, Feb. 2009.
- [25] T. Jagdhuber, I. Hajnsek, and K. P. Papathanassiou, “An iterative generalized hybrid decomposition for soil moisture retrieval under vegetation cover using fully polarimetric SAR”, *IEEE J. Sel. Top. Appl. Earth Obs. Remote Sens.*, vol. 8, no. 8, pp. 3911-3922, Aug. 2015.

- [26] I. Hajnsek, E. Pottier, and S. R. Cloude, "Inversion of surface parameters from polarimetric SAR", *IEEE Trans. Geosci. Remote Sens.*, vol. 41, no. 4, pp. 727-744, Apr. 2004.
- [27] H. Skriver, M. T. Svendsen, and A. G. Thomsen, "Multitemporal C- and L-band polarimetric signatures of crops", *IEEE Trans. Geosci. Remote Sens.*, vol. 37, no. 5, pp. 2413-2429, Sep. 1999.
- [28] S. R. Cloude, and E. Pottier, "An entropy based classification scheme for land applications of polarimetric SAR", *IEEE Trans. Geosci. Remote Sens.*, vol. 35, no. 1, pp. 68-78, Jan. 1997.
- [29] H. Joerg, M. Pardini, I. Hajnsek, K. P. Papathanassiou, "3-D Scattering Characterization of Agricultural Crops at C-Band using SAR Tomography", accepted for publication in *IEEE Trans. Geosci. Remote Sens.*, 2018.
- [30] S. R. Cloude, *Polarisation: Applications in Remote Sensing*. Oxford, U.K.: Oxford Univ. Press, 2009.
- [31] R. N. Treuhaft, and P. R. Siqueira, "Vertical Structure of Vegetated Land surfaces from Interferometric and Polarimetric Radar", *Radio Sci.*, vol. 35, no. 1, pp. 141-177, Feb. 2000.
- [32] S. R. Cloude, and K. P. Papathanassiou, "Three-Stage Inversion Process for Polarimetric SAR Interferometry", *Proc. Inst. Elect. Eng. - Radar, Sonar Navig.*, vol 150, no. 11, pp. 2352-2363, Jun. 2003.
- [33] J. D. Ballester-Berman, J. M. Lopez-Sanchez, and J. Fortuny-Guasch, "Retrieval of Biophysical Parameters of Agricultural Crops using Polarimetric SAR Interferometry", *IEEE Trans. Geosci. Remote Sens.*, vol. 43, no. 4, pp. 682-694, Apr. 2005.
- [34] M. Pichierri, I. Hajnsek, and K. P. Papathanassiou, "A Multi-Baseline Pol-InSAR Inversion Scheme for Crop Parameter Estimation at Different Frequencies", *IEEE Trans. Geosci. Remote Sens.*, vol. 54, no. 8, pp. 4952-4970, Aug. 2016.
- [35] M. Pichierri, and I. Hajnsek, "Comparing Performances of Crop Height Inversion Schemes From Multifrequency Pol-InSAR Data," *IEEE J. Sel. Top. Appl. Earth Obs. Remote Sens.*, vol. 10, no. 5, pp. 1727-1741, May 2017.
- [36] M. Pichierri, I. Hajnsek, S. Zwieback, and B. Rabus, "On the potential of Polarimetric SAR Interferometry to characterize the biomass, moisture and structure of agricultural crops at L-, C- and X-Bands", *Remote Sensing of Env.*, vol. 204, pp. 596-616, Jan. 2018.
- [37] A. Reigber, and A. Moreira, "First Demonstration of Airborne SAR Tomography using Multibaseline L-band Data", *IEEE Trans. Geosci. Remote Sens.*, vol. 38, no. 5, pp. 2142-2152, Sep. 2000.
- [38] F. Lombardini, and M. Pardini, "Experiments of Tomography-Based SAR Techniques with P-Band Polarimetric Data", in *Proc. PolInSAR*, Frascati, Italy, Jan. 2009.
- [39] O. Frey, and E. Meier, "3-D Time-Domain SAR Imaging of a Forest using Airborne Multibaseline Data at L- and P-Bands", *IEEE Trans. Geosci. Remote Sens.*, vol. 49, no. 10, pp. 3660-3664, Oct. 2011.

- [40] E. Aguilera, M. Nannini, M., and A. Reigber, “Wavelet-Based Compressed Sensing for SAR Tomography of Forested Areas”, *IEEE Trans. Geosci. Remote Sens.*, vol. 51, no. 12, pp. 5283-5295, Dec. 2013.
- [41] Y. Huang, L. Ferro-Famil, and A. Reigber, “Under-Foliage Object Imaging Using SAR Tomography and Polarimetric Spectral Estimators”, *IEEE Trans. Geosci. and Remote Sens.*, vol. 50, no. 6, pp. 2213-2225, Jun. 2012.
- [42] F. Lombardini, and F. Cai, “Temporal Decorrelation-Robust SAR Tomography”, *IEEE Trans. Geosci. Remote Sens.*, vol. 52, no. 9, pp. 5412-5421, Sep. 2014.
- [43] F. Gini, F. Lombardini, and M. Montanari, “Layover solution in multibaseline SAR interferometry”, *IEEE Trans. Aerosp. Electron. Syst.*, vol. 38, no. 4, 1344-1356, Oct. 2002.
- [44] M. Pardini, and K. Papathanassiou, “Sub-Canopy Topography Estimation: Experiments With Multibaseline SAR Data at L-Band”, in *Proc. of IGARSS*, pp. 4954 - 4957, Jul. 2012.
- [45] S. Tebaldini, “Algebraic Synthesis of Forest Scenarios from Multibaseline PolInSAR Data”, *IEEE Trans. Geosci. Remote Sens.*, vol. 47, no. 12, pp. 4132-4142, Dec. 2009.
- [46] M. Pardini, and K. Papathanassiou, “On the Estimation of Ground and Volume Polarimetric Covariances in Forest Scenarios With SAR Tomography”, *IEEE Geosci. Remote Sens. Lett.*, vol. 14, no. 10, pp. 1860-1864, Oct. 2017.
- [47] S. Tebaldini, and F. Rocca, “Multibaseline Polarimetric SAR Tomography of a Boreal Forest at P- and L-Bands”, *IEEE Trans. Geosci. Remote Sens.*, vol. 50, no. 1, pp. 232-246, Jan. 2012.
- [48] J. M. Lopez-Sanchez, J. Fortuny-Guasch, S. R. Cloude, and A. J. Sieber, “Indoor polarimetric radar measurements on vegetation samples at L, S, C and X band”, *J. Electromagn. Waves Appl.*, vol. 14, no.2, pp. 205-231, 2000.
- [49] S. C. M. Brown, S. Quegan, K. Morrison, J. C. Bennett, and G. Cookmartin, “High-Resolution Measurements of Scattering in Wheat Canopies – Implications for Crop Parameter Retrieval”, *IEEE Trans. Geosci. Remote Sens.*, vol. 41, no. 7, pp. 1602-1610, Jul. 2003.
- [50] J. M. Lopez-Sanchez, J. D. Ballester-Berman, and J. Fortuny-Guasch, “Indoor wide-band polarimetric measurements on maize plants: a study of the differential extinction coefficient”, *IEEE Trans. Geosci. Remote Sens.*, vol. 44, no. 4, pp. 758-767, Apr. 2006.
- [51] S. R. Cloude, “Dual-Baseline Coherence Tomography”, *IEEE Geosci. Remote Sens. Lett.*, vol. 4, no. 1, pp. 127-131, Jan. 2007.
- [52] T. Marzetta, “A New Interpretation for Capon’s Maximum Likelihood Method of Frequency-Wavenumber Spectral Estimation”, *IEEE Trans. Acoust. Speech, Signal Processing*, vol. 31, no.2, pp. 445-449, Apr. 1983.

Chapter 2

On the Separation of Ground and Volume Scattering Using Multi-Baseline SAR Data

H. Joerg, M. Pardini, I. Hajnsek, and K. P. Papathanassiou

IEEE Geoscience and Remote Sensing Letters

Published in vol. 14, no. 9, pp. 1570 - 1574, DOI:10.1109/LGRS.2017.2723980, July 2017

The author's contributions:

- Simulation of the MB SAR data and implementation of the two separation algorithms.
- Performance analysis of the two algorithms for separation of ground and volume component from MB SAR data.
- Evaluation of the results obtained from the performance analysis and writing of the manuscript.

The co-authors' contributions:

- M. Pardini suggested the implementation and the comparison of the two algorithms and supported the evaluation of the results.
- All co-authors reviewed the results and the manuscript.

On the Separation of Ground and Volume Scattering Using Multi-Baseline SAR Data

Hannah Joerg^{1,2}, Matteo Pardini¹, Irena Hajnsek^{2,1}, and Konstantinos P. Papathanassiou¹

¹ German Aerospace Center, Microwaves and Radar Institute, Wessling, Germany

² ETH Zurich, Institute of Environmental Engineering, Zurich, Switzerland

Abstract

In forest and agricultural scattering scenarios, the backscattered synthetic aperture radar (SAR) signature consists, depending on the frequency, of the superposition of ground and volume scattering contributions. Using multi-baseline (MB) SAR data, SAR Tomography techniques allow resolving contributions occurring at different heights. Two algorithms for the separation of ground and volume scattering are compared with respect to their ability to provide a coherent volume component that can be further used for parameter inversion, both of them requiring only the a priori known ground topography. Once the volume-only coherences are available, the total ground and volume scattering powers are estimated by means of a least squares fitting. The objective of this letter is to quantitatively evaluate the performance of this estimation by means of a Monte Carlo analysis with simulated data focusing on the impact of vertical resolution, errors in the knowledge of the ground topography and phase calibration residuals.

2.1 Introduction

The use of multi-baseline (MB) synthetic aperture radar (SAR) data and tomographic techniques has been proven to be a powerful tool for separating superimposed scattering contributions in height, such as point-like scatterers in layover in urban areas [1]-[3].

Vegetation scenarios are commonly modelled as two-layer media. In this context, the Random-Volume-over-Ground model appears to be a good compromise between the ability to describe the data and the number of parameters required for their parameterization. The availability of fully polarimetric data facilitates model inversion [4], but reaches its limit in the presence of anisotropic propagation through the volume. In this case, no closed form decomposition of the polarimetric MB volume coherences exists. Tomographic techniques are expected to allow a model-free separation of ground and volume scattering contributions even for single polarimetric MB data. However, when formulated in a maximum likelihood sense, the separation problem does not admit a unique solution [5].

In this letter, alternative solutions to the problem are considered employing a priori information, i.e. the knowledge of the ground topography. Two algorithms that directly benefit from this information for the separation of ground and volume scattering contributions are discussed and

compared, assuming that the ground vertical reflectivity is a Dirac-delta located at the ground height which is a priori known. The two algorithms follow different strategies for estimating the volume component from the MB data vector. The first one subtracts the ground signal, which is reconstructed based on Capon's asymptotic maximum likelihood (AML) method [5]. The second one coherently cancels the ground component using a matrix filter (MF) [6]. The ability of both algorithms to provide a coherent volume component that can be used for parameter inversion has not been investigated yet, and is addressed in the following. For instance, given the MB volume coherences estimated with either of the methodologies, the ground and volume powers can be estimated using a least squares fitting [7]. The separate analysis of ground and volume powers as well as the ground-to-volume power ratio can be used to characterize scattering scenarios [4,8]. For this purpose, the estimation performance for ground and volume powers obtained from both AML and MF is evaluated quantitatively by means of simulated data. In this analysis, particular emphasis has been posed on the influence of the tomographic vertical resolution, errors in the knowledge of the ground topography and phase calibration residuals.

2.2 Data Model and Problem Formulation

Let $\mathbf{y}(n)$ be the K -dimensional MB data vector in the n -th pixel of a N -dimensional multi-look cell, consisting of the complex backscatter amplitudes collected at K different tracks. The look-angle of the master (placed conventionally at the first element) is θ . The spatial separation of the tracks leads to a look-angle difference $\Delta\theta^i$ of the i -th track with respect to the master. The vertical wavenumber κ_z^i depends on $\Delta\theta^i$ and the wavelength λ as $\kappa_z^i \approx (4\pi/\lambda) \cdot (\Delta\theta^i / \sin\theta)$. The variation of the interferometric phase from track to track for a given height z is then expressed by the steering vector $\mathbf{a}(z) = [1, e^{-j\kappa_z^2 z}, \dots, e^{-j\kappa_z^K z}]^T$, with $\kappa_z^1 = 0$. The vertical Rayleigh resolution is defined by $\rho_z = 2\pi / (\max_i \kappa_z^i)$.

The MB data vector $\mathbf{y}(n)$ is modeled as the sum of a Dirac-delta shaped ground layer located at height z_G and a volume contribution located above. The ground layer has a complex reflectivity $\tau_G(n)$ distributed as a zero mean complex Gaussian process:

$$\mathbf{y}(n) = \tau_G(n)\mathbf{a}_G + \mathbf{y}_V(n), \quad n = 1, \dots, N, \quad (1)$$

where $\mathbf{a}_G := \mathbf{a}(z_G)$ and $\mathbf{y}_V(n)$ is the MB volume data vector. With ground power $p_G = E\{|\tau_G|^2\}$, volume power p_V and volume coherence matrix $\mathbf{\Gamma}_V$, the MB covariance matrix \mathbf{R} of $\mathbf{y}(n)$ can be written as:

$$\mathbf{R} = p_G \mathbf{a}_G \mathbf{a}_G^H + p_V \mathbf{\Gamma}_V. \quad (2)$$

For this two-layer model, no assumptions are posed on the volume scattering. Inside the multi-look cell, the scattering is assumed homogeneous and the topography constant. The phase center of the dihedral interactions between ground and volume is located at the ground and the associated contributions are therefore included in p_G . In principle, the model is generally valid at each frequency band, as long as a ground contribution is present.

In order to estimate the powers p_G and p_V by covariance matching from equation (2) [7], an estimate of $\mathbf{\Gamma}_V$, and therefore $\mathbf{y}_V(n)$, is required. However, the estimation problem as given by (1) has no unique solution in a maximum likelihood sense [5]. A way to overcome this limitation is to use a priori knowledge of z_G . For this case, two approaches to estimate $\mathbf{\Gamma}_V$ and p_G and p_V are discussed in the following. The first one employs an asymptotically optimal estimation of the ground reflectivity [5] while the second one directly cancels the ground layer using a band filter [6].

2.3 Separation Methodologies

2.3.1 Estimation of the Volume Coherences

In this Section, both methodologies for estimating the volume coherences starting from model (1) are described.

A. Asymptotic Maximum Likelihood Method

The volume signal $\mathbf{y}_V(n)$ is obtained in two subsequent steps. In the first step, the ground component is reconstructed, and requires an initial estimate of the ground reflectivity. An optimal estimate of $\tau_G(n)$, in the maximum likelihood sense, can be achieved only if the volume coherences are known. Nevertheless, the use of the full MB covariance matrix \mathbf{R} in Capon's AML method yields an initial estimate of the reflectivity at the a priori known ground height z_G [5]:

$$\hat{\tau}_G(n) = \frac{\mathbf{a}_G^H \mathbf{R}^{-1} \mathbf{y}(n)}{\mathbf{a}_G^H \mathbf{R}^{-1} \mathbf{a}_G}, n = 1, \dots, N. \quad (3)$$

For a sufficient number of looks N , the initial estimate in (3) converges asymptotically to the optimal estimate [5].

Finally, the volume data vector is obtained according to (1) as:

$$\mathbf{y}_V(n) = \mathbf{y}(n) - \tau_G(n) \mathbf{a}_G, n = 1, \dots, N. \quad (4)$$

B. Matrix Filter

This approach separates the two components by exploiting the fact that they are located at different heights. A MF, \mathbf{H} , is designed to cancel as much as possible the power components located in a stop band around the ground and to leave unaltered the power components at the heights inside the volume, where the pass band is located. Then the volume-only data vector is estimated as [6]:

$$\mathbf{y}_V(n) = \mathbf{H} \mathbf{y}(n), n = 1, \dots, N. \quad (5)$$

Retaining linearity, the availability of many filter coefficients makes the MF preferable to a vector filter. Many design criteria can be used for defining the filter; in the following, the filter is conditioned with respect to the steering vectors at given heights. The stop and the pass band are sampled at m_s and m_p heights respectively. The columns of the matrices $\mathbf{A}_{stop} \in \mathbb{C}^{k \times m_s}$ and

$\mathbf{A}_{pass} \in \mathbb{C}^{k \times m_p}$ are given by the steering vectors at the discretized heights inside the respective band. Then, an input steering matrix $\mathbf{A}_{in} = [\mathbf{A}_{stop} \ \mathbf{A}_{pass}]$ and an output steering matrix $\mathbf{A}_{out} = [\mathbf{0}_{k \times m_s} \ \mathbf{A}_{pass}]$ are defined, implying the cancellation of the power components in the stop band. The filter \mathbf{H} is the solution of:

$$\mathbf{H} = \underset{\mathbf{H}}{\operatorname{argmin}} \|\mathbf{H}\mathbf{A}_{in} - \mathbf{A}_{out}\|_F^2, \quad (6)$$

where $\|\cdot\|_F$ denotes the Frobenius norm. Adding a regularization factor η to avoid possible ill-conditioning, the solution of (6) is obtained in closed form as:

$$\mathbf{H} = \mathbf{A}_{out}\mathbf{A}_{in}^H(\mathbf{A}_{in}\mathbf{A}_{in}^H + \eta\mathbf{I})^{-1}. \quad (7)$$

The stop band, B_{stop} , is defined symmetrically around the a priori known ground height z_G while the pass band, B_{pass} , contains the volume component. The widths of stop and pass band are determined by the parameters δ and z_{top} :

$$\begin{aligned} B_{stop} &:= \{z, z \in [z_G - \delta, z_G + \delta]\} \\ B_{pass} &:= \{z, z \in [z_G + 2\delta, z_G + z_{top}]\}. \end{aligned} \quad (8)$$

The choice of δ and z_{top} influences the filtering performance. A good compromise between sufficient cancellation in the stop band and preservation in the pass band is achieved for selecting δ as 25% of the vertical Rayleigh resolution and z_{top} as an upper boundary of the expected height of the volume layer, e.g. obtained from preliminary tomographic analyses.

2.3.2 Power Estimation

After estimating the MB volume coherence matrix $\mathbf{\Gamma}_V$ from the \mathbf{y}_V obtained with one of the two approaches, covariance matching yields estimates for p_G and p_V by minimizing the following cost function based on equation (2) [7]:

$$Q(p_G, p_V) = \|\mathbf{R} - (p_G\mathbf{a}_G\mathbf{a}_G^H + p_V\mathbf{\Gamma}_V)\|_F^2. \quad (9)$$

The unweighted least squares solution of (9) is:

$$\begin{bmatrix} p_G \\ p_V \end{bmatrix} = (\mathbf{\Pi}^H\mathbf{\Pi})^{-1}\mathbf{\Pi}^H\operatorname{vec}(\mathbf{R}), \quad (10)$$

where $\mathbf{\Pi} = [\operatorname{vec}(\mathbf{a}_G\mathbf{a}_G^H) \ \operatorname{vec}(\mathbf{\Gamma}_V)]$ and $\operatorname{vec}(\cdot)$ is the vectorization operator converting a matrix to a column vector.

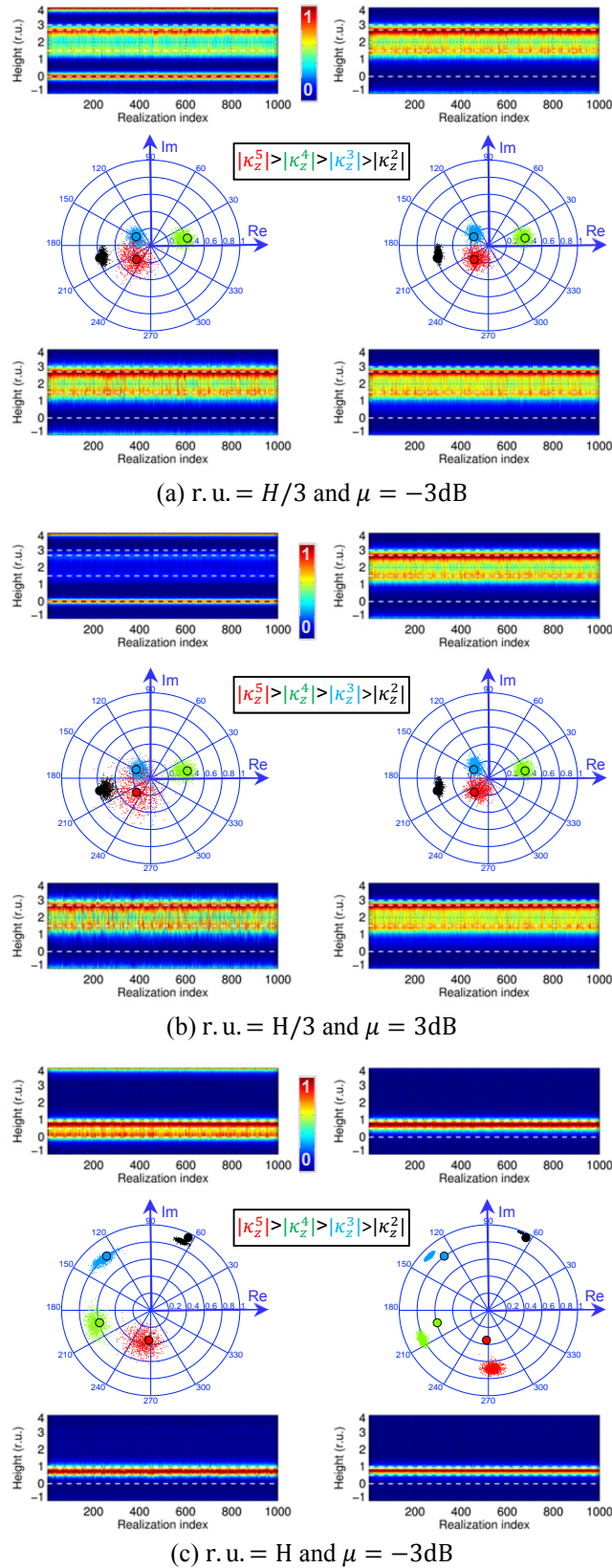


Fig. 1: For all panels (a)-(c): Top: Capon profiles of simulated MB (left) and volume-only MB (right) data. Middle: Coherence plot in the complex plane: comparison of the true volume coherences (circles) to the estimated volume coherences in 1000 realizations (dots) for the different baselines using AML (left) and MF (right). Bottom: Resulting volume-only Capon profiles using AML (left) and MF (right).

2.4 Numerical Results

2.4.1 Simulated MB Data

The MB data are simulated according to the model in (1) for $K = 5$ uniformly distributed tracks in absence of temporal decorrelation. For the sake of generality, the heights are expressed in Rayleigh resolution units (r.u.), defined as the height in meters divided by ρ_z . Hence, scenarios with different vertical resolution and absolute volume heights are covered by the variation of one parameter. $N = 100$ independent looks are used. White noise is added to the signal up to a signal-to-noise ratio of 20 dB.

Each scattering scenario is defined by two parameters: the volume height H (varying from one to three r.u.), and the ground-to-volume ratio $\mu := p_G/p_V$. By keeping p_V constant, the ground and volume powers are thus defined relative to each other. The volume layer is simulated as the sum of two Gaussian shaped layers, located at heights $z_1 = 0.9 H$ and $z_2 = 0.5 H$, with widths $w_1 = w_2 = 0.1 H$ and powers P_1 and P_2 , where $p_V = P_1 + P_2$ and $P_2/P_1 = 0.8$.

2.4.2 Estimated Volume Coherences

First, the MB volume coherence estimation from the simulated data is discussed for the two algorithms. In order to get a first understanding of their performance, Fig. 1 shows three different scenarios in terms of volume height and ground-to-volume power ratio. The vertical profiles estimated from the simulated MB data and the simulated volume-only MB data using the Capon beamformer are shown for 1000 Monte Carlo realizations (horizontal axis), normalized by their maximum power. The estimated volume-only complex coherences are compared to the “true” coherence values on the complex plane and the normalized Capon profiles are shown for AML (left) and MF (right). In the first two scenarios, the tomographic resolution is sufficiently high, i.e. r.u. = $H/3$. The MF outperforms AML in both scenarios. The volume coherences estimated by AML exhibit a larger phase noise in the ground dominated case than in the volume dominated scenario. This is coming from the inaccuracy of (3) in the estimation of the phase of τ_G . The application of (4) therefore results into a larger phase noise for the volume coherences in contrast to MF.

The third scenario is more critical, since the vertical Rayleigh resolution equals the volume height, i.e. r.u. = H , and makes the separation of the ground and the volume more challenging as now they are superimposed in the same height resolution cell. In this case, MF overestimates the coherence magnitudes while AML is able to recover the coherences better.

2.4.3 Estimation Performance

10^4 Monte Carlo runs are executed and the performance of the estimation methodologies is analyzed quantitatively in terms of root-mean-square error (RMSE) and bias of the estimates in Fig. 2, both normalized with respect to the true value. The estimates of interest are the powers of the ground and volume, \hat{p}_G and \hat{p}_V , and the ground-to-volume power ratio $\hat{\mu} = \hat{p}_G/\hat{p}_V$. The simulations are executed over a range of $\mu \in [-10 \text{ dB}, 10 \text{ dB}]$.

As already indicated, for r.u. = $H/3$, the MF performs equivalently or better than the AML and

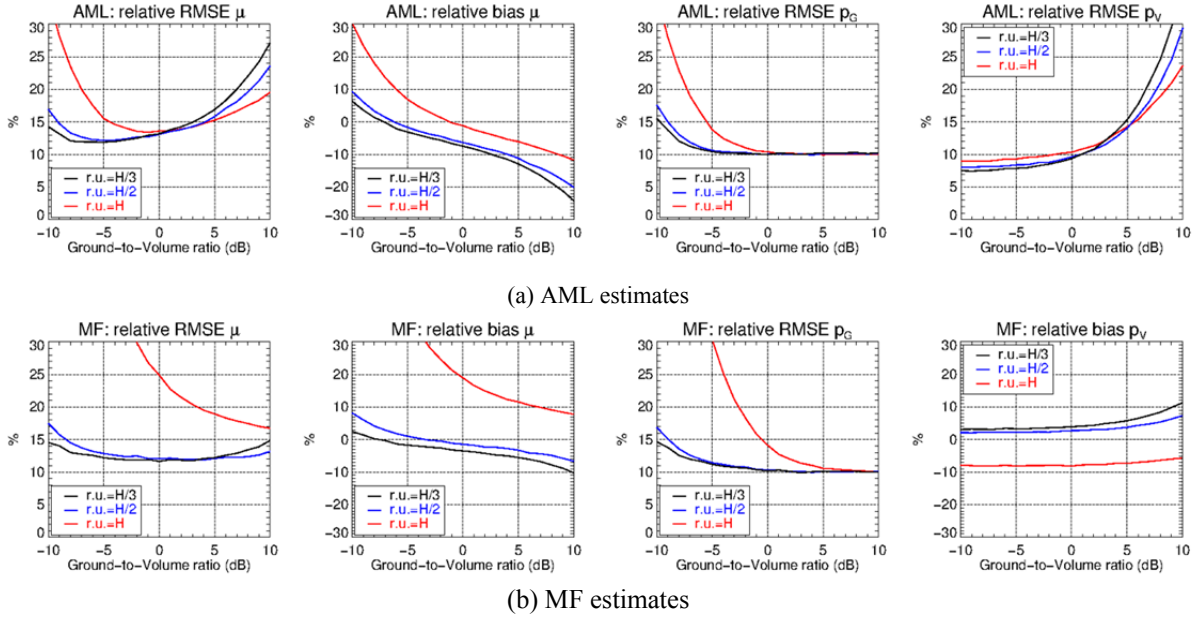


Fig. 2: Performance results over varying μ based on 10^4 Monte Carlo realizations for the estimation of \hat{p}_G , \hat{p}_V and $\hat{\mu} = \hat{p}_G/\hat{p}_V$.

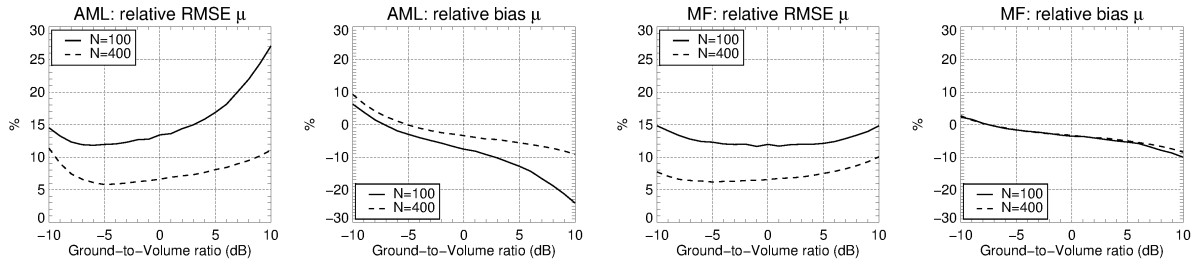


Fig. 3: RMSE($\hat{\mu}$) and bias($\hat{\mu}$) for r. u. = H/3 over varying μ with $N = 100$ and $N = 400$.

achieves $\text{RMSE}(\hat{\mu}) \leq 15\%$ over the whole range of μ . In general, for both methods the RMSE of the weaker power component tends to be higher, i.e. the $\text{RMSE}(\hat{p}_G)$ for low μ and the $\text{RMSE}(\hat{p}_V)$ for high μ , respectively. Going from r. u. = H/3 to r. u. = H/2 the performance of the algorithms does not change significantly.

For the critical case of r. u. = H, instead, the estimation performance of $\hat{\mu}$ decreases for both methods, essentially due to an increase of $\text{RMSE}(\hat{p}_G)$ and $\text{bias}(\hat{p}_G)$ at low μ levels. This effect is worse for the MF since, as discussed in Section 2.4.2., the coherence magnitudes are overestimated if the vertical resolution becomes on the order of the volume height. In fact, $\text{RMSE}(\hat{p}_G)$ of the MF exceeds 20% already for $\mu \leq -3$ dB, while for the AML this is the case only from $\mu \leq -7$ dB. For both algorithms, the tomographic resolution does not significantly influence the estimation performance of p_V .

Independently from the tomographic resolution, AML overestimates p_V for a dominant ground component leading to an underestimation of μ . The increased phase noise of the estimated volume coherences in this case (see Fig. 1) caused by the inaccuracy in the estimation of the ground reflectivity in (3) leads to the overestimation of p_V . However, the performance of the AML estimate of the ground reflectivity is expected to improve for a larger number of looks [5]. This is shown in Fig. 3 for the scenario with the best vertical resolution (r. u. = H/3). RMSE and bias of the AML

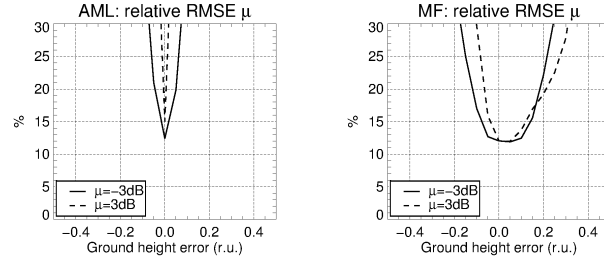


Fig. 4: RMSE($\hat{\mu}$) of AML and MF estimates for r. u. = $H/3$ over Δz_G .

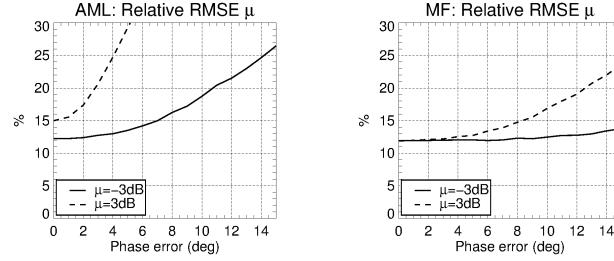


Fig. 5: RMSE($\hat{\mu}$) of AML and MF estimates for r. u. = $H/3$ over a randomly generated phase error.

estimates improve particularly for high μ due to an improvement of \hat{p}_V . Also for the MF, the RMSE($\hat{\mu}$) decreases for the whole range of μ while the bias($\hat{\mu}$) does not change.

An important point to consider is the impact of an error Δz_G caused by an error in the knowledge of the ground location or residual phase errors in the data which are linear with κ_z^l . The impact of the error Δz_G is shown in Fig. 4 for two reference scenarios with the best vertical resolution (r. u. = $H/3$) and $\mu = -3$ dB or $\mu = 3$ dB. The AML estimates are very sensitive to Δz_G that causes an underestimation of p_G and an overestimation of p_V . Aiming at a RMSE($\hat{\mu}$) better than 20%, even in the better performing case of $\mu = -3$ dB, only a range of $|\Delta z_G| \leq 0.05$ r. u. becomes acceptable. The MF estimates are more robust and acceptable results are still obtained for $\Delta z_G \in [-0.1 \text{ r. u.}, 0.2 \text{ r. u.}]$. For instance, the maximum acceptable error for a forest scenario with typically $\rho_z \approx 15$ m is 0.75 m. Agriculture applications with a high vertical resolution, i.e. $\rho_z \approx 1$ m, require an unrealistic precision up to 0.05 m for reasonable results with AML.

For (white) noise-like phase errors, which are distributed independently for each baseline, the behavior is different. Such phase errors strongly impact the AML estimates of p_G and p_V , resulting in RMSE($\hat{\mu}$) levels of 20% or even higher already for a phase error of 3 degrees for $\mu = -3$ dB and 11 degrees for $\mu = 3$ dB respectively (see Fig. 5). Instead, for the MF, only the volume power estimates for high μ are affected. A RMSE($\hat{\mu}$) of more than 20% is obtained for a phase error higher than 12 degrees in the volume dominating case.

The influence of the number of acquisitions, while keeping the total baseline, i.e. the vertical resolution, has also been investigated. Increasing the number of acquisitions from 5 up to 10 does not improve the performance of the MF estimates and neither the AML results change significantly.

Finally, differences in the scattering scenario can also affect the estimation performance. An increased width of the single volume layers makes it more difficult to resolve the layers. However, in the case of r. u. = $H/3$ and $\mu = -3$ dB, setting $w_{1,2}$ to 0.3 only leads to an insignificant nominal increase of RMSE($\hat{\mu}$) by 5-10% compared to $w_{1,2} = 0.1$ for both methods.

2.5 Conclusions

The performance of two algorithms, the AML and the MF approach, for the estimation of MB volume coherences and ground and volume backscattering powers from MB SAR data has been discussed, assuming that the ground topography is a priori known, which results to be a sufficient condition to enable a non-ambiguous separation. The performance of the two algorithms has been assessed and compared for different scattering properties and geometries. In principle, both algorithms can be applied at each frequency band, as long as a ground contribution is present.

The main limitation on the performance is the tomographic resolution. For volumes with heights on the order of the Rayleigh resolution, the AML estimates the volume coherences and the ground power with high accuracy. However, even for more favorable height resolutions, the volume power estimates may worsen especially for ground dominated scenarios, as a direct consequence of the uncertainties in the estimation of the ground reflectivity. This can be partially compensated by increasing the number of looks. It is worth remarking that for point-like scatterers, a higher number of acquisitions would have a similar effect. In the presence of volume scatterers, instead, increasing the number of acquisitions does not necessarily imply a (significant) performance improvement. In addition, the very high sensitivity to small errors in the knowledge of the ground location and to residual MB phase miscalibration imposes critical constraints on the practical application of this method.

If the tomographic Rayleigh resolution is sufficient, the MF provides good performance in the estimation of ground and volume powers. In addition, the MF is more robust against errors in the a priori required ground height and residual MB phase errors. Therefore, the application of MF is more reliable also with topographic estimates directly obtained from MB SAR data, e.g. by using [9].

The application of the discussed methodology on real (experimental) data has been demonstrated and discussed by the authors in [6] as well as in [8]. The achieved results are fully compliant with the conclusions drawn here. Future studies can be extended to other two-layer scattering scenarios like ice. Temporal decorrelation is expected to worsen the estimation performance, and the extent of it is left for future investigation. Finally, the benefit of additional polarimetric modelling and/or different optimization criteria of the filter response should be assessed.

Acknowledgements

This study was supported by the HGF (Helmholtz-Gemeinschaft Deutscher Forschungszentren) Alliance HA-310 ‘Remote Sensing and Earth System Dynamics’. The authors would like to thank the anonymous reviewers for their valuable comments, which have improved the quality of this paper.

2.6 References

- [1] F. Lombardini, M. Pardini, G. Fornaro, F. Serafino, L. Verrazzani, and M. Costantini, "Linear and Adaptive Spaceborne Threedimensional SAR Tomography: a Comparison on Real Data," *IET Radar, Sonar & Navigation*, vol.3, no.4, pp. 424-436, Aug. 2009.
- [2] X. X. Zhu, and R. Bamler, "Very High Resolution Spaceborne SAR Tomography in Urban Environment," in *IEEE Trans. Geosci. Remote Sens.*, vol. 48, no. 12, pp. 4296-4308, Dec. 2010.
- [3] Y. Huang, L. Ferro-Famil, and A. Reigber, "Under-Foliage Object Imaging Using SAR Tomography and Polarimetric Spectral Estimators," *IEEE Trans. Geosci. Remote Sens.*, vol. 50, no. 6, pp. 2213-2225, June 2012.
- [4] S. Tebaldini, and F. Rocca, "Multibaseline Polarimetric SAR Tomography of a Boreal Forest at P- and L-Bands," *IEEE Trans. Geosci. Remote Sens.*, vol. 50, no. 1, pp. 232-246, Jan. 2012.
- [5] T. Marzetta, "A New Interpretation for Capon's Maximum Likelihood Method of Frequency-Wavenumber Spectral Estimation," *IEEE Trans. Acoust. Speech, Signal Processing*, vol. 31, no. 2, pp. 445-449, Apr. 1983.
- [6] F. Lombardini, and M. Pardini, "Experiments of Tomography-Based SAR Techniques with P-Band Polarimetric Data," in *Proc. PolInSAR*, Frascati, Italy, Jan. 2009.
- [7] B. Ottersten, P. Stoica, and R. Roy, "Covariance matching estimation techniques for array signal processing and applications," *Digital Signal Processing*, vol. 8, no. 3, pp. 185-210, July 1998.
- [8] H. Joerg, M. Pardini, K. P. Papathanassiou, and I. Hajnsek, "Analysis of Orientation Effects of Crop Vegetation Volumes by Means of SAR Tomography at Different Frequencies," in *Proc. of EUSAR*, Hamburg, Germany, June 2016.
- [9] M. Pardini, and K.P. Papathanassiou, "Sub-Canopy Topography Estimation: Experiments with Multibaseline SAR Data at L-Band," in *Proc. IEEE IGARSS*, pp. 4954-4957, July 2012.

Chapter 3

3-D Scattering Characterization of Agricultural Crops at C-band using SAR Tomography

H. Joerg, M. Pardini, I. Hajnsek, and K. P. Papathanassiou

IEEE Transactions on Geoscience and Remote Sensing

Accepted for publication in January 2018

The author's contributions:

- Planning of the airborne MB SAR acquisitions and the ground measurement collection of the CROPEX 2014 campaign.
- Coordination of and participation in the ground measurement collection.
- Tomographic processing of the MB SAR data and implementation of the Matrix Filter for ground and volume separation.
- Interpretation and evaluation the estimated ground and volume parameters in relation with the changes in soil and plant parameters.
- Writing of the manuscript.

The co-authors' contributions:

- M. Pardini supervised the tomographic processing of the data and suggested the implementation of the Matrix Filter approach for the ground and volume separation.
- I. Hajnsek suggested and initiated the CROPEX 2014 campaign.
- K. P. Papathanassiou suggested the evaluation of the center of mass.
- All co-authors helped in discussing the results, reviewing and editing of the manuscript.

3-D Scattering Characterization of Agricultural Crops at C-band using SAR Tomography

Hannah Joerg^{1,2}, Matteo Pardini¹, Irena Hajnsek^{2,1}, and Konstantinos P. Papathanassiou¹

¹ German Aerospace Center, Microwaves and Radar Institute, Wessling, Germany

² ETH Zurich, Institute of Environmental Engineering, Zurich, Switzerland

Abstract

The aim of this paper is to interpret and characterize changes of the 3-D polarimetric scattering signatures of agricultural crops at C-band and to relate them to temporal changes of the soil and plant parameters. For this, a time series of multi-baseline (MB) synthetic aperture radar (SAR) data acquired at C-band by the airborne F-SAR system of the German Aerospace Center (DLR) over the Wallerfing test site in Germany was analyzed. The availability of MB SAR data enables the resolution of scattering contributions in height by means of SAR Tomography. The tomographic profiles at the different polarizations were analyzed regarding temporal changes for different crop types. First, it was investigated if the center of mass of the vertical reflectivity profiles as a single parameter enables the tracking of changes in soil and vegetation. The results show that the vertical reflectivity profiles and their center of mass do not allow resolving the ambiguity if a change originates from soil or vegetation dynamics as expected. Thus, the scattering contributions from ground and volume were separated in height, using a filtering approach, and used for the estimation of the ground and volume scattering powers by means of covariance matching. Comparing the outputs with coincident ground measurements showed that dielectric as well as geometric changes in the vegetation are traceable by the separated ground and volume powers. Finally, the estimated powers were analyzed with respect to orientation effects, i.e. to polarimetric anisotropic behavior. They were found to be not significant for the crops under study at C-band.

3.1 Introduction

Synthetic Aperture Radar (SAR) remote sensing has shown great potential for monitoring agricultural vegetation. Due to the sensitivity of microwaves to dielectric properties of the individual plant components and of the underlying soil, SAR measurements contain information which can be used to retrieve bio- and geophysical parameters and monitor their dynamics [1-13]. For instance, polarimetric SAR (PolSAR) was successfully applied for crop classification [3], estimation of plant phenology [5], crop productivity retrieval [3] or water stress detection [6,7]. Reliable and robust estimates of agricultural crop height are obtained by polarimetric

interferometric SAR techniques using single or multi-baseline (MB) fully-polarimetric acquisitions along spatially separated tracks [8-15].

Nevertheless, many questions are remaining particularly regarding the understanding of the scattering processes in the vegetation [2-4,8,9]. Conventional PolSAR cannot resolve scattering contributions at different heights and therefore changes in the underlying soil are often misinterpreted as changes in the vegetation and vice versa [2-6]. Furthermore, the scattering is influenced by both plant geometry (such as the alignment of stalks and leaves) and dielectric properties of the vegetation (as for instance water content) [2-4].

In order to address these questions, indoor and outdoor ground based experiments were conducted to resolve the 3-D scattering of wheat [16], corn at [17-19] and rice [20] at different frequencies. However, there are no systematic experiments assessing the temporal variation of the 3-D scattering signature of agricultural crops induced by phenological changes in the vegetation and/or changes in the soil.

In this paper, MB data at C-band are investigated due to their penetration capability into the vegetation canopy and the sensitivity to the individual plant components. Tomographic techniques allow a direct estimation of the vertical reflectivity by exploiting the amplitude and phase variation between acquisitions from several spatially separated tracks [21,22]. Even if the required number and distribution of the acquired tracks limits the wide application of airborne SAR Tomography to date, they are critical regarding the understanding of the 3-D scattering characteristics.

The objective of this paper is to investigate the changes in the 3-D scattering of agricultural crops over time at C-band. This requires the identification of the parameters which characterize the 3-D scattering signature of vegetated agricultural fields. At the same time the paper aims to provide some understanding on the potential of a reduced observation scenario that does not allow a tomographic reflectivity reconstruction. For this, the center of mass of the vertical reflectivity profiles is evaluated as it corresponds - at least in first order - to the interferometric phase center that can be estimated by means of single-baseline data [23].

In the presented analysis, the ground and volume scattering components are separated by applying a filtering approach directly to the MB data vector. The separation algorithm exploits the distinct location of the scattering components in height, assuming that the ground topography is known [24,25]. No further assumptions are necessary. The ground and volume powers can then be estimated by covariance matching [26]. The temporal variation of the retrieved parameters, such as the vertical reflectivity, the center of mass and the ground and volume powers, is evaluated regarding relations with changes in the soil and plant parameters. Finally, the significance of anisotropic propagation effects is assessed by directly comparing the ground and volume powers estimated under the oriented volume hypothesis with the ones estimated assuming a random volume.

The analysis is carried out using a time series of fully polarimetric MB data acquired by F-SAR, the DLR airborne sensor, in the frame of the Crop Experiment (CROPEX) 2014 campaign, over the agricultural Wallerfing test site located in southern Germany.

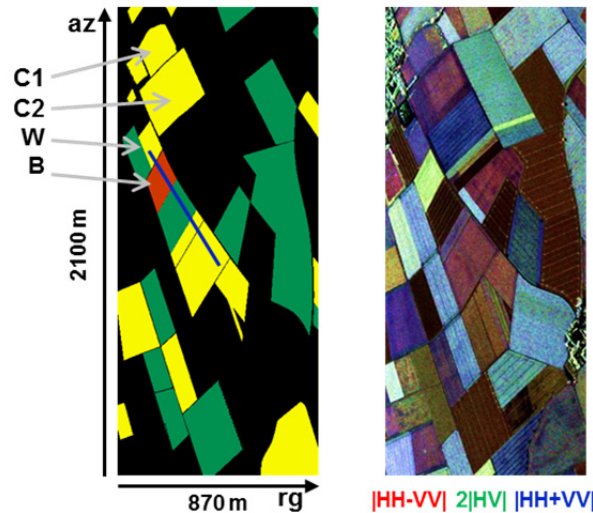


Fig. 1: Left: Land use of the patch under study: corn (yellow), wheat (green) and barley (red); other crop types, settlements and forests are masked out (black). C1, C2, W and B are the intensive measurement fields. The blue line indicates the transect for the analysis. Right: Pauli RGB composite image on June 18, 2014.

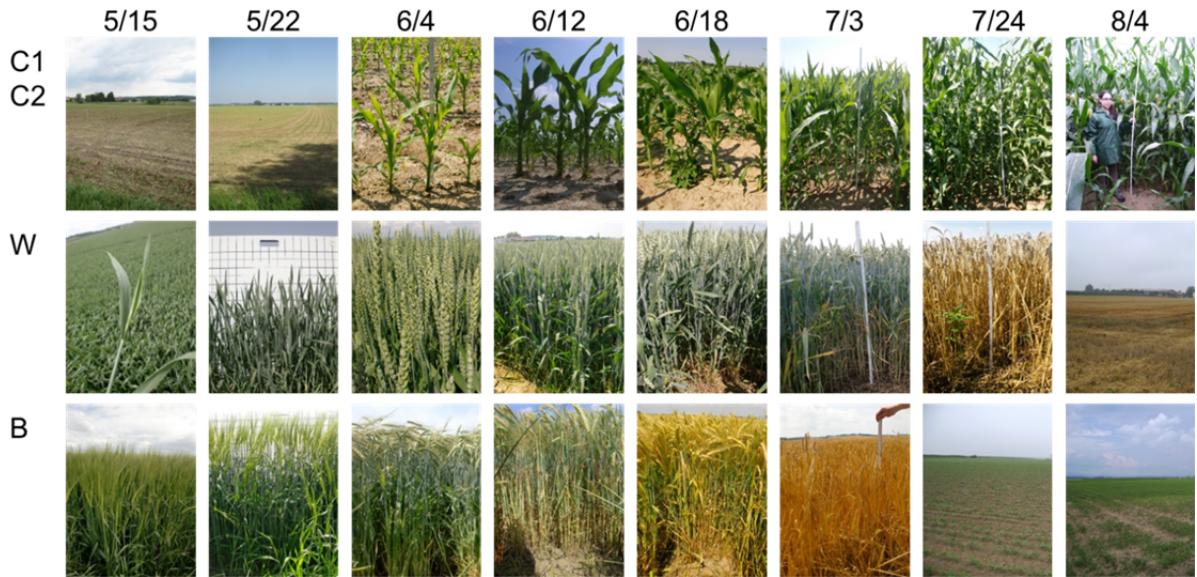
3.2 The CROPEX 2014 Campaign

The CROPEX 2014 campaign was designed to cover different phenological stages of mainly three crop types, namely corn, wheat and barley. For this purpose, repeat pass polarimetric MB SAR acquisitions by DLR's F-SAR and extensive ground measurements were carried out on eight days from May to August 2014. Both data sets are described in the following.

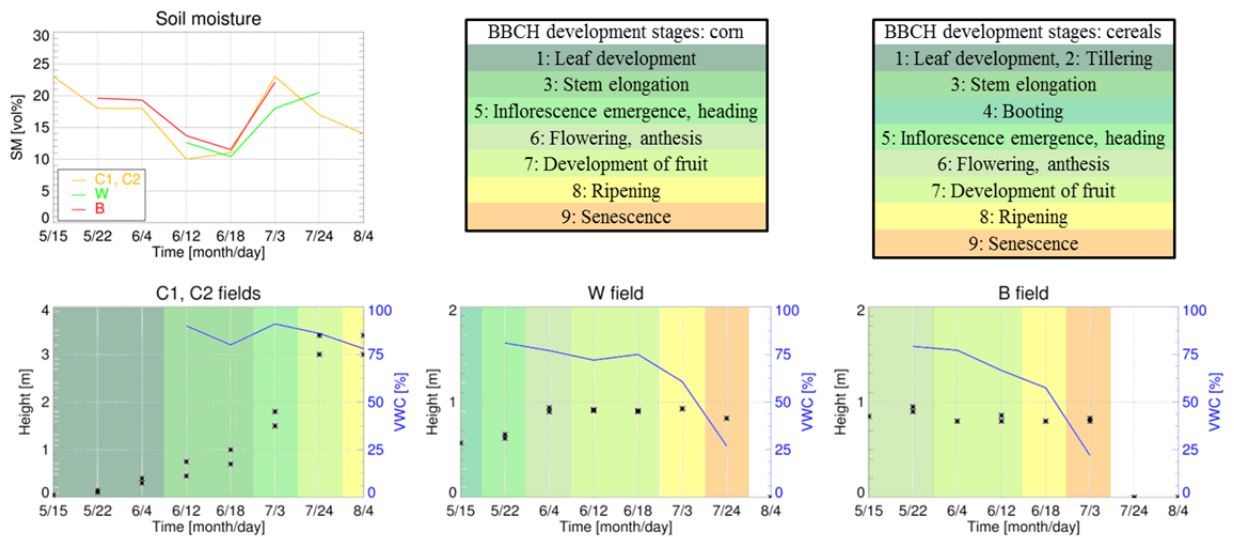
3.2.1 Test Site and Ground Measurements

The test site (located at 48.68 N, 12.88 E) is dominated by agricultural fields on a rather flat terrain with topography varying across the test site by less than 15 m. The land use of the patch under study, restricted to the crop types of interest, is shown in Fig. 1 on the left and a Pauli RGB image of the same area on the right. The latter reveals the differences between the crop types: the barley field appears in yellow indicating a mixture of volume and dihedral scattering; the wheat fields are very dark but still dominated by double bounce scattering; the corn fields show a mixture of surface and double bounce scattering and some differences are present within the fields, mainly due to row planting characteristics. A bigger row distance enables more dihedral scattering, like in the near range of field C1 and in the far range of field C2 (with row distances of 0.8 m). The other areas in the fields C1 and C2 with less dihedral scattering correspond to areas with smaller row distances between 0.7 and 0.75 m.

The intensive measurement fields chosen for validation are the corn fields indicated with C1 and C2, the wheat field W and the barley field B. On these fields, plant height was measured and the plant development stage was determined according to the BBCH scale (from *Biologische Bundesanstalt, Bundessortenamt und Chemische Industrie*) [27] for each of the campaign dates. Row orientation and row spacing were measured and pictures were taken for reference. After the



(a) Pictures of the intensive measurement fields.



(b) Soil moisture and plant parameters (minimum and maximum plant height, VWC, BBCH stage).

Fig. 2: Overview of the ground measurements on the intensive measurement fields on the acquisition dates.

plants reached a certain development stage, a small patch (0.25 m^2 for wheat and barley and 1 m^2 for corn) was harvested at two locations inside the fields on every campaign date to estimate the Vegetation Water Content (VWC) from the normalized weight difference of fresh and dried samples. Soil moisture was measured in vol% using a Frequency Domain Reflectometry (FDR) probe at the harvested points and on a more detailed grid consisting of 35 measurement locations distributed within the fields C1 and C2. On each location, 5 measurements were taken and averaged. A soil moisture value of 0 vol% corresponds to an oven-dry soil and 50 vol% to a water-saturated soil (for the type of soil in this area).

The pictures in Fig. 2(a) give an overview of the state of the plants on the campaign dates. The mean values of the measured soil moisture and vegetation parameters are shown in Fig. 2(b).

Soil moisture measurements for the W and the B field do not cover the whole campaign period. However, on coinciding dates, the soil moisture levels of all fields show a similar trend as C1 and C2. The soil moisture values start from a relatively high level of almost 25 vol% in May and decrease down to 10 vol% until June 12. They stay at this lower level of about 10-13 vol% until June 18 before they reach again 25 vol% on the next date, followed by a less pronounced decrease until the end of the campaign. Since the fields have not been irrigated, the soil moisture variations are due to precipitation documented by a meteorological station in the study area.

The plant development on the fields C1, C2, W and B is described in the following:

- For the corn fields, the campaign covers the beginning of the plant development until the ripening stage. The corn was planted with a row distance of 0.7-0.8 m and with 6 to 7 plants per meter. During the leaf development at the end of May, the plants start to develop and reach a height of approximately 0.4 m on June 4, and continue to grow up to a final height of 3.5 m until July 24. On this date, the fruit development is at its early milky stage. On the last date, the fruits are further advanced, reaching the ripening phase in the dough stage. The drying of the plants is not fully covered by the acquisitions; the VWC starts to decrease at the end of the campaign.
- The wheat plants are booting in May and the plant height is around 0.6 m. The spacing of the planted rows is 0.1 m with more than 100 plants per meter. The plants reach full height (around 0.8 m) on June 4, when the fruit development starts. After June 18, the wheat ripens and the VWC decreases from around 75% to 27% on July 24. On the last date, the wheat has been harvested and the stubbles are still present on the field.
- The barley plants have reached full height (around 0.9 m) and the first awns are visible already at the beginning of the campaign. The row spacing and the number of plants for the barley field are similar to the wheat field. From May 22 to June 4, the heads bend from a vertical to a horizontal position, which is also visible in the slight decrease in plant height. The fruit development reaches the early dough stage by the mid of June. Just before, the drying process starts which is reflected in the VWC measurements decreasing from around 75% (June 4) to 25% (July 3). On July 24, the plants have been harvested.

3.2.2 Multi-Baseline SAR Acquisitions

On each date of the campaign one MB data set was acquired consisting of K individual tracks. The relevant system and acquisition geometry parameters are summarized in Table I. The spatial resolution is 0.5 m in slant-range as well as in azimuth. The analyzed patch (see Fig. 1) is a subset of the acquired scene and the incidence angle θ ranges from 30° to 47° and from 30° to 37° in the area of the intensive measurement fields.

The spatial baseline configuration was chosen to fulfill the required high vertical resolution, i.e. of preferably less than one meter, demanding a large maximum baseline. The spatial baseline between the master and the k -th track leads to an incidence angle difference $\Delta\theta_k$ compared to the incidence angle of the master. The vertical wavenumber $\kappa_{z,k}$ depends on $\Delta\theta_k$ and the wavelength λ as $\kappa_{z,k} = (4\pi/\lambda) \cdot (\Delta\theta_k / \sin \theta)$ [28]. The vertical Rayleigh resolution ρ_z is inversely proportional

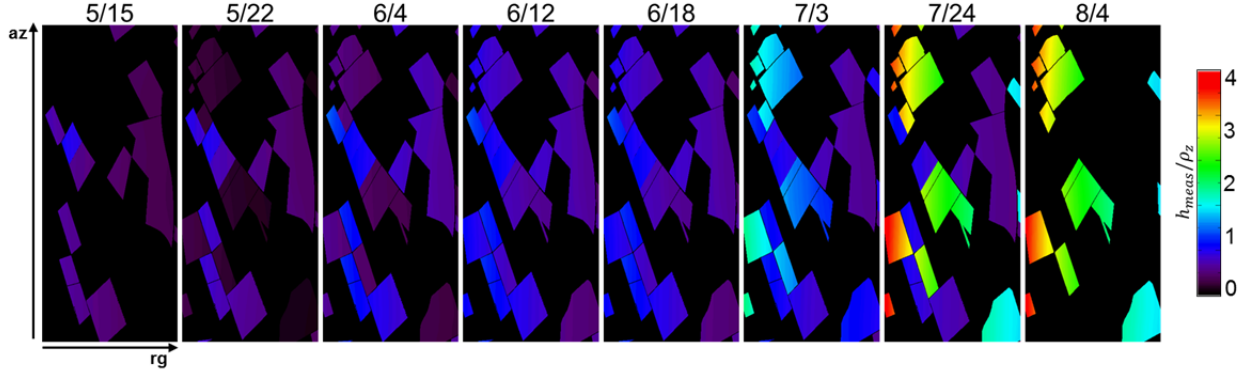


Fig. 3: Resolution units ρ_z per plant height h_{meas} for the fields in the patch under study on the acquisition dates.

TABLE I
SYSTEM AND ACQUISITION PARAMETERS OF THE EXPERIMENTAL DATA SET

Frequency	5.3 GHz (C-band)
System bandwidth W	384 MHz
Resolution in slant-range and azimuth	0.5m
Flight height	3110 m
Variation of incidence angle θ within the patch under study	$[30^\circ, 47^\circ]$
Variation of $\max_k \kappa_z^{(k)}$ within the patch under study	$[7.8 \text{ rad/m}, 3 \text{ rad/m}]$
Variation of ρ_z within the patch under study	$[0.8 \text{ m}, 2.1 \text{ m}]$
Number of tracks K :	
5/15	3
6/18	5
8/4	8
5/22, 6/4, 6/12, 7/3, 7/24	9

to the maximum baseline, i.e. the maximum $\kappa_{z,k}$ within the tracks, and given by [21]

$$\rho_z = \frac{2\pi}{\max_k \kappa_{z,k}}. \quad (1)$$

The maximum baseline of the tracks must be traded against the critical baseline which is defined as the baseline inducing a spectral shift between two tracks equal to the processed range bandwidth W [28]. Considering this constraint, $\max_k \kappa_{z,k} = 7.8 \text{ rad/m}$ was achieved on each date of the campaign resulting into a vertical Rayleigh resolution of 0.8 m. Due to the incidence angle dependency of $\kappa_{z,k}$ the vertical resolution decreases down to 2 m at the far range of the patch. The

pictures in Fig. 3 visualize the measured plant heights in Rayleigh resolution units. The height of the wheat and barley plants never exceeds 1 m, which is on the order or even below the Rayleigh resolution. Only the corn plants on the last three dates considerably exceed one Rayleigh resolution unit. However, the intensive measurement fields (see Fig. 1) were chosen in an area with a more favorable resolution.

The minimum baseline results from the desired non-ambiguous height range ΔH [21]

$$\min_k \kappa_{z,k} \leq \frac{2\pi}{\Delta H}. \quad (2)$$

In this experiment, $\min_k \kappa_{z,k} \approx 0.62$ rad/m at $\theta = 30^\circ$ results in $\Delta H \approx 10$ m, which is sufficient since the plants are not expected to become higher than 4 m.

The number of tracks varies from 3 to 9 for the different campaign dates due to imposed time constraints. The data were acquired around 10 a.m. within approximately 90 minutes. Following the constraints on the maximum and minimum baseline mentioned above, the remaining tracks were distributed in a non-uniform way. However, taking into account all possible combinations among the available tracks, a uniformly sampled κ_z space is obtained allowing a better conditioned tomographic SAR imaging.

3.3 Multi-Baseline Data Analysis

In this Section, the estimated vertical reflectivity profiles at the different polarizations and dates are analyzed qualitatively especially regarding the influence of temporal changes in soil and vegetation.

Prior to any tomographic processing, a careful phase calibration is mandatory to compensate for residual phase screens resulting from platform motion [29]. Since the phase distortion is proportional to the baseline error normalized to the wavelength, accurate phase calibration at higher frequencies becomes challenging. After a first order phase calibration a minimum entropy autofocus was applied to improve the radiometric accuracy [30].

The MB data vector $\mathbf{y}^i = [y_1^i, \dots, y_K^i]^T$ contains the K complex single look images at a given polarimetric channel $i \in \{\text{HH}, \text{HV}, \text{VV}\}$. In the case of distributed scatterers, statistical descriptors are necessary to characterize the scattering signature requiring spatial multi-looking. The MB data vector in a multi-look cell of N neighboring samples can be assumed to be a K -dimensional complex-valued zero mean Gaussian process. Hence, the scattering signature of distributed scatterers is fully described by an estimate $\hat{\mathbf{R}}^i$ of the $(K \times K)$ -dimensional MB covariance matrix \mathbf{R}^i

$$\hat{\mathbf{R}}^i = \frac{1}{N} \sum_{n=1}^N \mathbf{y}^i(n) \mathbf{y}^i(n)^H. \quad (3)$$

A quadratic multi-look cell of 7.5 m in slant-range and azimuth, corresponding to 225 independent looks, is used for retrieving the MB covariances defining the horizontal extent of the tomographic resolution cell.

The interferometric phase variation at a given elevation z is given by the steering vector $\mathbf{a}(z) = [1, e^{-j\kappa_{z,2}z}, \dots, e^{-j\kappa_{z,K}z}]^T$, with $\kappa_{z,1} = 0$ [24]. Spectral estimation methods can be used to estimate the vertical reflectivity distribution from the MB covariance matrix and $\mathbf{a}(z)$. Here, the Capon adaptive beamformer is used since it provides good side lobe suppression and enhanced resolution when compared to Fourier beamforming [22,24].

Fig. 4 shows the Capon profiles along the transect indicated by the blue line in Fig. 1 on five selected dates. The transect is 450 m long, crosses two corn fields, a wheat and a barley field and ends in another corn field. The topographic phase, known from a LiDAR derived digital terrain model, is compensated so that the ground is imaged at a height of 0 m indicated by the white line. The black line corresponds to the center of mass (CoM) of the vertical profiles. At least for a medium vertical resolution, like the one at hand, the center of mass is equivalent to the interferometric phase center [16]. For each resolution cell, the center of mass of the vertical reflectivity profile is defined by A quadratic multi-look cell of 7.5 m in slant-range and azimuth, corresponding to 225 independent looks, is used for retrieving the MB covariances defining the horizontal extent of the tomographic resolution cell.

The interferometric phase variation at a given elevation z is given by the steering vector $\mathbf{a}(z) = [1, e^{-j\kappa_{z,2}z}, \dots, e^{-j\kappa_{z,K}z}]^T$, with $\kappa_{z,1} = 0$ [24]. Spectral estimation methods can be used to estimate the vertical reflectivity distribution from the MB covariance matrix and $\mathbf{a}(z)$. Here, the Capon adaptive beamformer is used since it provides good side lobe suppression and enhanced resolution when compared to Fourier beamforming [22,24].

Fig. 4 shows the Capon profiles along the transect indicated by the blue line in Fig. 1 on five selected dates. The transect is 450 m long, crosses two corn fields, a wheat and a barley field and ends in another corn field. The topographic phase, known from a LiDAR derived digital terrain model, is compensated so that the ground is imaged at a height of 0 m indicated by the white line. The black line corresponds to the center of mass (CoM) of the vertical profiles. At least for the given vertical resolution, the center of mass is equivalent to the interferometric phase center [23]. For each resolution cell, the center of mass of the vertical reflectivity profile is defined by

$$COM^i = \frac{\int_{0-\delta}^{z_{top}+\delta} P^i(z) z dz}{\int_{0-\delta}^{z_{top}+\delta} P^i(z) dz}, \quad (4)$$

where $P^i(z)$ is the vertical reflectivity at a given polarization $i \in \{HH, HV, VV\}$. In order to ensure that the vertical reflectivity profile is fully within the limits of the integral, they are chosen conservatively by extending the expected height range of the reflectivity profile in both directions. Since the ground phase has been compensated, the lower limit is just below the ground at $0 \text{ m} - \delta$ and the upper limit slightly above the maximum expected height at $\max(z_{top} + \delta, 0.6)$, where $\delta = 0.2 \text{ m}$ corresponds to approximately 25% of the vertical resolution. The center of mass in each resolution cell is calculated from the vertical reflectivity profile estimated from the multi-looked covariances.

In general, the vertical reflectivity profiles in Fig. 4 show an effective suppression of side lobes and ambiguities suggesting that the MB data are well calibrated. In the following, the vertical

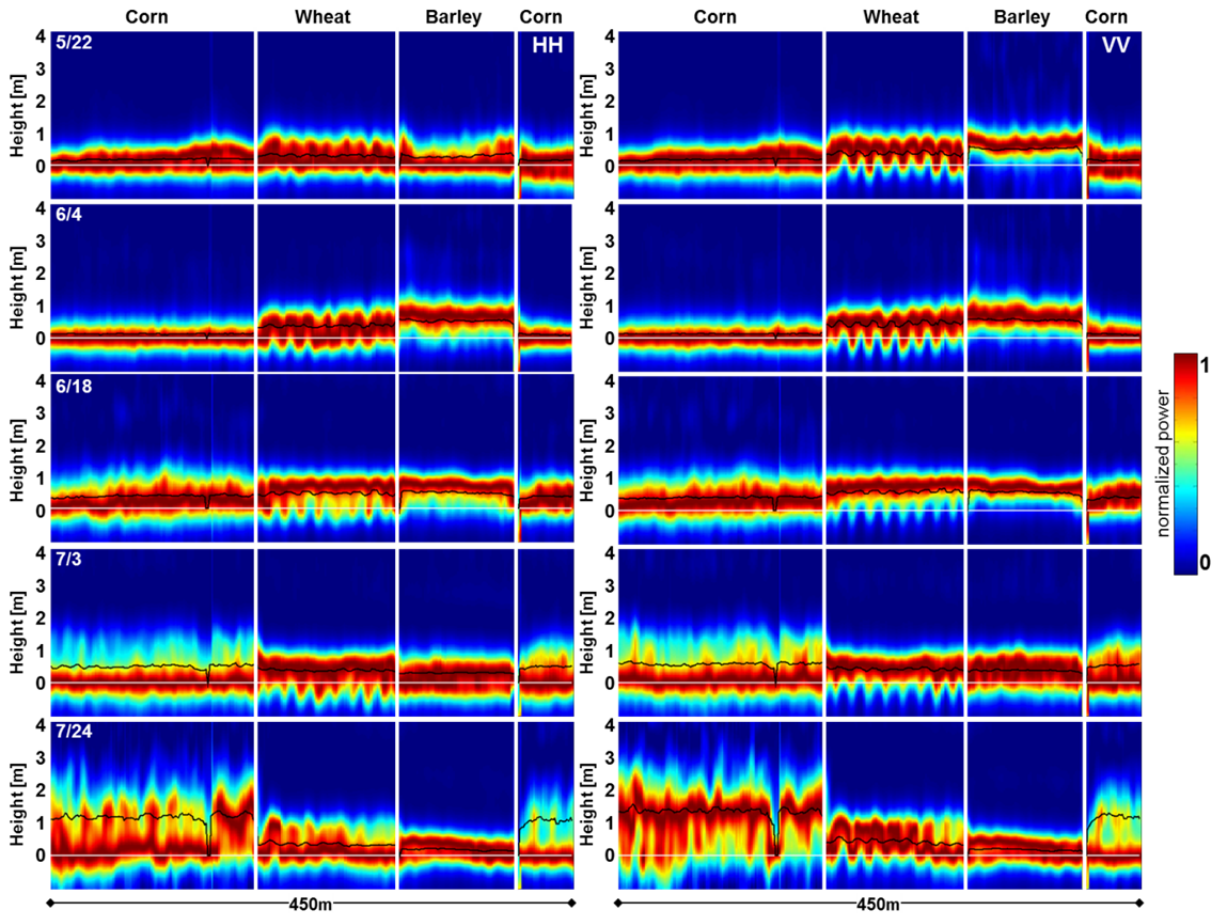


Fig. 4: Vertical reflectivity profiles along the line outlined in Fig. 1 (passing from corn through barley and wheat and ending again in corn) estimated using the Capon beamformer in HH (left) and VV (right) for selected acquisition dates. The reconstructed profiles are normalized to the maximum power at each inversion point. The white line corresponds to the ground imaged at a height of 0 m and the black line corresponds to the center of mass of the vertical reflectivity profiles.

profiles in HH and VV polarization are discussed since they show the maximum differences. The HV profiles represent an intermediate case between HH and VV and their discussion is omitted.

The transitions between the fields can be clearly seen, as the crops have different scattering characteristics and their scattering behavior changes with the development stage. In the following, these changes are discussed in detail for each crop type separately.

- The height of the corn on the first two dates is lower than 50 cm and only a ground scattering response is seen in the reflectivity profiles. On June 4, the ground contribution is stronger compared to May 22. On June 18, the plant height reaches almost 1 m and the profiles become more extended in height. However, ground and vegetation cannot be distinguished from each other. Despite the fact that the vegetation is growing up to 1.9 m, the vertical reflectivity profiles on July 3 still show a dominant scattering at the ground and do not reveal the full plant extent. Even though the reflectivity profiles in VV are slightly more sensitive to the vegetation, the difference between the polarizations is rather small. Finally, on July 24, the reflectivity profiles become more diverse due to a change of plant

morphology (fruit and leaves) and an increase of plant height up to 3.5 m. Certainly, the improved plant height-to-vertical resolution ratio allows to appreciate better these differences. While the profile in HH shows still dominant scattering at the ground, the scattering center in VV is primarily located in the vegetation layer.

- On the first two dates, the vertical reflectivity profiles of the wheat show a stronger scattering component at the ground in HH than in VV, where the maximum of the reflectivity profile is located towards the top of the vegetation. In both polarizations, the tractor trails are clearly visible with a distance of approximately 22 m, characterized by a relevant ground contribution. On the second date, a slight increase of the vegetation scattering appears in HH, probably because the wheat plants are in the flowering stage with more evolved heads. Starting from June 18, the trails appear less pronounced than in the earlier dates. At the same time, the maximum of the vertical reflectivity profile in HH moves towards the vegetation top. This might be due to the fact that towards the end of the fruit development stage the vertically oriented heads of the plants start to bend. Afterwards, the VWC starts to decrease due to the drying of the plants. Hence, starting on July 3 and, more obvious on July 24, the maximum of the vertical reflectivity profiles moves towards the ground in both polarizations. At the same time, the profiles are more extended in height, indicating that the lower VWC causes the vegetation volume to be more transparent allowing scattering from the lower parts of the vegetation volume.
- In the barley, the reflectivity profiles on the first dates are very different at the two polarizations. In HH the ground is very dominant while in VV the reflectivity profile has a very distinct maximum at the top of the vegetation layer. Two weeks later, the profiles at the two polarizations become much more similar. With the start of the ripening stage, the heads of the barley plants bend from vertical to horizontal. Since the grains are still milky, they become the main scattering contribution in HH. The scattering center in VV is still at the top of the vegetation. On June 18, the drying of the vegetation extends the profiles in height. On the last date, the vegetation has been harvested and the afterwards planted beans just emerged.

To summarize, main events in the phenological cycle can be observed at the vertical reflectivity profiles for all three crop types. The 3-D scattering signature reflects both the geometric changes, like the bending of the heads in the cereals, and the dielectric changes, like the drying of the plants. From these observations, the question rises, whether it is possible to monitor the changes, i.e. transitions between phenological stages, by means of a single parameter retrieved from the vertical reflectivity profiles, like the center of mass. Fig. 5 shows the variation of its mean value at the different polarizations over the corn (fields C1 and C2), wheat (field W) and barley (field B) fields in relation to the measured plant height.

- In the corn, on the first dates until July 3, the variation of the center of mass reflects the observations made for the profiles above. It does not exceed 0.5 m despite the increasing plant height, indicating that the dominant scattering component is located on the ground. On the last two dates, the center of mass in all polarizations is located in the vegetation, but

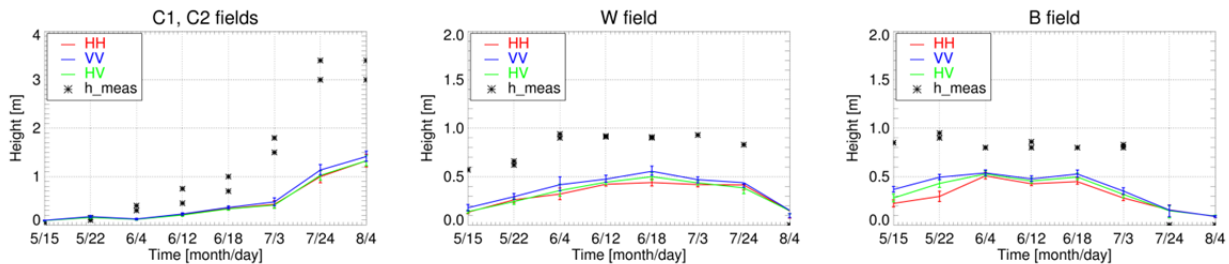


Fig. 5: Mean value of the center of mass of the vertical reflectivity over the intensive measurement fields compared to the minimum and maximum measured plant height on the different acquisition dates. The error bars correspond to the 60% confidence interval.

does not exceed 50% of the measured plant height. Such a deep penetration is usually not expected for the late development stage of the corn plants at C-band. At this point, it is not possible to conclude whether this is due to a strong ground contribution or a weaker (top) volume component. In contrast to the profiles in Fig. 4, on July 24 the center of mass is not significantly changing across the polarizations.

- In the cereals, the information provided by the center of mass matches the observations at the profiles even though the observed variations are not as strong. For instance, the center of mass in the wheat is slightly higher at VV than at HH until June 18. Afterwards, the polarizations are more similar and the ground becomes more dominant with the start of the drying process. In the barley, the bending of the heads between May 22 and June 4 leads to a higher center of mass at HH, making the center of mass more similar at the different polarizations. After June 18, the center of mass lowers due to the drying of the plants.

The variations due to phenological developments are reflected by the center of mass. However, a variation in the center of mass itself does not enable to distinguish whether it is caused by a change in the ground or in the volume scattering.

Additionally, differences in the profiles, or the center of mass, at different polarizations could either be due to a polarization dependency of the volume scattering or caused by the strongly polarized ground scattering component [31,32]. In order to address this, the ground and volume component need to be separated from each other.

3.4 Ground and Volume Separation

In the following, a scattering scenario consisting of two layers is assumed where the ground layer is located at height z_G under a volume layer. In general, this separation problem formulated in a maximum likelihood sense does not admit a unique solution [33]. Uniqueness can be achieved by regularization imposed in form of assumptions or electromagnetic models. However, model-based approaches might be limited since they can lead to a misinterpretation of scattering components [34].

As shown in the following using MB data, the knowledge of the ground topography z_G is a sufficient condition to overcome the ill-posedness. In agricultural applications, the ground topography could be for instance provided by an interferometric acquisition performed before the

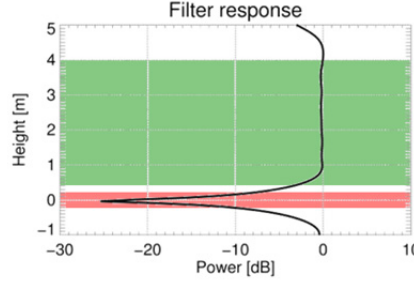


Fig. 6: Response $g(z) = \|\mathbf{H}\mathbf{a}(z)\|_2^2/K$ with $z \in [-1 \text{ m}, 5 \text{ m}]$ for $z_G = 0 \text{ m}$ and $z_{top} = 4 \text{ m}$ (red: stop band, green: pass band).

start of the growing season.

3.4.1 Data Model

Following a two-layer model, the MB data vector $\mathbf{y}^i(n)$ at a given polarization $i \in \{\text{HH}, \text{HV}, \text{VV}\}$ for each sample n in a multi-look cell of N samples can be modeled as the sum of a Dirac-delta shaped ground layer located at height z_G and a volume contribution located above

$$\mathbf{y}^i(n) = \tau_G^i(n)\mathbf{a}_G + \mathbf{y}_V^i(n), \quad n = 1, \dots, N, \quad (5)$$

with $\mathbf{a}_G := \mathbf{a}(z_G)$ and $\tau_G^i(n)$, the complex reflectivity of the ground component, described by a zero-mean complex Gaussian process. The MB data covariance matrix at polarization i can be written as

$$\mathbf{R}^i = p_G^i \mathbf{a}_G \mathbf{a}_G^H + p_V^i \mathbf{\Gamma}_V^i, \quad (6)$$

with ground power $p_G^i = E\{|\tau_G^i|^2\}$ and volume power p_V^i . Particularly with respect to the physical interpretation of ground power changes, it is worth to remark that p_G^i contains surface and dihedral scattering powers since the phase center of both interactions is located at the ground. The MB volume coherence matrix $\mathbf{\Gamma}_V^i$ defines the vertical structure of the volume component at polarization i . $\mathbf{\Gamma}_V^i$ can be estimated from the volume only MB data vector

$$\hat{\mathbf{\Gamma}}_{Vlm}^i = \frac{1}{N} \sum_{n=1}^N \frac{\hat{y}_{Vl}^i(n) \hat{y}_{Vm}^i(n)^*}{\|\hat{y}_{Vl}^i(n)\|_2 \|\hat{y}_{Vm}^i(n)\|_2}, \quad 1 \leq l, m \leq K. \quad (7)$$

3.4.2 Estimation of Volume Signal

The separation of the two layers is performed by a filter designed to cancel as much as possible the contributions in the stop band positioned around the ground and to leave unaltered the contributions of the volume [24,25]. In this case, a filter in the form of a matrix is chosen as the MB data vector is too short to allow a good filtering performance with a classical finite impulse response filter [35].

An advantageous feature of this approach is the preservation of the coherent structure of the filtered data. Besides this, any other optimal filtering approach based on second order statistics of the volume-only MB data vector cannot be applied because they are unknown.

The volume data vector $\mathbf{y}_V^i(n)$ at each polarization $i \in \{\text{HH}, \text{HV}, \text{VV}\}$ for a sample n is then estimated by applying the filter \mathbf{H} to $\mathbf{y}^i(n)$

$$\mathbf{y}_V^i(n) = \mathbf{H}\mathbf{y}^i(n), \quad n = 1, \dots, N. \quad (8)$$

The stop band, B_{stop} , is defined symmetrically around the ground height z_G and the pass band, B_{pass} , contains the vegetation volume above. The stop and the pass band are sampled at m_s and m_p heights respectively. The steering vectors evaluated at the particular heights are stored in the columns of the matrices $\mathbf{A}_{stop} \in \mathbb{C}^{K \times m_s}$ and $\mathbf{A}_{pass} \in \mathbb{C}^{K \times m_p}$ representing signal components. The constraints demanding a maximum possible cancellation of the signal in the stop band and its preservation in the pass band lead to the definition of an input steering matrix $\mathbf{A}_{in} = [\mathbf{A}_{stop} \quad \mathbf{A}_{pass}]$ and an output steering matrix $\mathbf{A}_{out} = [\mathbf{0}_{K \times m_s} \quad \mathbf{A}_{pass}]$. Thus, the filter \mathbf{H} is given by the following minimization problem

$$\mathbf{H} = \underset{\mathbf{H}}{\operatorname{argmin}} \|\mathbf{H}\mathbf{A}_{in} - \mathbf{A}_{out}\|_F^2, \quad (9)$$

where $\|\cdot\|_F$ denotes the Frobenius norm. Adding the real regularization factor η to avoid possible ill-conditioning and to increase robustness to noise and phase calibration residuals, the solution of (9) is obtained in closed form as

$$\mathbf{H} = \mathbf{A}_{out}\mathbf{A}_{in}^H(\mathbf{A}_{in}\mathbf{A}_{in}^H + \eta\mathbf{I})^{-1}. \quad (10)$$

The filtering performance depends on the choice of stop and pass band which are fixed as

$$\begin{aligned} B_{stop} &:= \{z, z \in [z_G - 0.2 \text{ m}, z_G + 0.2 \text{ m}]\} \\ B_{pass} &:= \{z, z \in [z_G + 0.4 \text{ m}, z_G + z_{top}]\}. \end{aligned} \quad (11)$$

The width of the stop band is 0.4 m corresponding to approximately 50% of the vertical resolution. The pass band starts 0.2 m above the stop band until $z_{top} \leq 4\text{m}$, which is slightly higher than the expected maximum plant height. The response $g(z) = \|\mathbf{H}\mathbf{a}(z)\|_2^2/K$ is plotted in Fig. 6 in dB for $z \in [-1 \text{ m}, 5 \text{ m}]$ with a filter designed for $z_G = 0 \text{ m}$ and $z_{top} = 4 \text{ m}$. The transient of $g(z)$ between ground cancellation and volume preservation depends on the vertical resolution and the number of filter coefficients. For the given resolution, the width of B_{stop} and the separation between the bands as defined in (11) seem to be sufficient. The maximum attenuation in the stop band is 26 dB, while the signal is preserved in the pass band. By design, the filter is not able to resolve a volume component that is lower than 0.4 m. Besides, the separation of the components can be critical for plant heights below or in the order of the vertical resolution since the two components are then superimposed in one resolution cell or when z_G varies across the N estimation

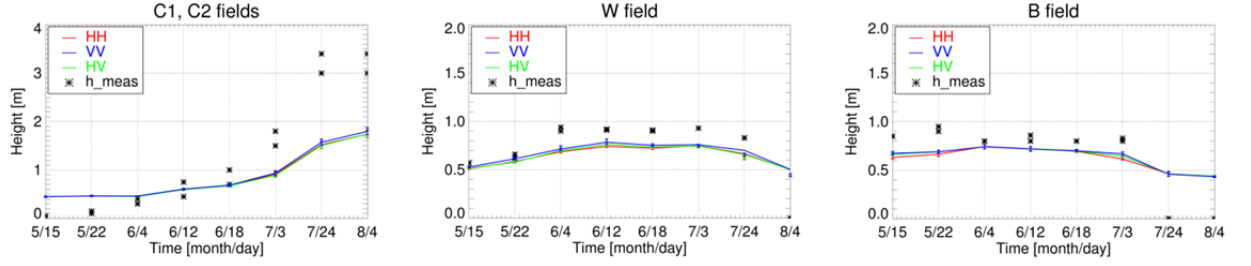


Fig. 7: Mean value of the center of mass of the volume vertical reflectivity over the intensive measurement fields compared to the maximum and minimum measured plant height on the different acquisition dates. The error bars correspond to the 60% confidence interval.

samples. Additionally, in the design of the filter, no constraints are set outside the bands since no scattering is assumed underground or above the vegetation. However, no positive gain, associated with an increase of the noise level in these areas, is observed in the response.

3.4.3 Power Estimation

Once the volume signal and the MB volume coherence matrix Γ_V^i are estimated for each polarization $i \in \{HH, HV, VV\}$, estimates for p_G^i and p_V^i are calculated by covariance matching [26], i.e. by minimizing the following cost function according to equation (6)

$$Q(p_G^i, p_V^i) = \|\hat{\mathbf{R}}^i - (p_G^i \mathbf{a}_G \mathbf{a}_G^H + p_V^i \hat{\Gamma}_V^i)\|_F^2. \quad (12)$$

With a sufficient number of looks N , the (unweighted) least squares solution of (12) is:

$$\begin{bmatrix} p_G^i \\ p_V^i \end{bmatrix} = (\mathbf{\Pi}^H \mathbf{\Pi})^{-1} \mathbf{\Pi}^H \text{vec}(\hat{\mathbf{R}}^i), \quad (13)$$

where $\mathbf{\Pi} = [\text{vec}(\mathbf{a}_G \mathbf{a}_G^H) \quad \text{vec}(\hat{\Gamma}_V^i)]$ and $\text{vec}(\cdot)$ is the vectorization operator that transforms a matrix into a column vector.

If the plant height is on the order of the vertical resolution the estimation of the powers becomes less accurate. Simulations showed that the root-mean-square error for p_V is always below 15% and not significantly worse than for cases with a better height-to-vertical resolution ratio. In contrast, p_G is overestimated by 30% for volume-dominated scenarios if the ground and volume components are contained in one vertical resolution cell compared to 10% for two vertical resolution cells available. [25]

3.5 Results

3.5.1 Volume Only Multi-Baseline Data Analysis

The volume only vertical reflectivity profile and its center of mass, referred to as volume center of mass in the following, can be retrieved from the estimated volume component. Fig. 7 relates the mean volume centers of mass for the corn, wheat and barley fields to the measured plant heights.

- Until June 18, the volume center of mass in the corn is located closely to the top of the plants. Afterwards, the volume center of mass does not increase at the same rate as the plants grow. In the last two dates, it lies more than 1 m below the measured height indicating that the main scattering contribution of the volume comes from a lower part of the plants than on earlier dates.
- Until harvest, the volume center of mass in the cereals stays close to the top of the plants and does not show further significant variation over time. This can be also due to the limited vertical resolution since the plant height never exceeds 0.9 m and hence is always on the order of the vertical resolution.

For all three crop types, no significant differences between polarizations are observed. For low plant heights, as in the early dates for the corn and for the cereals, this might be due to the limited vertical resolution. Nevertheless, it also suggests that the polarization dependency before separation (see Fig. 4 and 5) is due to the ground component and that the volume component is widely polarization independent, particularly for the higher vegetation in the corn on the later dates. Even though the volume center of mass at the different polarizations can be interpreted as an indicator for the polarization dependency of the volume component, it might not fully describe the vertical structure of the vegetation. Therefore, the absence of differences between the location of the volume center of mass at the different polarizations does not necessarily imply the absence of anisotropic propagation effects.

3.5.2 Ground and Volume Scattering Powers

The temporal analysis of the estimated ground and volume scattering powers provides further insights on their relation to the changes in soil and plant parameters. Fig. 8 shows the polarimetric, spatial and temporal variation of the estimated ground-to-volume power ratios over the patch under study for five different dates. The ground-to-volume ratio in VV is always lower than in HH (while the values in HV are in between). This is due to the weaker ground power in VV originating from the weaker dihedral contribution in this channel for the same volume power [9]. Variations can be observed not only between different crop types and development stages but also within individual fields. For instance, the spatial pattern in the C1 and C2 fields, observed particularly on July 3 and July 24, is caused by the varying planting row density and orientation. Also here, the tractor trails in the wheat fields appear as a stripe-like pattern. Further, spatial heterogeneity in soil constitution or in dielectric properties of the soil and/or plants can impact the ground-to-volume ratio.

In the following, the temporal variation of the ground and volume scattering power and their ratio is quantitatively analyzed against the available ground measurements. Fig. 9 shows the mean values obtained by averaging over the intensive measurement fields. The ground and volume powers are normalized with respect to the values in HH on May 15.

- For the corn, the initial plant growth leads to an increase in the volume power p_V and hence a decreasing ground-to-volume ratio until June 18. Even though the ground-to-volume ratio

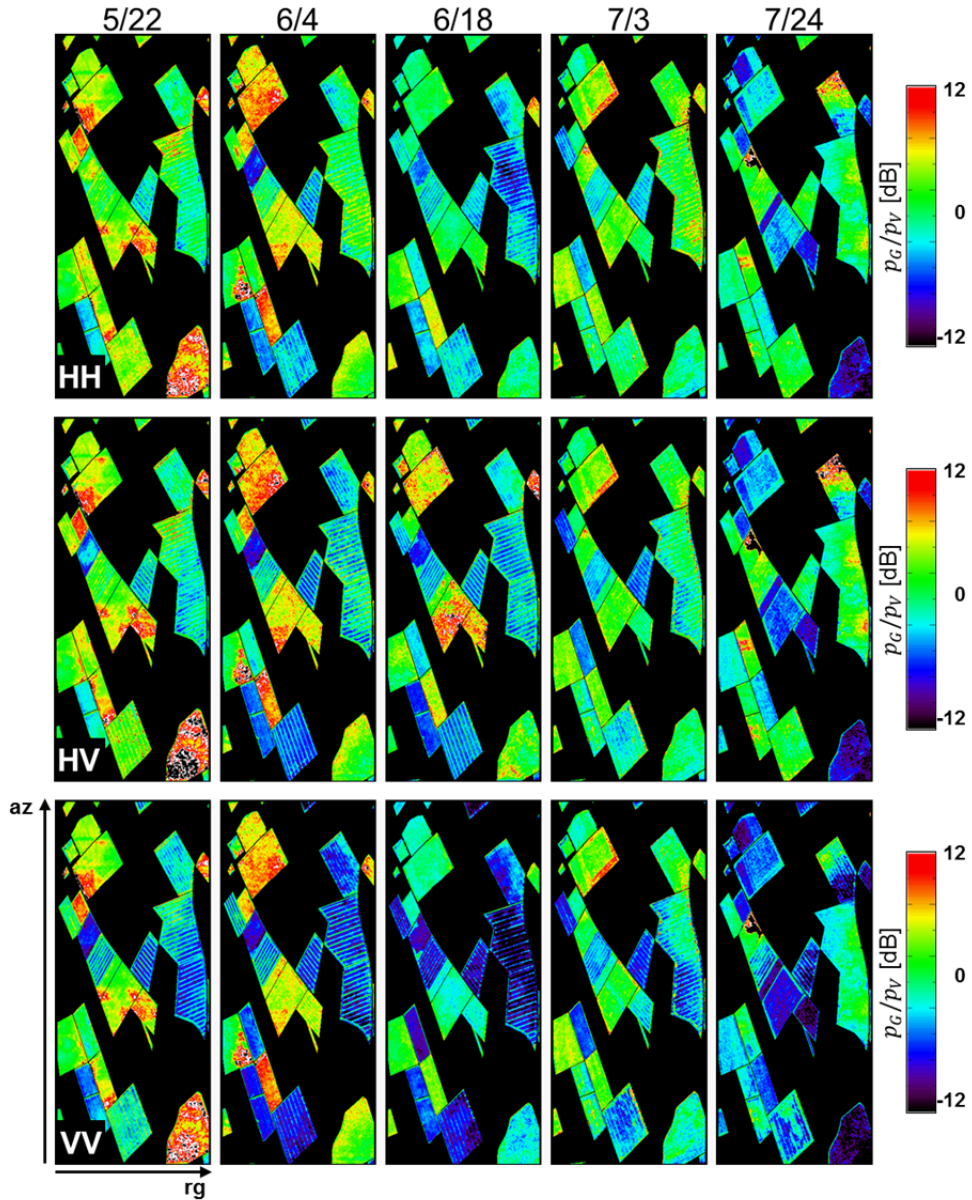
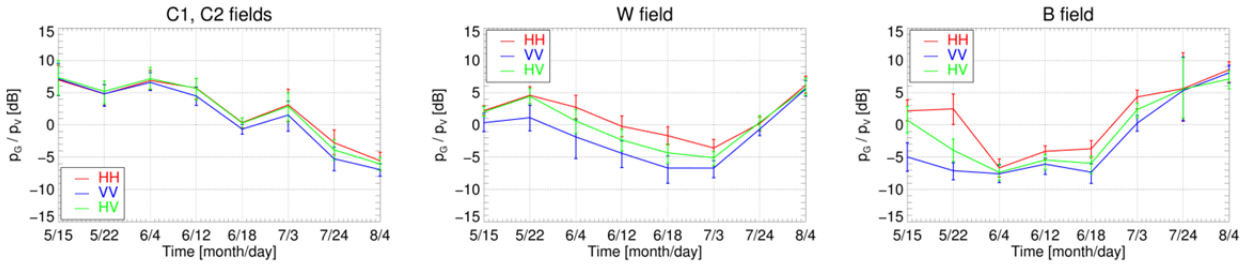
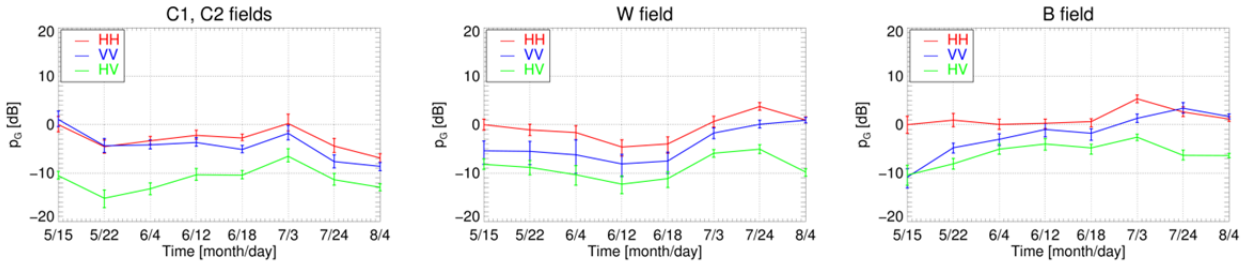


Fig. 8: Retrieved ground-to-volume power ratio on the different dates in HH (top), HV (middle) and VV (bottom).

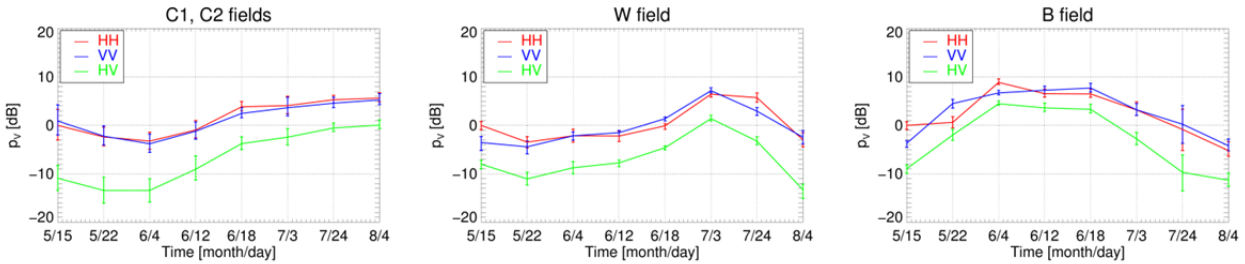
might be overestimated due to a possible overestimation of the ground power p_G for the lower plant heights, the decreasing trend can be trusted since it arises from the change of p_V . The increase of the ground-to-volume ratio from June 18 to July 3 is related to the change from dry to wet soil (11 vol% to 23 vol%) causing p_G to increase by 3 dB while p_V stays constant. Afterwards, the ground-to-volume ratio decreases again due to a decrease in p_G , while p_V stays constant even though the plant growth continues until maximum height in the last two dates. The drop in soil moisture (from 23 vol% to 17 vol%) after July 3 is too small to cause the observed decrease of 5 dB in p_G . Field experiments have shown that the water content is evenly distributed in the corn plants until the start of the fruit development, while afterwards the water is concentrated in the lower third of the plant [4,36,37]. For the corn



(a) Ground-to-volume power ratio estimates



(b) Ground power estimates



(c) Volume power estimates

Fig. 9: Mean value of the estimated ground-to-volume power ratio (a), the ground power (b) and the volume power (c) over the intensive measurement fields on the different acquisition dates. The error bars correspond to the 60% confidence interval. The ground and volume powers are normalized by the power in the HH channel on May 15.

fields under study, the fruit development starts after July 3. Due to the lower VWC in the upper two thirds of the plant, those plant components become electromagnetically more transparent leading to a constant volume power despite the ongoing plant growth. Furthermore, the change in VWC distribution increases the density of VWC in the lower third of the plant resulting in a weaker contribution from the ground height. This also explains the small extent of the vertical reflectivity profiles and the low center of mass compared to the plant height on the later dates. In this case, the effect of plant growth on the estimated tomographic parameters is concealed by the dielectric change, i.e. the redistribution of water within the plant, which has a bigger impact.

- The ground-to-volume power ratio for the wheat is always higher in HH than in VV due to the higher p_G in HH. The ongoing growth of the wheat leads to a decrease in all polarizations until June 12. From June 18, the vegetation water content decreases from 75% to 60% and finally down to 27% before the plants are harvested on the last date. The drying of the plants causes p_G to increase while the variation of p_V is divided in two phases: it

increases until July 3 and decreases afterwards. A possible explanation for this might be that the drying process initially enables a deeper penetration of the electromagnetic wave into the vegetation volume leading to an increasing p_V . After a certain point, further drying causes the decrease of p_V , which, in combination with the increasing p_G , leads to an increase of the ground-to-volume ratio. The loss of water content in the vertical stalks at this stage makes the bended heads to be the dominant scatterers in the volume. Therefore, the decrease of p_V is stronger in VV than in HH.

- Also in the barley, the variation of the ground-to-volume power ratio matches the changes documented by the ground measurements. The mentioned bending of the heads, between May 22 and June 4, is detected in the powers as well. In HH, p_V increases by more than 8 dB between the two dates, changing from a ground dominant to a volume dominant scattering scenario. In VV instead, p_G increases slightly and the ground-to-volume ratios become very similar in all polarizations. Finally, the drying process is spread over more acquisition dates than in the wheat. It can be observed by a steadily increasing ground-to-volume ratio, although the significant rise is after June 18. The increase in soil moisture from 11 vol% to 23 vol% after June 18 certainly contributes to this as well.

3.5.3 Significance of Anisotropic Propagation Effects

In the presence of anisotropic propagation effects, the vertical reflectivity function of the vegetation volume becomes polarization dependent while the volume only vertical reflectivity function of a random volume is, besides a scaling factor, the same across the polarimetric channels. Both the very small variation of the volume center of mass and marginal difference between the co-polar volume powers indicate that at C-band anisotropic propagation effects might not play a significant role for the different crop types considered. To further investigate this, the differences between a random volume hypothesis and the generalized (oriented volume) case are assessed in this Section based on the ground filtered MB data.

As proposed by [38] for the single-baseline case, a test for the validity of the random volume hypothesis can be realized by investigating the linearity of the polarimetric interferometric coherences. Also for MB data, one way to evaluate the presence of anisotropic propagation effects is to use a statistical test for the random volume hypothesis [39]. However, the selection of an accurate threshold for the acceptance of the hypothesis is based on the estimation of the independent number of looks from the ground filtered MB data. This is problematic preventing to assess the reliability of the results on this basis.

Another way is to directly compare the ground and volume scattering powers predicted by the random volume model to the ones obtained from the data. The fully-polarimetric MB data vector is formed by stacking the single-polarimetric MB data vectors \mathbf{y}^i , $i \in \{\text{HH}, \text{HV}, \text{VV}\}$, on top of each other. By applying the filtering approach to the fully-polarimetric MB data vector, the polarimetric MB volume covariance matrix $\widehat{\mathbf{W}}_V \in \mathbb{C}^{3K \times 3K}$ is estimated. In the random volume case, the volume structure matrix is polarization independent. Thus, the random volume covariance matrix, \mathbf{W}_V^{RV} , can be written as the Kronecker product of the polarimetric volume covariance matrix \mathbf{C}_V and the volume interferometric coherence matrix Γ_V^{RV} [40]

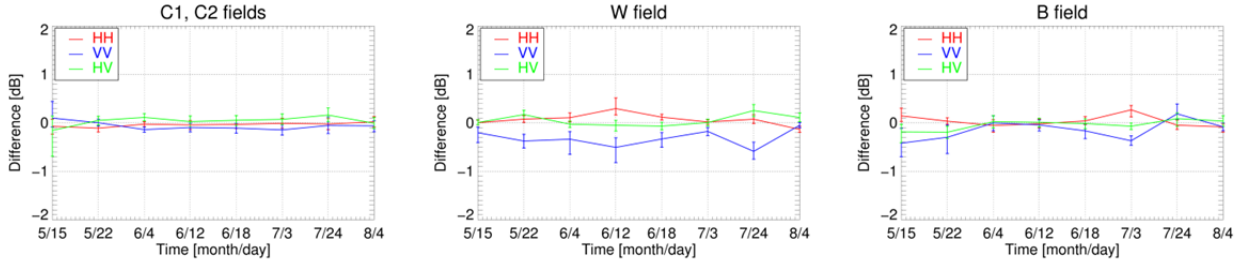


Fig. 10: Mean value of the difference between the retrieved ground-to-volume power ratio under the random volume hypothesis and the oriented one over the intensive measurement fields on the different acquisition dates. The error bars correspond to the 60% confidence interval.

$$\mathbf{W}_V^{RV} = \mathbf{C}_V \otimes \Gamma_V^{RV}. \quad (14)$$

Fitting this model to the estimated MB volume covariance matrix $\widehat{\mathbf{W}}_V$ yields the estimate $\widehat{\mathbf{W}}_V^{RV}$ of \mathbf{W}_V^{RV} .

Afterwards, the polarimetric signatures of ground and volume scattering components, \mathbf{C}_G and \mathbf{C}_V , are estimated analogously to (12) and (13) by covariance matching using the fully-polarimetric MB data covariance matrix $\widehat{\mathbf{W}}$ [25]

$$Q(\mathbf{C}_G, \mathbf{C}_V) = \|\widehat{\mathbf{W}} - (\mathbf{C}_G \otimes \mathbf{a}_G \mathbf{a}_G^H + \mathbf{C}_V \otimes \widehat{\Gamma}_V^{RV})\|_F^2. \quad (15)$$

Fig. 10 shows the difference between the estimated ground-to-volume power ratio under the random volume hypothesis and the oriented one for the intensive measurement fields for corn, wheat and barley.

- For the corn fields, the differences are negligible: the vegetation volume in the corn seems to be well represented by a random volume.
- Bigger deviations are observed in the cereal cases in the time between flowering and fruit development and just before harvest. In these cases, the ground-to-volume ratio under the random volume hypothesis is lower in VV and higher in HH compared to the general one. However, the deviations are smaller than 1 dB which is on the order of the accuracy of the method [25] and the SAR data itself. Therefore, the temporal variation retrieved under the random volume hypothesis leads to the same conclusions as the general one. This could also be attributed to the low plant height when compared to the vertical resolution.

3.6 Discussion and Conclusions

In this paper, airborne SAR Tomography at C-band was applied for the first time over agricultural crops. The polarimetric 3-D scattering of agricultural crops was investigated using MB SAR acquisitions on different dates across the phenological cycle. Tomographic processing techniques were employed to retrieve the vertical reflectivity profiles and their center of mass.

A filtering approach was applied to separate ground and volume scattering components based on the knowledge of the ground height z_G which is a sufficient condition for an unambiguous

separation. The separation yields the MB volume only coherences and allows the estimation of the ground and volume powers. The filtering performance is essentially limited by the vertical (tomographic) resolution and by the topographic variation within the horizontal resolution cell. Indeed, a vertical resolution in the order of the plant height results into a worsening of the estimation performance of the ground power. Nevertheless, the filter is robust to errors in the knowledge of the ground topography and residual phase miscalibration. In particular, the matrix filter can be used with a low number of looks, and the filtering performance is not impaired sensitively by a low number of baselines. [25]

Temporal changes of the estimated 3-D reflectivity and the separated ground and volume components were analyzed and interpreted using ground measured soil moisture and plant parameters. However, no measurements of the temporal variation of surface roughness were available. Being aware of the critical impact of surface roughness on the ground scattering, there was no indication of its effect in the data.

Summarizing, following changes at or in the volume layer can be detected by the individual techniques in the time span covered by the experiment:

- For the corn, the initial growth can be detected by using the profiles, the center of mass and the separated ground and volume powers. The redistribution of water content inside the plants due to the fruit development leads to a higher water density in the lower third of the plants [4,36,37]. This effect can be observed in the vertical profiles but also in the center of mass that moves towards the lower part of the vegetation. The growth of the corn in these dates is not detectable since the water redistribution within the plants increases the electromagnetic transparency of the upper part of the plants. Even though the temporal changes of the profiles and the center of mass can be explained by this effect, only the separated ground and volume powers enable to resolve its impact on the scattering characteristics. The ground power is finally affected by soil moisture variations.
- In the cereals, the dryout of the plants is reflected in the temporal variation of the vertical profiles, the center of mass and the ground-to-volume power ratio. Furthermore, the analysis of different polarizations indicates which plant components are changing geometrically or dielectrically. For instance, the bending of the heads in the barley can be observed by big polarimetric differences in all the tomographic observables. Further, the loss of VWC in the stalks of the wheat causes a faster decrease of the volume power in VV than in HH. Due to the low plant height of the cereals compared to the vertical resolution, the ground and volume separation is more critical and particularly the ground power might be overestimated in volume dominated scenarios which has to be considered when interpreting the results.

Even though the variation of the center of mass reflects the soil and plant dynamics over time, it is important to mention that it cannot resolve whether a change occurs on the ground or in the volume component. The complete understanding of the resulting scattering characteristics is strongly driven by the analysis of the powers enabling to draw conclusions on the behavior of the center of mass a posteriori.

In general, it can be concluded that geometric changes are only significant if the involved plant components have sufficient water content, as for instance the heads in the barley with the milky grains.

Further, the presence of anisotropic effects in the vegetation volume has been addressed by estimating the powers from the MB volume coherences fitted to a random volume model. In the corn, no differences compared to the results of the general, oriented volume hypothesis have been detected. For wheat and barley, very small, and probably not significant differences in the results under the oriented and the random volume assumption have been detected on some acquisition dates.

Towards larger scale applications, it is of interest to reduce the number of tracks. The impact of the reduction has to be evaluated in future work.

An open issue is still the use of the extracted ground component for soil moisture estimation. The estimated ground power contains the direct scattering from the ground but also the dihedral scattering component that depends also on the plant dielectric. The volume component instead is sensitive to changes in the VWC. This information is important since the detection of water stress of plants can be an indicator for soil moisture variation [7]. Future research should therefore further investigate the physical inversion of VWC from (volume only) MB SAR data. Besides, the differences in sensitivity to biophysical parameters at different frequencies should be investigated to understand if complementary information could be obtained by a multi-frequency approach.

Acknowledgements

The authors would like to thank the team from the Ludwig-Maximilians-Universität in Munich for their help in the ground parameter collection. This study was supported by the HGF Alliance HA-310 ‘Remote Sensing and Earth System Dynamics’.

3.7 References

- [1] I. Hajnsek, T. Jagdhuber, H. Schon, and K. P. Papathanassiou, “Potential of Estimating Soil Moisture Under Vegetation Cover by Means of PolSAR”, *IEEE Trans. Geosci. Remote Sens.*, vol. 47, no. 2, pp. 442-454, Feb. 2009.
- [2] H. Skriver, M. T. Svendsen, and A. G. Thomsen, “Multitemporal C- and L-band polarimetric signatures of crops”, *IEEE Trans. Geosci. Remote Sens.*, vol. 37, no. 5, pp. 2413-2429, Sep. 1999.
- [3] H. McNairn, and B. Brisco, “The Application of C-band Polarimetric SAR for Agriculture: A Review”, *Can. J. Remote Sen.*, vol. 30, no. 3, pp. 525-542, Ju. 2004.
- [4] S. C. Steele-Dunne, H. McNairn, A. Monsivais-Huertero, J. Judge, P. W. Liu, K. P. Papathanassiou, “Radar Remote Sensing of Agricultural Canopies: A Review”, *IEEE J. Sel. Top. Appl. Earth Obs. Remote Sens.*, vol. 10, no. 5, pp. 2249-2273, May 2017.
- [5] L. Mascolo, J. M. Lopez-Sanchez, F. Vicente-Guijalba, F. Nunziata, M. Migliaccio, and G. Mazzarella, “A Complete Procedure for Crop Phenology Estimation with PolSAR Data Based

- on the Complex Wishart Classifier”, *IEEE Trans. Geosci. Remote Sens.*, vol. 54, no. 11, pp. 6505-6515, Nov. 2016.
- [6] H. Vereecken, L. Weihermüller, F. Jonard, and C. Montzka, “Characterization of Crop Canopies and Water Stress Related Phenomena using Microwave Remote Sensing Methods: A Review”, *Vadose Zone J.*, vol. 11, no. 2, May 2012.
- [7] T. van Emmerik, S.C. Steele-Dunne, J. Judge, and N. van de Giesen, “Impact of Diurnal Variation in Vegetation Water Content on Radar Backscatter From Maize During Water Stress”, *IEEE Trans. Geosci. Remote Sens.*, vol. 53, no. 7, pp. 3855-3869, Jul. 2015.
- [8] J. M. Lopez-Sanchez, and J. D. Ballester-Berman, “Potentials of Polarimetric SAR Interferometry for Agriculture Monitoring”, *Radio Sci.*, vol. 44, no. 2, pp. 141-177, Mar. 2009.
- [9] J. M. Lopez-Sanchez, J. D. Ballester-Berman, and Y. Marequez-Moreno, “Model Limitations and Parameter-Estimation Methods for Agricultural Applications of Polarimetric SAR Interferometry”, *IEEE Trans. Geosci. Remote Sens.*, vol. 55, no. 11, pp. 3481-3493, Nov. 2007.
- [10] J. D. Ballester-Berman, J. M. Lopez-Sanchez, and J. Fortuny-Guasch, “Retrieval of Biophysical Parameters of Agricultural Crops using Polarimetric SAR Interferometry”, *IEEE Trans. Geosci. Remote Sens.*, vol. 43, no. 4, pp. 682-694, Apr. 2005.
- [11] M. Pichierri, I. Hajnsek, and K. P. Papathanassiou, “A Multi-Baseline Pol-InSAR Inversion Scheme for Crop Parameter Estimation at Different Frequencies”, *IEEE Trans. Geosci. Remote Sens.*, vol. 54, no. 8, pp. 4952-4970, Aug. 2016.
- [12] M. Pichierri and I. Hajnsek, “Comparing Performances of Crop Height Inversion Schemes From Multifrequency Pol-InSAR Data,” *IEEE J. Sel. Top. Appl. Earth Obs. Remote Sens.*, vol. 10, no. 5, pp. 1727-1741, May 2017.
- [13] J. M. Lopez-Sanchez, F. Vicente-Guijalba, E. Erten, M. Campos-Taberner, and F. J. Garcia-Haro, “Retrieval of vegetation height in rice fields using polarimetric SAR interferometry with TanDEM-X data”, *Remote Sensing of Env.*, vol. 192, , pp. 30-44, Feb. 2017.
- [14] S. R. Cloude, and K. P. Papathanassiou, “Three-Stage Inversion Process for Polarimetric SAR Interferometry”, *Proc. Inst. Elect. Eng. - Radar, Sonar Navig.*, vol 150., no. 11, pp. 2352-2363, Jun. 2003.
- [15] R. N. Treuhaft, and P. R. Siqueira, “Vertical Structure of Vegetated Land surfaces from Interferometric and Polarimetric Radar”, *Radio Sci.*, vol. 35, no. 1, pp. 141-177, Feb. 2000.
- [16] S. C. M. Brown, S. Quegan, K. Morrison, J. C. Bennett, and G. Cookmartin, “High-Resolution Measurements of Scattering in Wheat Canopies – Implications for Crop Parameter Retrieval”, *IEEE Trans. Geosci. Remote Sens.*, vol. 41, no. 7, pp. 1602-1610, Jul. 2003.

- [17] J. M. Lopez-Sanchez, J. Fortuny-Guasch, S. R. Cloude, and A. J. Sieber, "Indoor polarimetric radar measurements on vegetation samples at L, S, C and X band", *J. Electromagn. Waves Appl.*, vol. 14, no.2, pp. 205-231, 2000.
- [18] J. M. Lopez-Sanchez, J. D. Ballester-Berman, and J. Fortuny-Guasch, "Indoor wide-band polarimetric measurements on maize plants: a study of the differential extinction coefficient", *IEEE Trans. Geosci. Remote Sens.*, vol. 44, no. 4, pp. 758-767, Apr. 2006.
- [19] S. R. Cloude, "Dual-Baseline Coherence Tomography", *IEEE Geosci. Remote Sens. Lett.*, vol. 4, no. 1, pp. 127-13, Jan. 2007.
- [20] M. J. Sanjuan, J. M. Lopez-Sanchez, and J. D. Ballester-Berman, "Microwave Scattering Profiles of a Rice Sample by means of Polarization Coherence Tomography", in *Proc. IEEE IGARSS*, vol. 3, pp. 554-557, Jul. 2008.
- [21] A. Reigber, and A. Moreira, "First Demonstration of Airborne SAR Tomography using Multibaseline L-band Data", *IEEE Trans. Geosci. Remote Sens.*, vol. 38, no. 5, pp. 2142-2152, Sep. 2000.
- [22] O. Frey, and E. Meier, "3-D Time-Domain SAR Imaging of a Forest using Airborne Multibaseline Data at L- and P-Bands", *IEEE Trans. Geosci. Remote Sens.*, vol. 49, no. 10, pp. 3660-3664, Oct. 2011.
- [23] K. Morrison, J. Bennet and S. Solberg, "Ground-based C-band tomographic profiling of a conifer forest stand.", *International Journal of Remote Sensing*, vol. 34, no. 21, pp. 7839-7853, Sep. 2013.
- [24] F. Lombardini, and M. Pardini, "Experiments of Tomography-Based SAR Techniques with P-Band Polarimetric Data", in *Proc. PolInSAR*, Frascati, Italy, Jan. 2009.
- [25] H. Joerg, M. Pardini, I. Hajnsek, and K. P. Papathanassiou, "On the Separation of Ground and Volume Scattering Using Multibaseline SAR Data", *IEEE. Geosci. Remote Sens. Lett.*, vol. 14, no. 9, pp.1570-1574, Jul. 2017.
- [26] B. Ottersten, P. Stoica, and R. Roy, "Covariance matching estimation techniques for array signal processing and applications", *Digital Signal Processing*, vol. 8, no. 3, pp. 185-21, Jul. 1998.
- [27] U. Meier, et al. "The BBCH system to coding the phenological growth stages of plants – history and publications", *Journal of Cultivated Plants*, vol. 61, no. 2, pp. 41-52, 2009.
- [28] S. R. Cloude, *Polarisation: Applications in Remote Sensing*. Oxford, U.K.: Oxford Univ. Press, 2009.
- [29] A. Reigber, P. Prats, and J.J. Mallorqui, "Refined Estimation of Time-Varying Baseline Errors in Airborne SAR Interferometry", *IEEE Geosci. Remote Sens. Lett.*, vol. 3, no. 1, pp. 145-149, Jan. 2006.
- [30] M. Pardini, and K. P. Papathanassiou, "A Two-Step Phase Calibration Method for Tomographic Applications with Airborne SAR Data", in *Proc. EUSAR*, vol. 10, Jun. 2014.

- [31] H. Joerg, M. Pardini, I. Hajnsek, and K. P. Papathanassiou, "Application of SAR Tomography on Agricultural Vegetation for Scattering Characterisation", in *Proc. PolInSAR*, Frascati, Italy, Jan. 2015.
- [32] H. Joerg, M. Pardini, and I. Hajnsek, "Spatial and Temporal Characterization of Agricultural Crop Volumes by means of Polarimetric SAR Tomography at C-Band", in *Proc. IEEE IGARSS*, pp. 5292 - 5295, Jul. 2015.
- [33] T. Marzetta, "A New Interpretation for Capon's Maximum Likelihood Method of Frequency-Wavenumber Spectral Estimation", *IEEE Trans. Acoust. Speech, Signal Processing*, vol. 31, no.2, pp. 445-449, Apr. 1983.
- [34] J. D. Ballester-Berman, and J. M. Lopez-Sanchez, "Applying the Freeman–Durden Decomposition Concept to Polarimetric SAR Interferometry", *IEEE Trans. Geosci. Remote Sens.*, vol. 48, no. 1, pp. 466-479, Jan. 2010.
- [35] Z. W. Zhu, W. Shi, H. Leung, and Z. Ding, "Matrix filter design using semi-infinite programming with application to DOA estimation", *IEEE Trans. Signal Process.*, vol. 48, no. 1, pp. 267-271, Jan. 2000.
- [36] C. Igathinathane, A. R. Womac, S. Sokhansanj, and L. O. Pordesimo, "Mass and moisture distribution in aboveground components of standing corn plants.", *Transactions of the ASABE*, vol. 49, no. 1, pp. 97-106, 2006.
- [37] J. Casanova, M. Jang and J. Judge, "Transmission of Microwaves through a Dynamic Corn Canopy in Emission Models", in *Proc. IEEE IGARSS*, pp. 2025-2027, Jul. 2006.
- [38] C. Lopez-Martinez and A. Alonso-Gonzalez, "Assessment and Estimation of the RVoG Model in Polarimetric SAR Interferometry", *IEEE Trans. Geosci. Remote Sens.*, vol. 52, no. 6, pp. 3091–3106, Jun. 2014.
- [39] K. Werner, M. Jansson, and P. Stoica, "On Estimation of Covariance Matrices With Kronecker Product Structure", *IEEE Trans. Signal Process.*, vol. 56, no. 2, pp. 478-491, Jan. 2008.
- [40] S. Tebaldini, "Algebraic Synthesis of Forest Scenarios from Multibaseline PolInSAR Data", *IEEE Trans. Geosci. Remote Sens.*, vol. 47, no. 12, pp. 4132-4142, Dec. 2009.

Chapter 4

Sensitivity of SAR Tomography to the Phenological Cycle of Agricultural Crops at X-, C- and L-band

H. Joerg, M. Pardini, I. Hajnsek, and K. P. Papathanassiou

IEEE Journal of Selected Topics in Applied Earth Observations and Remote Sensing

Submitted in November 2017

The author's contributions:

- Planning of the airborne MB SAR acquisitions and the ground measurement collection of the CROPEX 2014 campaign.
- Coordination of and participation in the ground measurement collection.
- Identification of phenological transitions of interest and implementation of the processing steps for estimating the tomographic parameters.
- Interpretation and evaluation of the estimated parameters for the specific phenological transitions.
- Writing of the manuscript.

The co-authors' contributions:

- M. Pardini supervised the tomographic processing of the data and suggested the implementation of the Matrix Filter approach for the ground and volume separation.
- I. Hajnsek suggested and initiated the CROPEX 2014 campaign.
- K. P. Papathanassiou suggested the evaluation of the center of mass.
- All co-authors helped in discussing the results, reviewing and editing of the manuscript.

Sensitivity of SAR Tomography to the Phenological Cycle of Agricultural Crops at X-, C- and L-band

Hannah Joerg^{1,2}, Matteo Pardini¹, Irena Hajnsek^{2,1}, and Konstantinos P. Papathanassiou¹

¹ German Aerospace Center, Microwaves and Radar Institute, Wessling, Germany

² ETH Zurich, Institute of Environmental Engineering, Zurich, Switzerland

Abstract

Understanding the impact of changes of soil and plant parameters in agriculture on Synthetic Aperture Radar (SAR) measurements is of great interest when it comes to monitor the temporal evolution of agricultural crops by means of SAR. In this regard, specific transitions between phenological stages in corn, barley and wheat have been identified associated to certain dielectric and geometric changes, based on a time series of fully polarimetric multi-baseline SAR data and in-situ measurements acquired in the frame of the DLR's CROPEX 2014 campaign between May and July. The experiments reported in this paper address the sensitivity of X-, C- and L-band to these phenological transitions exploiting the availability of multiple baselines on each acquisition date. The application of tomographic techniques enables the estimation of the 3-D backscatter distribution and the separation of ground and volume scattering components. Tomographic parameters have been derived at different frequencies, namely the center of mass of the profiles of the total and of the volume-only 3-D backscatter, and the ground and volume powers. Their sensitivity and ability to detect changes occurring on the ground and in the vegetation volume have been evaluated focusing on the added value provided by the 3-D resolution at the different frequencies and polarizations available.

4.1 Introduction

Plant height, morphology, water content and biomass vary among different agricultural crop types but also for the same crop type during the phenological cycle. Synthetic Aperture Radar (SAR) remote sensing is a powerful tool for monitoring this temporal and spatial diversity mainly due to the ability to provide data with high spatial and temporal resolution and sensitive at the same time to dielectric and geometric soil and vegetation properties [1,2]. Based on this, time series of polarimetric SAR have been successfully exploited for classification of crop types [1,3] and phenological stages [4], while monitoring of plant height is facilitated by its robust inversion from polarimetric-interferometric SAR methodologies [5-8].

However, due to the complexity of the scattering mechanisms occurring within the vegetation there is still limited understanding of how biophysical parameters and their changes impact SAR measurements as a function of frequency [6]. Both scattering and propagation are influenced by the

amount of water contained in the vegetation and by the geometric 3-D distribution of the plant components [9,10]. At the same time, scattering mechanisms change with frequency, as the wavelength drives the sensitivity to different plant components [9,11]. A first insight on the relation between SAR measurements and biophysical parameters can be gained by correlating temporal variations [1,2,12,13]. However, the generalization is rather limited, since changes on the ground can be misinterpreted as changes in the vegetation and vice versa. This underlines the major difficulty at any frequency which is the unique interpretation of the high complexity of scattering mechanisms by electromagnetic models able to separate between soil and plant dynamics in the frame of a limited observation space.

SAR Tomography (TomoSAR) contributes to the understanding of the ongoing scattering processes. Without using scattering models, TomoSAR techniques estimate the 3-D backscatter distribution by combining multiple spatially separated acquisitions [14]. First indoor and outdoor ground-based experiments have been conducted for wheat at X- and C-band in [15] and for corn at X-, C- and L-band in [16-18]. Profiles of the 3-D backscatter were analyzed as a function of polarization, incidence angle and frequency. However, these experiments were carried out for only one phenological stage and no separation between ground and volume scattering was attempted.

To fill this experimental gap, the Crop Experiment (CROPEX) campaign was carried out by DLR in 2014 providing a time series of airborne polarimetric multi-baseline SAR data at X-, C- and L-band with coincident ground measurements over the Wallerfing test site.

In order to distinguish between changes in scattering components located on the ground and in the vegetation volume a TomoSAR filtering technique has been applied allowing the estimation of the volume interferometric coherences and the ground and volume powers [19]. This enables the distinct analysis of the volume-only 3-D backscatter and ground and volume power changes in time related to the changes in the plants along the phenological cycle.

To this purpose, characteristic transitions between phenological stages related to dielectric (e.g. dynamics of the water content) and geometric (e.g. alignments of plant components) changes have been identified within the monitored time period for the crop types under study, i.e. corn, barley and wheat. The objective of the experimental results reported in this paper is to investigate the sensitivity of TomoSAR parameters to these phenological transitions across frequencies. Additionally, the study intends to give insights on the added value of the ground-volume separation and on the importance of polarimetric observation diversity.

4.2 Data Time Series

The experimental data are part of the CROPEX 2014 campaign and consist of a time series of multi-baseline SAR data acquisitions and simultaneously collected ground measurements over the agricultural Wallerfing test site located in South Germany [20]. Fully polarimetric SAR acquisitions are available at X-, C- and L-band on six dates between May and July. This Section introduces the test site and briefly describes the phenological development of corn, barley and wheat in this time period.

Fig. 1 (a) shows the land use of the area under study limited to the crop types of interest. On each campaign date, several plant parameters were intensively measured within selected fields (indicated in Fig. 1 (a)) including row distance, number of plants per meter and plant height. Additionally, the

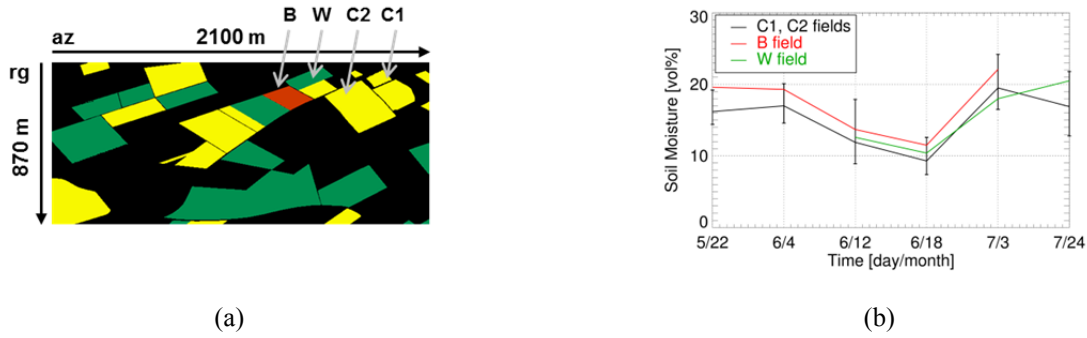


Fig. 1: (a): Land use of the area under study in the range (rg) - azimuth (az) coordinate system: corn (yellow), wheat (green) and barley (red); other crop types, settlements and forests are masked out (black). C1, C2, W and B are the intensively measured fields. (b): Temporal variation of soil moisture. The error bars correspond to the 60% confidence interval.

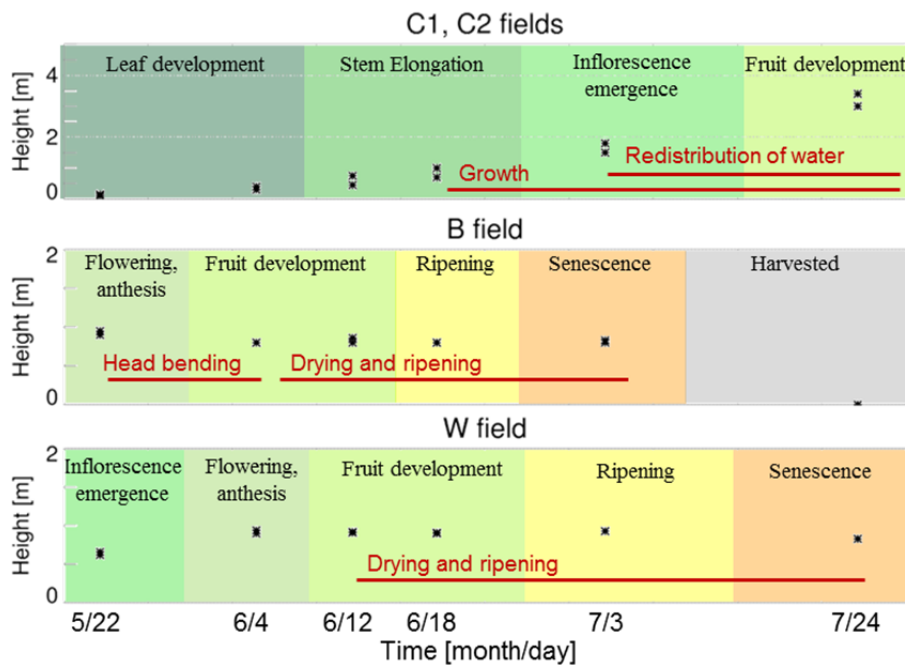


Fig. 2: Phenological development and height of the plants on the intensively measured fields across the monitored time period. The red lines indicate the start and end of the transitions under study per crop type.

phenological stage of the plants was identified according to the BBCH scale (from *Biologische Bundesanstalt, Bundessortenamt und Chemische Industrie*) [21]. A small patch (0.25 m^2 for wheat and barley and 1 m^2 for corn) was harvested at two locations within those fields. The weight of the harvested plants yields the wet biomass per square meter. By drying samples of the harvested plants, the Vegetation Water Content (VWC) per square meter was obtained as the difference of the wet and dry sample weight which was upscaled to 1 m^2 . Soil moisture measurements were collected using a Frequency Domain Reflectometry probe on the locations where the plant parameters were measured and additionally on a denser grid on the fields C1 and C2 (see Fig. 1 (a)). This grid consists of approximately 35 measurement locations, and 5 measurements were taken per location. The soil moisture variation on the corn fields (see Fig. 1 (b)) is therefore statistically more representative. However, the sparser measurements in the wheat and barley fields show a similar

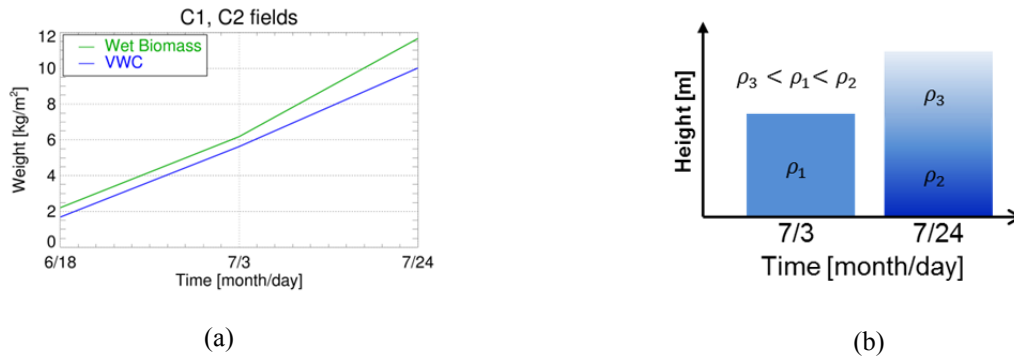


Fig. 3: C1, C2 fields: (a): Wet biomass and VWC on the relevant dates. (b): Schematic view of the redistribution of water. Darker colors indicate higher density of water.

trend, as it is reasonable to expect.

Fig. 2 illustrates the evolution of plant heights and phenological development on the intensively measured fields as a function of the campaign dates. Based on these dates and the available experimental data (both on ground and from the SAR), specific transitions between two or more phenological stages have been selected for this study. The focus lies on dielectric changes and geometric changes of plant components with high water content. The time frames for the analyzed transitions are indicated by the red lines for each crop type and they are described separately in the following.

4.2.1 Corn

The corn was planted with a row distance from 0.7 to 0.8 m and 6 to 7 plants per meter. During the monitored time period, the corn plants grow until full height and reach the fruit development phase on the last date.

From a crop monitoring perspective, the plant growth is of interest. Here, the last three dates from June 18 until July 24 are analyzed, where the wet biomass accumulates (see Fig. 3 (a)). The plants consist mainly of water, as indicated by the high VWC compared to the wet biomass. Besides that, the corn adapts its VWC distribution within the plant to the development stage. This is illustrated schematically in Fig. 3 (b). At first while the plant is still growing, the water is uniformly distributed in height with a certain water density ρ_1 . Once the fruit development starts, here after July 3, the water content is redistributed in height leading to an increased water density ρ_2 in the lower part of the plants to support the fruit located there and a lower water density ρ_3 above [2,22].

4.2.2 Barley

The barley is planted in rows of approximately 0.1 m distance and around 100 plants per meter. On May 22, the barley plants are in the flowering stage, and the time series observes the second part of the phenological cycle until harvest. Barley is a cereal and it has characteristically long awns of approximately the same length as the heads.

During the transition from the flowering to the fruit development phase, the heads of the barley bend from a vertical to a rather horizontal position (see Fig. 4 (a)). This occurred between May 22 and June 4. While the dielectric properties do not change significantly during this event, the drying

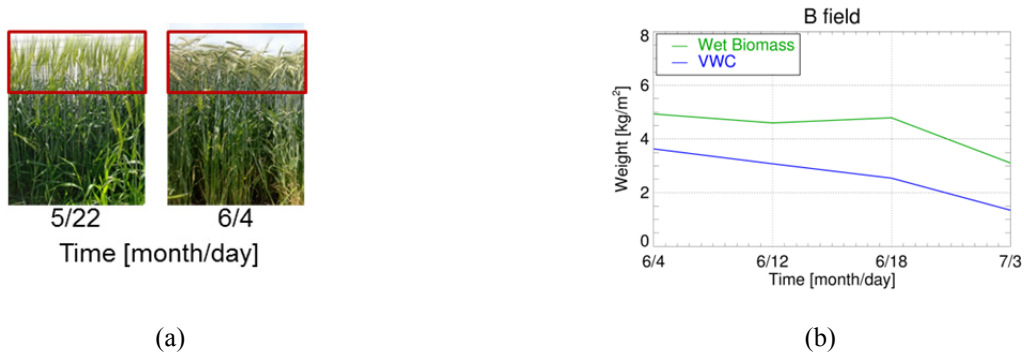


Fig. 4: B field: (a): Pictures of the bending of the heads. (b): Wet biomass and VWC on the relevant dates for the drying and ripening.

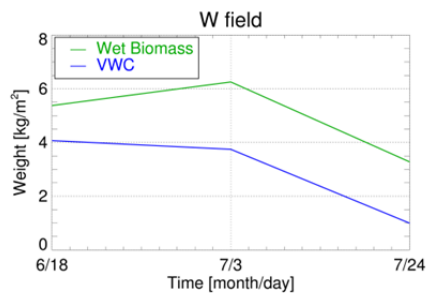


Fig. 5: W field: Wet biomass and VWC on the relevant dates for the drying and ripening.

and ripening processes happen simultaneously after June 4. The plot in Fig. 4 (b) shows a continuous decrease of VWC. The wet biomass instead stays high until June 18, which is due to an increase of dry plant material because of the ripening.

4.2.3 Wheat

Wheat is a cereal and the planting characteristics are very similar to the ones in the barley. The biggest differences to barley are the very short awns, and the fact that the heads keep oriented vertically, bending slightly only when ripening. The campaign observed the second part of the wheat phenological cycle and after June 18 the simultaneous drying and ripening of the plants take place. However, the development stages are shifted with respect to the barley, since the wheat plants are in the inflorescence stage on the first date. In contrast to barley, the VWC stays high during the increase of dry biomass after June 18 and it only decreases after July 3 (see Fig. 5).

4.3 Tomographic Algorithms and Parameters

The phenological transitions introduced in Section 4.2 are associated to dielectric and/or geometric changes that affect the scattering and attenuation behavior at the different frequencies. Fig. 6 shows the VV backscattered power images on four selected dates at the different frequencies. The spatial and temporal variability is clearly noticeable. The fact that an unambiguous interpretation of changes occurring on the ground and in the vegetation between the dates by means of the backscattered power alone is not possible motivates the use of TomoSAR techniques.

This Section shortly describes the SAR acquisitions and the principle of TomoSAR. The a

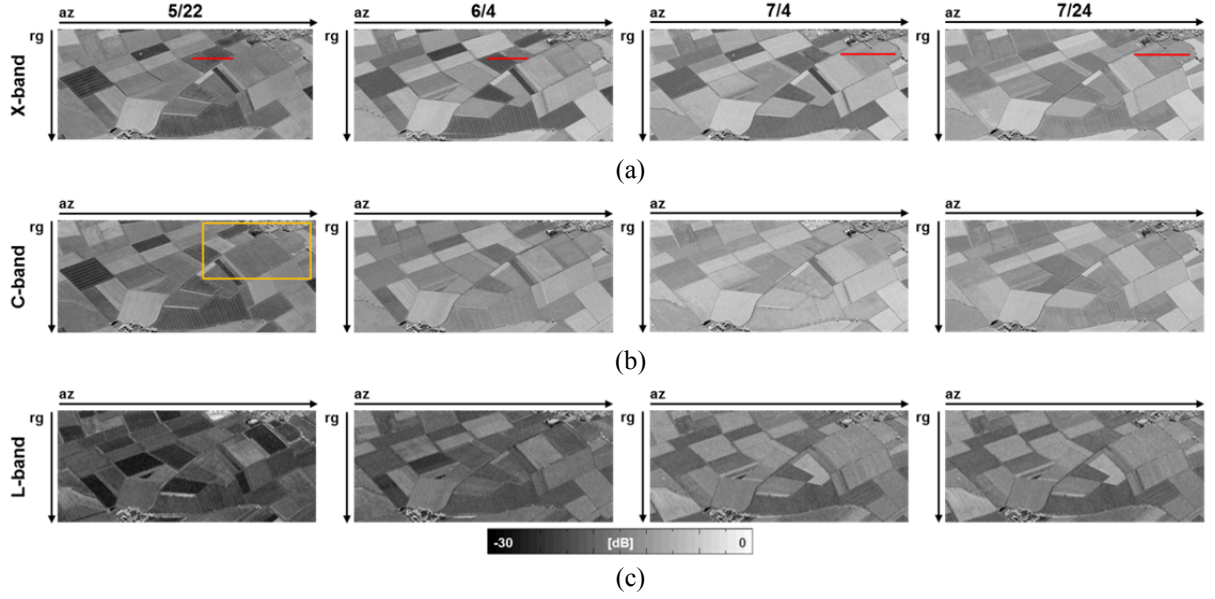


Fig. 6 (a)-(c): VV backscattered power images on selected dates at X-, C- and L-band. The yellow box indicates the area of the intensively measured fields and the red lines the transect for the tomographic examples presented in Section 4.3.2.

algorithm used for separating ground and volume scattering components is outlined together with the parameters that will be used to quantify the changes related to the phenological changes.

4.3.1 Acquisition Parameters

The acquisition parameters are given for the area where the intensively measured fields are located, indicated by the yellow box in Fig. 6, and are summarized in Table I. Since the X- and C-band acquisitions were carried out simultaneously, their incidence angle (34°), spatial resolution and number of tracks are identical. At L-band, the spatial resolution is coarser and the incidence angle larger (40°).

Each acquisition consists of K tracks acquired on the same day, with an approximate temporal sampling of ten minutes. The tracks are separated by increasing horizontal baselines. At the k -th track this separation induces a difference $\Delta\theta_k$ compared to the incidence angle θ of the first track. The variation of the interferometric phase between the tracks provides sensitivity to height differences. This sensitivity is expressed by the vertical wavenumber κ_z^k measured in rad/m between the first and the k -th track as $\kappa_z^k \approx 4\pi/\lambda \cdot \Delta\theta_k/\sin\theta$, where λ stands for the wavelength [23]. Then the variation of the interferometric phase for a given height z is stored in the steering vector $\mathbf{a}(z) = [1 e^{-j\kappa_z^2 z} \dots e^{-j\kappa_z^K z}]^T$, with $\kappa_z^1 = 0$ corresponding to the master track. The vertical Rayleigh resolution is inversely proportional to the maximum available vertical wavenumber [14] and is given by

$$r_z = \frac{2\pi}{\max_k \kappa_z^k}. \quad (1)$$

TABLE I
ACQUISITION PARAMETERS GIVEN FOR THE AREA OF THE INTENSIVELY MEASURED FIELDS
AT THE DIFFERENT FREQUENCIES

Frequency band	X-band (9.6 GHz)	C-band (5.4 GHz)	L-band (1.3 GHz)
Resolution in slant-range and azimuth	0.5 m × 0.5 m		1.3 m × 0.5 m
Mean local incidence angle at the intensively measured fields	34°		40°
Number of tracks	May 22:	9	8
	June 4:	9	6
	June 12:	9	7
	June 18:	8	7
	July 3:	9	8
	July 24:	9	7
Maximum vertical wavenumber at the intensively measured fields	11.2 rad/m	6.2 rad/m	4.2 rad/m
Vertical Rayleigh resolution achieved at the intensively measured fields	0.55 m	0.9 m	1.4 m

The requirements and rationale for the baseline design are described in [20,24]. For all six dates, a mean vertical resolution of 0.5 m, 0.9 m and 1.4 m at X-, C- and L-band is attained in the region of the intensively measured fields; slightly higher in near range and slightly lower in far range. With reference to Fig. 2, the vertical resolution becomes critical at L- and C-band for low plant heights as in barley and wheat, and in the early development stages of corn, while X-band vertical resolution seems adequate. This has to be considered when interpreting the results, since it is challenging to distinguish scattering contributions within the same tomographic resolution cell.

4.3.2 SAR Tomography

The data vector $\mathbf{y}^i \in \mathbb{C}^K$ at each polarimetric channel $i \in \{HH, HV, VV\}$ contains the complex single look images from the different tracks, after performing the necessary interferometric processing steps (co-registration, flat-earth compensation [23] and phase calibration [25,26]). In the case of distributed scatterers, such as vegetation, a spatial multi-looking is required and the scattering signature is fully described by the covariance matrix $\mathbf{R}^i \in \mathbb{C}^{K \times K}$ estimated by averaging over N neighbouring samples

$$\hat{\mathbf{R}}^i = \frac{1}{N} \sum_{n=1}^N \mathbf{y}^i(n) \mathbf{y}^i(n)^H, \quad i \in \{HH, HV, VV\}. \quad (2)$$

For the data set at hand, the spatial multi-looking is performed by using a square window of 7.5 m × 7.5 m resulting in 220 independent looks at X- and C-band and 90 independent looks at L-band.

On each campaign date, all the tracks were acquired in repeat- pass mode within 90 minutes. No evidence of significant temporal decorrelation has been observed from the comparison of the

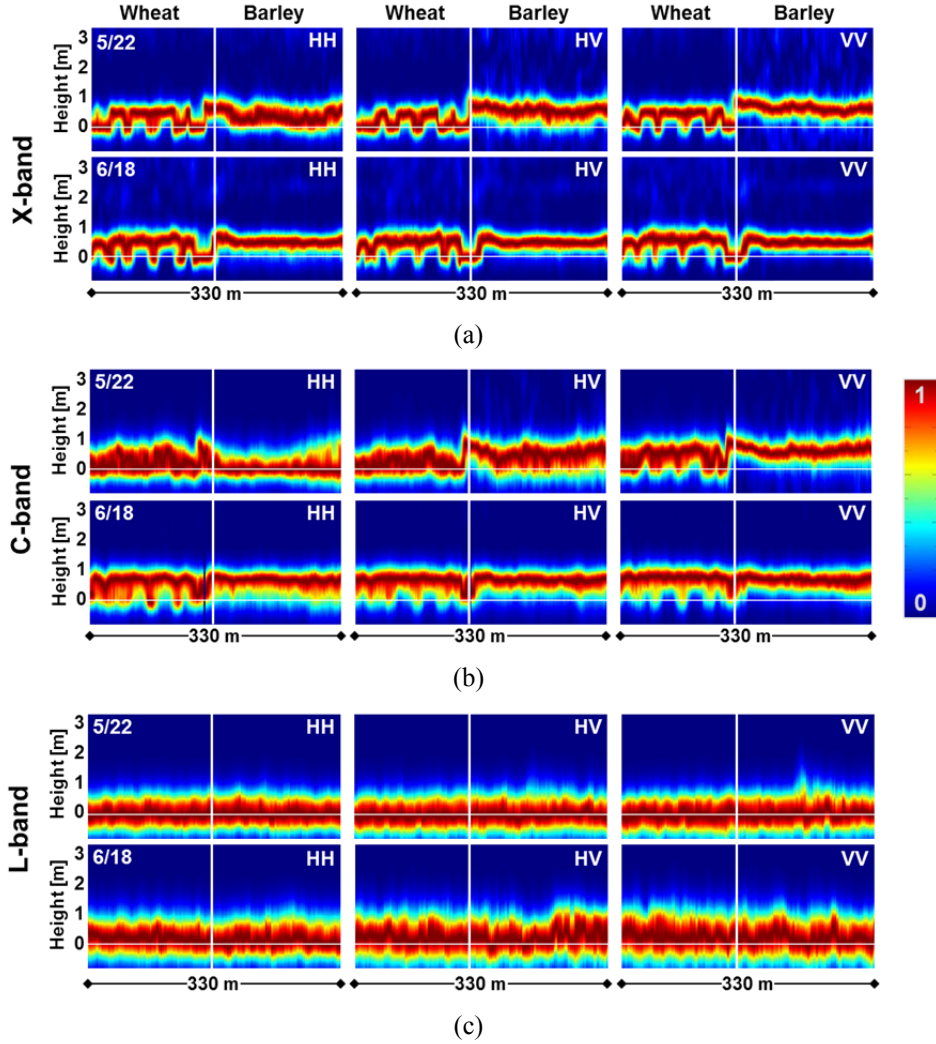


Fig. 7: (a)-(c): Wheat and Barley: Profiles of the 3-D backscatter along the transect outlined in Fig. 6 on May 22 (top) and June 18 (bottom) at X-, C- and L-band. The profiles are estimated using the Capon beamformer and normalized to the maximum power at each inversion point.

magnitude of interferometric coherences corresponding to the same (small) vertical wavenumbers. The 3-D backscatter is estimated from $\hat{\mathbf{R}}^i$ by applying spectral estimation methods using $\mathbf{a}(z)$ [27,28]. Examples of profiles of the 3-D backscatter estimated using the Capon beamformer¹ along the transects indicated by the red lines in Fig. 6 are given for wheat and barley on May 22 and June 18 (Fig. 7), and for corn on July 3 and July 24 (Fig. 8) for each polarization at the different frequencies. The topographic phase, known from a LiDAR digital terrain model, has been compensated so that the ground is imaged at a height of 0 m. The largest differences are observed between the HH and VV channels, while at HV the profiles show always a behavior in between. Changes in the vegetation characteristics can be qualitatively observed by the change of the profiles of the 3-D backscatter between the dates.

¹ No differences have been found in the estimated profiles if the full-rank polarimetric Capon beamformer [29] is used instead.

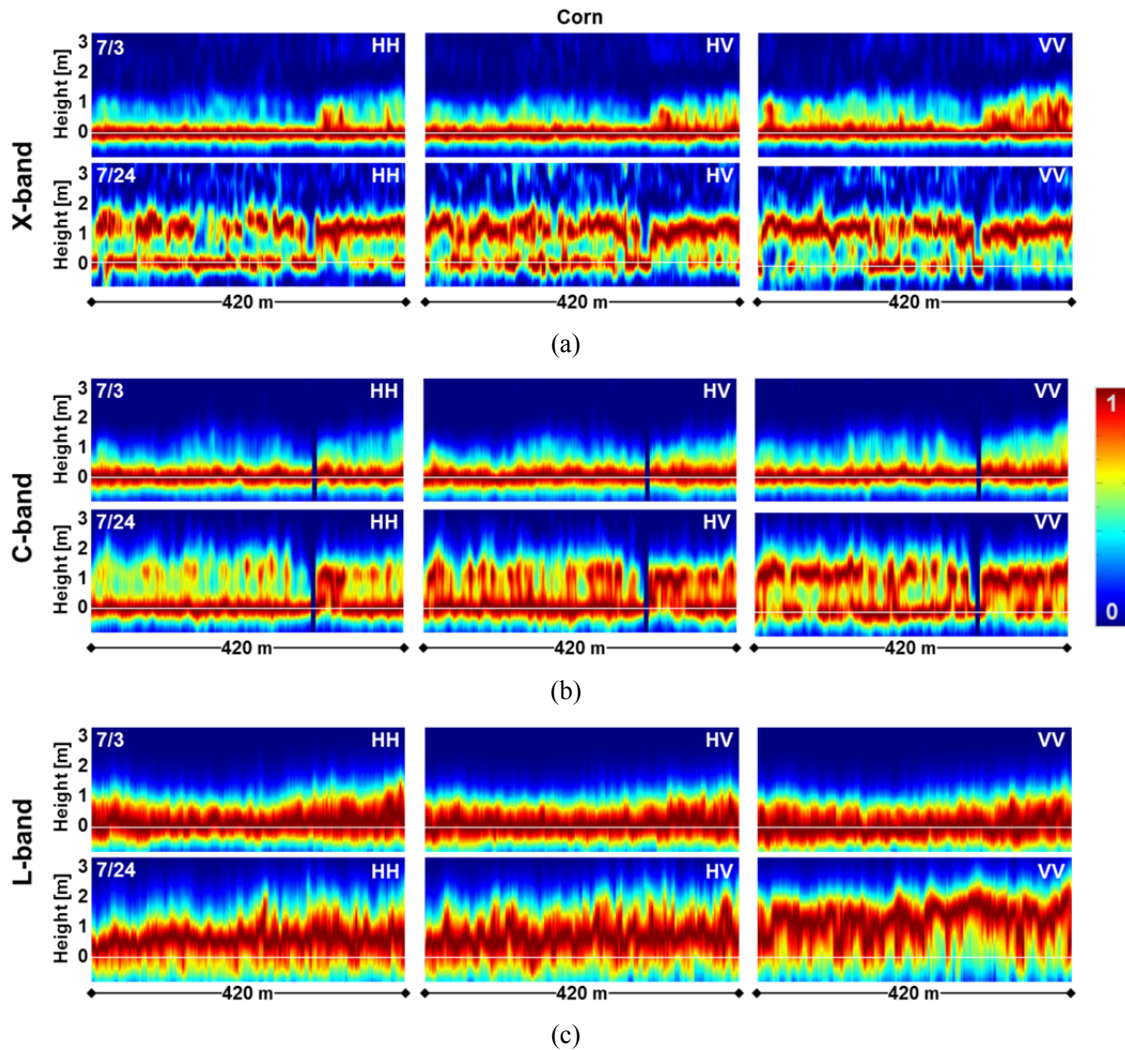


Fig. 8: (a)-(c): Corn: Profiles of the 3-D backscatter along the transect outlined in Fig. 6 on July 3 (top) and July 24 (bottom) at X-, C- and L-band. The profiles are estimated using the Capon beamformer and normalized to the maximum power at each inversion point.

At L-band, wheat and barley (see Fig. 7) cannot be distinguished from their profiles and they show almost no differences between the two dates. Even though L-band is expected to be more ground dominated, this spatial and temporal insensitivity might also be due to the fact that Capon super-resolution capabilities are hampered by the presence of a wide volume. On the contrary, at X- and C-band, the profiles vary with crop type, polarization, time and frequency. The tractor tracks are clearly visible in the wheat, particularly when the profiles are volume dominated. For both cereals, the maximum of the profiles at X-band is located close to the top of the vegetation and polarization differences are less pronounced. At C-band, the profiles on May 22 are rather ground dominated at HH when compared to VV while the location of the maximum of the profiles on June 18 moves to the top of the vegetation at all polarizations due to the evolved cereal heads. However, C-band still penetrates more suggesting sensitivity to the full vegetation volume while X-band is rather attenuated at the top.

For the corn (see Fig. 8), the profiles at L-band are still ground dominated on July 3, despite a plant height of up to 1.9 m. The location of the maximum of the profiles at HH moves slightly

upwards on July 24, while VV appears more sensitive to the vegetation. At X- and C-band the profiles reflect the growth between the two dates, the morphological change and spatial differences. The latter relate mainly to the density of the planting rows. Additionally, the extent of the profiles on both dates is smaller than the actual plant height (around 1.9 m and 3.2 m) indicating that the plant top is semi-transparent even at the small wavelengths.

From these examples, it is already apparent that for ground-dominated scenarios and low vertical resolution compared to the plant heights the analysis of vegetation parameters from the 3-D backscatter is limited.

In general, looking at the whole profiles, it is not possible to clearly distinguish changes on the ground from changes in the volume nor to quantify the differences between the dates. This motivates the necessity of separating ground and volume scattering components.

4.3.3 Separation of Ground and Volume

The scattering scenario is modelled by means of an impenetrable ground and a semi-transparent vegetation layer. The Capon spectral estimator, even in its polarimetric full-rank implementation [29], cannot separate ground and volume scattering contributions in terms of ground / volume powers and volume-only interferometric coherences. Additionally, the ground power estimates are intrinsically biased due to the presence of the volume [30]. Therefore, a different separation methodology has to be used.

Model-based algorithms, including the decomposition in [31], provide non-unique solutions due to the intrinsic ambiguity in the separation (see the discussion in [19] and [30]), that can be overcome by introducing regularization constraints. However, the same modelling assumptions may not hold at all frequencies and phenological stages. To overcome these limitations, a model-free matrix filter has been used for estimating the volume-only coherences. The matrix filter was initially proposed in [27] and analyzed regarding estimation performance in [19]. The algorithm requires the knowledge of the ground topography. It provides a unique solution without posing any assumption on the individual scattering processes, regardless of the frequency and of the polarimetric channel.

To simplify the notation, the index i indicating the polarimetric channel is omitted in the following.

A. Data Model

Under the assumption that the ground layer can be approximated by a Dirac- δ positioned at the ground height z_G [19], the covariance matrix for a single polarimetric channel can be written as

$$\mathbf{R} = p_G \mathbf{a}_G \mathbf{a}_G^H + p_V \mathbf{\Gamma}_V, \quad (3)$$

where p_G and p_V are the ground and volume powers and $\mathbf{a}_G = \mathbf{a}(z_G)$. The matrix $\mathbf{\Gamma}_V$ contains the volume-only interferometric coherences at the different baselines. The ground power p_G contains contributions from both direct surface and dihedral scattering mechanisms since the phase center of dihedral interactions between trunk and surface is located on the ground.

B. Estimation of Volume Coherences

A matrix filter \mathbf{H} is designed according to [19,27] in order to cancel the scattering contributions in a stopband around the a priori known ground height and to preserve the ones in a passband including all the volume components. Applying this filter to the data covariance matrix $\hat{\mathbf{R}}$ yields an estimate of the volume covariance matrix $\hat{\mathbf{R}}_V$ as

$$\hat{\mathbf{R}}_V = \mathbf{H} \hat{\mathbf{R}} \mathbf{H}^H. \quad (4)$$

The knowledge of the ground topography is a sufficient condition to overcome the intrinsic ambiguity of estimating the two layers from the multi-baseline SAR data [19,30]. Particularly for agricultural applications, the knowledge of the ground topography can easily be gained for instance from an interferometric acquisition before the growing season.

If the plant height is in the order of the vertical resolution and the two components are located within the same vertical resolution cell, the separation becomes more critical than for higher vertical resolutions. In this case, as shown by numerical simulations, the volume coherence magnitudes and phases are overestimated particularly for low ground-to-volume power ratios [19].

C. Estimation of Ground and Volume Powers

The matrix $\hat{\mathbf{R}}_V$ estimated according to equation (4) yields the volume coherences $\hat{\mathbf{\Gamma}}_V$ after a proper normalization. Following the model in (3), the ground and volume powers can be jointly estimated by covariance matching [32]

$$\begin{bmatrix} p_G \\ p_V \end{bmatrix} = (\mathbf{\Pi}^H \mathbf{\Pi})^{-1} \mathbf{\Pi}^H \text{vec}(\hat{\mathbf{R}}), \quad (5)$$

where $\mathbf{\Pi} = [\text{vec}(\mathbf{a}_G \mathbf{a}_G^H) \quad \text{vec}(\hat{\mathbf{\Gamma}}_V)]$, and $\text{vec}(\cdot)$ is the vectorization operator that transforms a matrix into a column vector. In the critical case of only one vertical resolution unit per plant height, the overestimated volume coherences cause an overestimation of p_G for volume-dominated scenarios. For a ground-to-volume power ratio of -5 dB, the root-mean-square error in the estimation of p_G increases from 10% (two vertical resolution units per plant height) to 30% for only one vertical resolution unit per plant height, while for p_V it is always below 15% [19].

4.3.4 Discussion of TomoSAR Parameters

The TomoSAR parameters used to evaluate the sensitivity of the different frequencies to the phenological transitions are summarized and discussed in the following.

- The *center of mass* of the 3-D backscatter is estimated for each resolution cell from the vertical backscatter profile $P^i(z)$, estimated by the Capon beamformer as

$$CoM^i = \frac{\int_{0-\delta}^{z_{top}+\Delta} P^i(z) z dz}{\int_{0-\Delta}^{z_{top}+\Delta} P^i(z) dz}, \quad i \in \{HH, HV, VV\}. \quad (6)$$

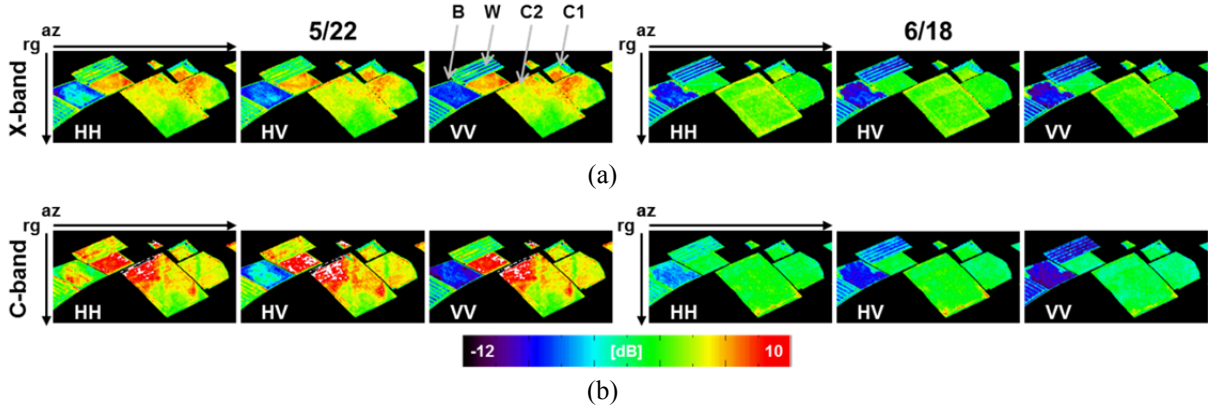


Fig. 9: (a)-(b): Estimated ground-to-volume power ratio at HH, HV and VV on May 22 (left) and June 18 (right) at X- and C-band.

In order to ensure that the limits of the integral fully include the tomographic profile, they are chosen conservatively by extending the expected height range of the tomographic profile in both directions. Since the ground phase has been compensated, the lower limit is just below the ground at $0 \text{ m} - \Delta$ and the upper limit slightly above the maximum expected height at $z_{top} + \Delta$, where $\Delta = 0.2 \text{ m}$.

After separation (see Section 4.3.3), the *volume center of mass*, i.e. the center of mass of the volume-only 3-D backscatter, is estimated in analogy to (6).

It is worth to remark that the center of mass corresponds – at least in the first order – to the interferometric phase center that could be estimated by only two tracks.

- The variation of the *ground and volume powers* (see Section 4.3.3.) is a quantitative measurement for incoherent changes. Besides, the directly resulting *ground-to-volume power ratio* $\mu^i = p_G^i / p_V^i$ at the different polarizations $i \in \{HH, HV, VV\}$ indicates if ground or volume is the dominant scattering.

The coherent polarimetric signatures and therefore polarimetric observables such as entropy and alpha angle of the ground and volume are not analyzed here. The polarimetry of the volume does not provide additional information since the presence of complex scattering mechanisms saturates the entropy to high levels with limited added value to the interpretation of the scattering mechanisms. On the other hand, the vertical resolution is limited for low plant heights and the interference from the volume component on the estimated ground component is too severe for a meaningful interpretation of the ground polarimetry. As already commented, the power estimates are more robust in this regard enabling a quantification of the changes for vertical resolutions larger than or in the order of the plant heights. The analysis of the L-band results is restricted to the corn in the following due to the very critical resolution conditions in the cereals where the height to vertical resolution ratio is much lower than one.

Fig. 9 shows the maps of the ground-to-volume power ratios for X- and C-band at the different polarizations on the dates where the profiles in the cereals were discussed, i.e. May 22 and June 18. In general, the ground-to-volume power ratio is lower at VV than at HH while the values at HV lie in between. The scattering scenario in the cereals is at X-band more dominated by the volume than

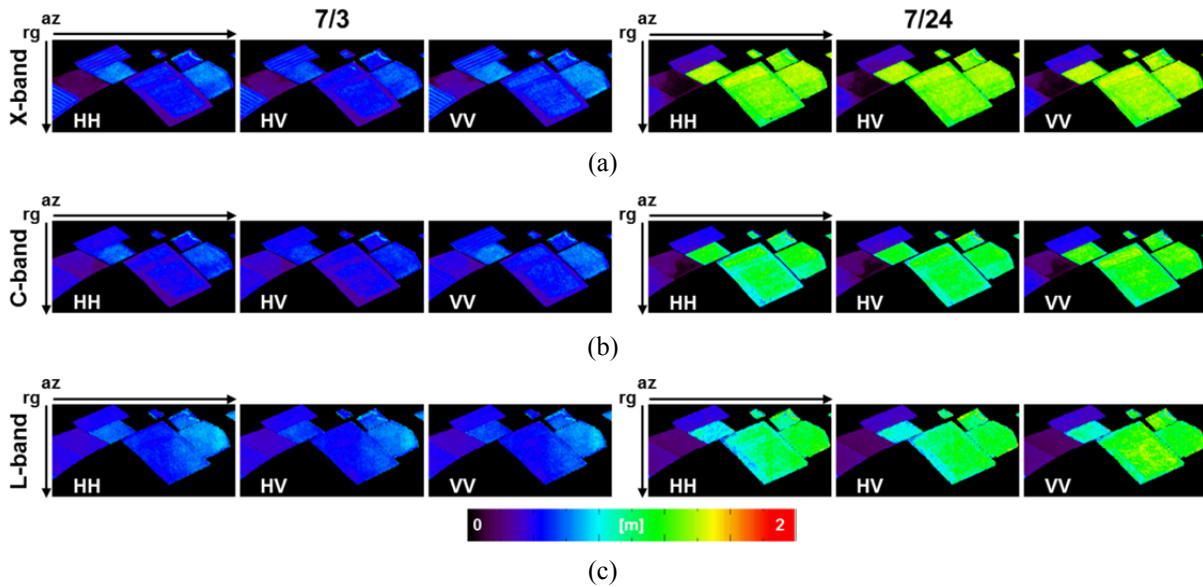


Fig. 10 (a)-(c): Height of the estimated center of mass of the 3-D backscatter at HH, HV and VV on July 3 (left) and July 24 (right) at X-, C- and L-band.

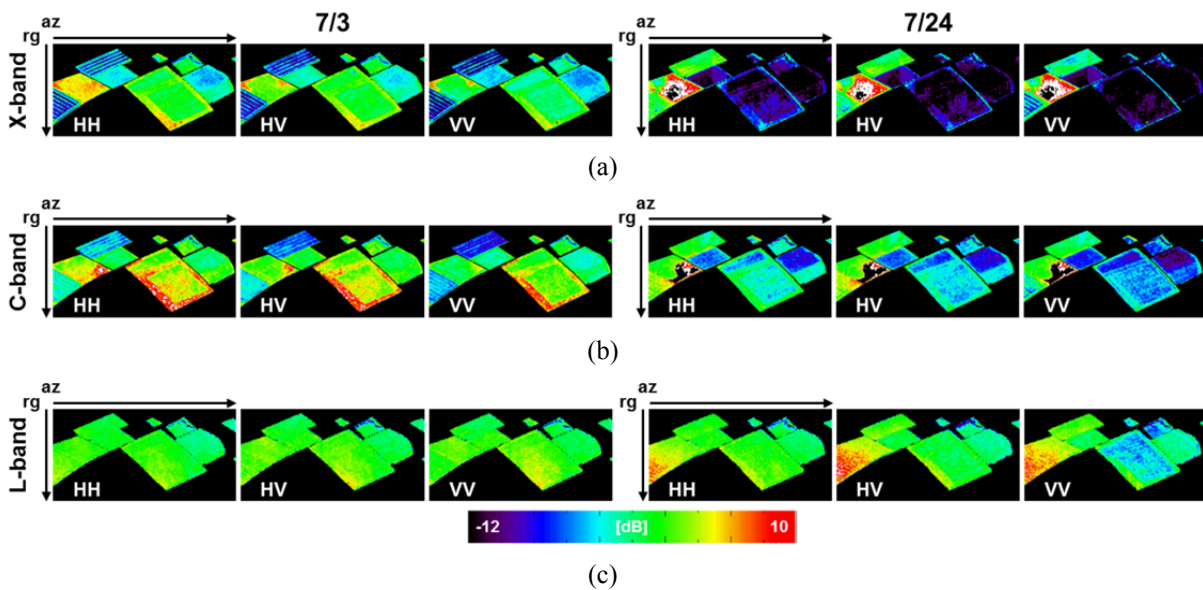


Fig. 11: (a)-(c): Estimated ground-to-volume power ratio at HH, HV and VV on July 3 (left) and the July 24 (right) at X-, C- and L-band.

at C-band. On June 18, the scattering becomes more volume-dominated both in the wheat and the barley field compared to May 22. The tractor tracks are visible in the wheat with a higher ground-to-volume ratio.

Also for the corn, the center of mass and the ground-to-volume power ratio on July 3 and July 24 (see Figs. 10 and 11) show that X-band is more volume dominated than C-band with similar spatial patterns. The comparison with the measured planting parameters show that the bigger the row distances are and/or the more they are oriented in parallel to the line-of-sight, the higher the ground power is. This is observed explicitly on July 3. Later, in areas with closer row distances, the center of mass is located higher, the volume power is higher and the ground power is lower. No big spatial

variability is observed at L-band, as already indicated from the profiles in the previous Section. In some areas, the ground-to-volume ratio is even lower at L-band than at C-band on July 3, which is unexpected. This may be explained by the difference in incidence angle, which is steeper at C-band than at L-band, resulting in less sensitivity to the gaps between the rows at L-band. On July 24 instead, the ground-to-volume ratios at L-band become higher than at the higher frequencies. This change might have been induced by a change of plant morphology and/or dielectric properties.

In terms of polarimetry, the biggest differences are observed between HH and VV. This is expected and has been reported in previous studies [17]. Therefore, the analysis of the abovementioned parameters in the next Section is restricted to the two co-pol channels.

4.4 Sensitivity to Phenological Transitions at Different Frequencies

In this Section, the introduced parameters are analyzed regarding their sensitivity to the phenological transitions described in Section 4.2. Over the relevant dates for each transition (indicated in Fig. 2), the trends of the mean values of the TomoSAR parameters are discussed at field level. This can be justified by the low standard deviation of the values despite the spatial differences discussed in Section 4.3., especially in the corn.

4.4.1 Corn

The growth of the corn plants is associated with a strong increase of VWC during the monitored phenological stages. The higher VWC together with the taller vegetation is expected to influence both the volume power and the ground power: an increase of the volume power is expected to be weakened by the higher attenuation due to the larger amount of water, which at the same time causes the ground power to decrease. In addition to the plant growth, the water distribution within the plant changes from a uniform to a non-uniform distribution once the fruit development starts, i.e. after July 3. This redistribution implies a change of water density as depicted in Fig. 3 (b). From the electromagnetic point of view, a lower water density causes a higher transparency of the plant components and a higher water density an increased attenuation. This redistribution of water changes the height of the center of mass, which is expected to be located lower with respect to the total measured plant height after the redistribution.

Fig. 12 shows the variation of the center of mass (solid line) and the volume center of mass (dashed line) at the different frequencies compared to the actual measured plant height. Across all frequencies, the center of mass is low compared to the plant height. However, this observation can be biased since it can result from a strong ground component. The volume center of mass is located around 50% of the plant height at all the frequencies on the last date. The height of the volume center of mass increases slightly with frequency, from 1.5 m at L-band to 1.7 m at X-band. This indicates the differences in attenuation after the water redistribution within the plants (compare Fig. 3 (b)). The lower layer with higher water density ρ_2 causes a higher attenuation at higher frequencies, and the upper layer with lower water density ρ_3 an increased electromagnetic transparency at lower frequencies, as expected.

Accordingly, the ground power (see Fig. 13) at X- and C-band decreases after July 3 due to the increased attenuation caused by the increase of VWC. At L-band, instead, the ground power is

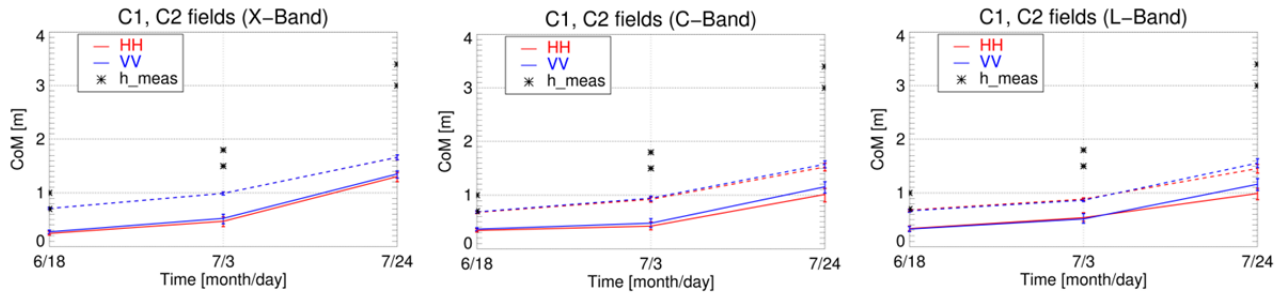


Fig. 12: C1, C2 fields: Mean value of the height of the estimated center of mass of the total (solid lines) and the volume (dashed lines) 3-D backscatter compared to the measured plant height on the relevant dates at X-, C- and L-band. The error bars correspond to the 60% confidence interval.

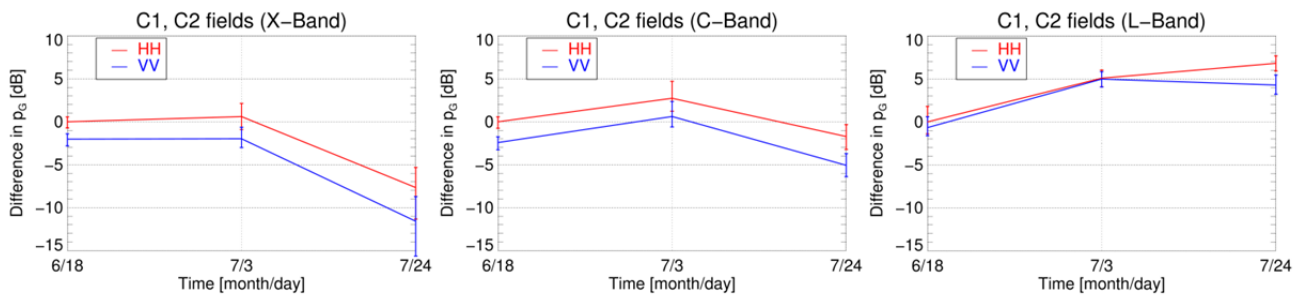


Fig. 13: C1, C2 fields: Mean value of the difference in the estimated ground power (normalized to the ground power at HH on June 18) on the relevant dates at X-, C- and L-band. The error bars correspond to the 60% confidence interval.

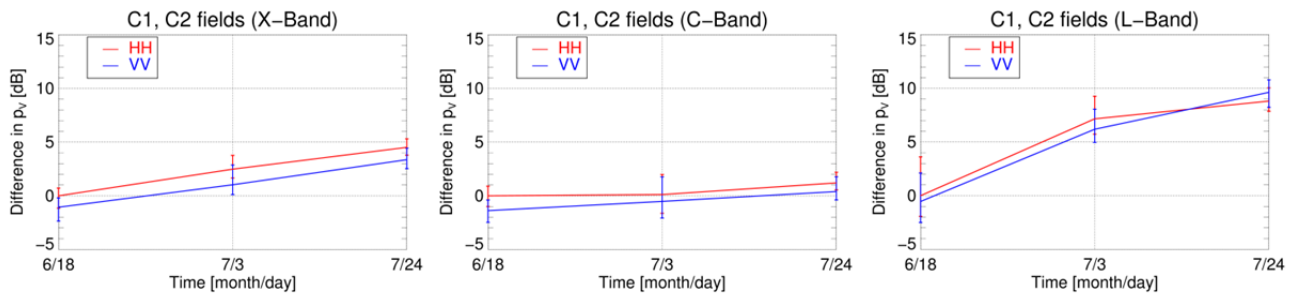


Fig. 14: C1, C2 fields: Mean value of the difference in the estimated volume power (normalized to the volume power at HH on June 18) on the relevant dates at X-, C- and L-band. The error bars correspond to the 60% confidence interval.

constant at VV and slightly increasing at HH indicating that the increase is associated to the dihedral scattering interpreted by the increase of water content of the stalks close to the ground. It is worth to comment that the ground power is for sure influenced by soil moisture variations, which are reported in Fig. 1 (b), as well. However, the variation of the ground power at X-band is dominated by the increasing attenuation rather than the soil moisture variation. At C-band the progressive increase and decrease resembles the soil moisture variation. However, the 5 dB decrease after July 3 seems too large to be caused solely by a decrease in soil moisture of around 4 vol%, especially when compared to the increase of 10 vol% before in hand with a ground power increase of only 3 dB. Even though L-band does not suffer from the attenuation to the same extent,

its ground power variation cannot be connected solely to the soil moisture variation since surface and dihedral scattering contributions are mixed.

At X- and L-band, the volume power increases during the plant growth (see Fig. 14). Between the last two dates this increase is similar at the order of 3 to 4 dB. As concluded from the analysis of the ground power, L-band is not as affected by the attenuation as the higher frequencies. Therefore, the sensitivity to the lower part of the stalks explains the increase of volume power with VWC. The volume power at C-band remains almost constant over the three dates and is not sensitive to the increase of VWC. This fact might be explained by the two layers with different densities (see Fig. 3 (b)). The layer with higher water density ρ_2 attenuates the wave, while the lower density ρ_3 of the layer above results in an increased transparency. Also X-band is attenuated by the dense water layer close to the ground. However, a possible explanation for the still present increase of volume power can be that the upper layer is not as transparent as at C-band enabling more scattering contributions possibly due to morphological changes (e.g. the leaves). A second possibility could be multiple scattering between the different plants, as previously observed at C-band in tropical forests [33].

To summarize, the penetration is significant at all frequencies due to the non-uniform distribution of the water content that increases the semi-transparency of the top vegetation layer with time. The ability to resolve the 3-D scattering is critical for identifying this redistribution in the TomoSAR separated parameters. Specifically, the joint analysis of the ground and volume powers and the height of the volume-only center of mass could resolve any interpretation ambiguity. Besides, the variation of the ground power is impacted by several factors, such as changes in attenuation, the amount of dihedral power and by soil moisture variations. The relative significance of each of the factors changes depending on the frequency. The volume power variation shows some sensitivity to VWC at X- and L-band, but the contributing scattering mechanisms are different.

4.4.2 Barley

A. Bending of the Heads

The heads of the barley contain the still milky grains when they change their orientation between May 22 and June 4. Particularly due to the awns (longer than 10 cm), it might be expected that the different orientation of the heads causes a difference in penetration and volume power as a function of polarization in the two dates. At the same time, no significant dielectric change occurs since the VWC level is high.

Indeed, as shown in Fig. 15, for vertically oriented heads the volume power at C-band is approximately 4 dB higher at VV than at HH on May 22. The center of mass is lower at HH as well, indicating a deeper penetration. The change of orientation causes the volume power at HH to increase by 8 dB and the center of mass becomes similar at the two polarizations. In contrast, almost no polarization differences are observed at X-band. The bending of the heads causes a lifting of the center of mass at both polarizations to a similar extent indicating that the electromagnetic wave interacts with a bigger part of the vegetation volume before the bending of the heads occurs than after. Still at X-band, the bending of the heads effects an increase of the volume power at both polarizations by approximately 6 dB.

To summarize, polarization differences at C-band allow the identification of the bending of the

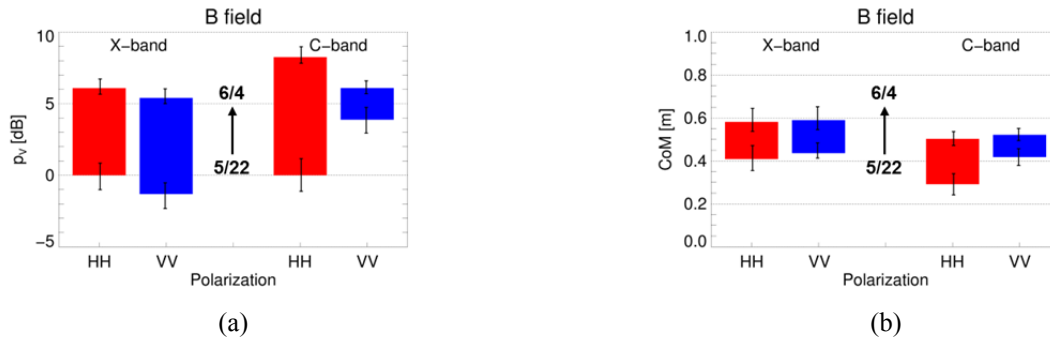


Fig. 15: B field: (a): Mean value of the estimated volume power normalized to the volume power at HH on May 22. (b): Mean value of the height of the estimated center of mass of the 3-D backscatter (right). The lower and upper value of the colored bars corresponds to the respective mean values on May 22 and June 4. The related black error bars correspond to the 60% confidence interval.

heads very clearly. This difference across the co-pol channels is not given at X-band in either the center mass or the volume power. Similarly to C-band, between May 22 and June 4 they both increase, but this does not necessarily correspond to the change of orientation of the main scattering mechanism in the volume.

B. Drying and Ripening

As introduced in Section 4.2, the barley plants loose VWC after June 4. At the same time, the ripening contributes to an increase of dry plant material and thus the wet biomass only decreases significantly after June 18 (see Fig. 4). The decrease of VWC is expected to impact the estimated volume power and to effect an increased penetration through the vegetation volume that could be seen from a higher scattering contribution from the ground.

Indeed, the volume powers at X- and C-band (see Fig. 16) show a decreasing trend over the four relevant dates with a strong drop on the order of 3 to 4 dB after June 18. This probably corresponds to the drop in wet biomass rather than to the decrease of VWC.

As expected, the ground powers (see Fig. 17) show an increase at both frequencies. Besides the lower percentage of water in the vegetation, the soil moisture variation certainly impacts the ground power variation. However, X-band is less affected by soil moisture variation in the earlier dates due to the higher attenuation by the vegetation. This can be seen in an increase of approximately 3 dB after June 4 despite the decreasing soil moisture trend. At C-band, the ground power only increases slightly at VV. However, the increase of soil moisture after June 18 certainly supports the upward trend of the ground power at both frequencies, but at the same time is not distinguishable from the decrease of percentage of water in the vegetation.

To summarize, the estimated volume powers at X- and C-band can be related to the wet biomass. The ground power instead increases for decreasing water content but the increase of soil moisture cannot be neglected, especially at the later dates.

4.4.3 Wheat

In the wheat field the wet biomass increases after June 18 while the VWC stays high and only drops after July 3, as shown in Fig. 5. This distinguishes the observations during the drying process of the

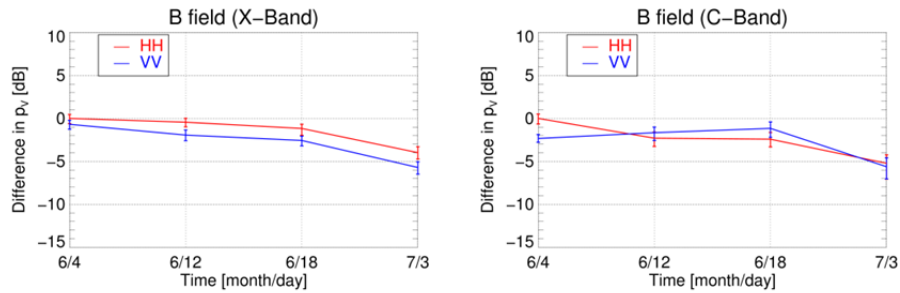


Fig. 16. B field: Mean value of the difference in the estimated volume power (normalized to the volume power at HH on June 4) on the relevant dates at X- and C-band. The error bars correspond to the 60% confidence interval.

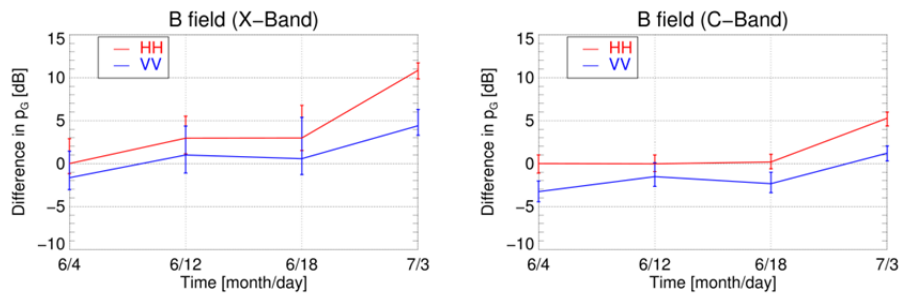


Fig. 17. B field: Mean value of the difference in the estimated ground power (normalized to the ground power at HH on June 4) on the relevant dates at X- and C-band. The error bars correspond to the 60% confidence interval.

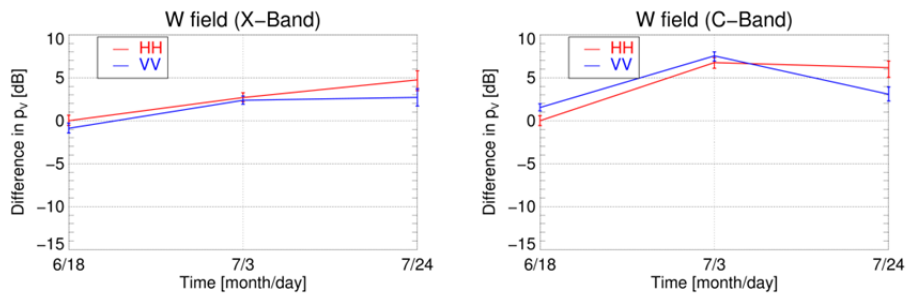


Fig. 18. W field: Mean value of the difference in the estimated volume power (normalized to the volume power at HH on June 18) on the relevant dates at X- and C-band. The error bars correspond to the 60% confidence interval.

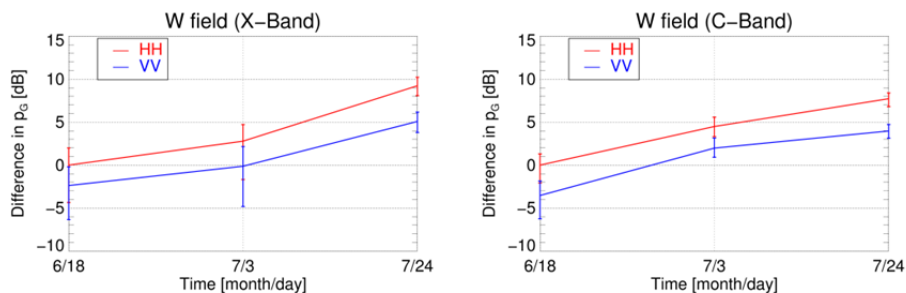


Fig. 19. W field: Mean value of the difference in the estimated ground power (normalized to the ground power at HH on June 18) on the relevant dates at X- and C-band. The error bars correspond to the 60% confidence interval.

wheat from the ones of the barley that are characterized by a continuous decrease of VWC. This behavior is expected to be reflected on the volume power. On July 3, while the VWC stays constant the wet biomass increases due to an increase of dry biomass. This relative loss in VWC is expected to be associated to an increase of backscattered power from the ground.

Indeed, the volume powers (see Fig. 18) increase after June 18, particularly at C-band. Afterwards, the decrease of wet biomass, due to the lower VWC, is only slightly visible at C-band and not at all at X-band. The attenuation by the high VWC is higher at X-band [9]. This explains the approximately 5 dB lower increase before July 3 compared to C-band. Since the volume power is slightly higher at HH on July 24 at both frequencies, the main scattering components seem to be the heads which bend after ripening to some extent while the stalks are losing water.

The upward trend of the ground power (see Fig. 19) reflects the reducing percentage of water contained in the plants at both frequencies, while C-band seems to be slightly more influenced by soil moisture variations. Comparing C-band to X-band, the increase of ground power is 2 dB stronger before July 3 when soil moisture increases. The weaker increase by 2 dB afterwards is consistent with the decrease of soil moisture on the more representative measurement grid, while the increase exhibited by the moisture measurements on the W field could be outliers.

To summarize, the increase of wet biomass is more explicit at C-band, while X-band might still be more affected by attenuation by the high VWC level at this stage. Differences in the polarizations allow insights to the contributing scattering components. In turn, X-band might be better suited for the detection of the relative loss in VWC since it is less sensitive to the soil moisture variation than C-band.

4.4.4 Discussion

The analysis of the phenological transitions benefits from the separation of the ground and the volume power variations. This enables to distinguish changes on the ground and in the vegetation which would not be possible by means of the total backscattered power.

The behavior of the center of mass supports the interpretation of the power variations and is able to track the redistribution of water content in the corn.

Since the volume power is independent from changes on the soil, it was expected to be sensitive to variations of VWC and wet biomass. Indeed, in the cereals, the wet biomass variation is reflected in the variation of the volume power. However, if the VWC is too high, attenuation might dominate, as for instance at X-band in the wheat case. Similar reasoning applies to C-band in the corn, while L-band appears sensitive to the increase of VWC which, on the early development stages, is almost identical to the wet biomass. Still for corn, the non-uniform water redistribution during the growth of the plants complicates the interpretation of the changes of volume power showing an increase at X- and L-band while C-band is almost insensitive. The unexpected behavior with frequency requires further analysis particularly regarding the ongoing scattering mechanisms at X-band. Despite C-band not being sensitive to the VWC increase at the analyzed dates, it might still be affected by the decrease of the VWC afterwards. Unfortunately, the subsequent growth stages are not monitored here.

Differences in the volume power between HH and VV at C-band can help to identify changes such as the bending of the heads in the barley. Further, the availability of the co-pol channels allows

insights to the scatterers contributing to the volume power and indicates the presence of dihedral scattering on the ground.

The ground power is impacted by changes in attenuation through the vegetation volume, soil moisture and dihedral scattering contribution. In general, the higher the frequency is, the lower the impact of soil moisture, as observed for X- and C-band in the corn and X-band in the cereals. A vegetation volume with high VWC causes more attenuation and the effect increases with frequency. Thus, the ground power change at high frequencies can give an idea on changes in VWC, as observed particularly for X-band in all crop types. It is worth to remark that in the analysis of the ground power the effect of surface roughness was not addressed. Generally, it has a bigger effect at higher frequencies. However, it is expected that the attenuation from the vegetation volume weakens the ground power making the influence of roughness changes not decisive for the presented observations.

Despite the resolved ambiguity of scattering contributions in height, the problem of relating them to biophysical measurements is still open. For the volume power, complex models would be required accounting for a mixture of scattering and attenuation by the vegetation volume and including non-uniform water distributions within the plants. Similar conclusions regarding the necessity to adapt existing models are drawn in a recent study assessing the relation of polarimetric interferometric SAR parameters and biophysical measurements in agricultural crops [34]. At the same time, the ground power is impacted by several parameters limiting modeling approaches for actual parameter inversion. In any case, an incoherent polarimetric observation space is expected to be insufficient for modelling these dependencies as well as for parameter inversion.

4.5 Conclusions

This paper discusses the sensitivity of parameters estimated from tomographic SAR data to specific phenological transitions in corn, wheat and barley at different frequencies. The separation of ground and volume components enables to quantify changes at different heights, and the center of mass of the total and the volume-only 3-D backscatter supports the interpretation of these changes. For one dominant scattering mechanism, the center of mass is unique while it cannot provide unambiguous information on changes for more than one scattering mechanisms. The analysis, although limited to backscattered powers and center of mass, highlights that 3-D parameters are sensitive to changes in the vegetation volume in all frequencies. The results are particularly interesting in view of developing crop monitoring applications with current and future spaceborne SAR missions.

The added value of the 3-D information provided by TomoSAR is the distinct analysis of ground and volume. This enables to relate ground power variations to changes in attenuation where higher frequencies, such as X- and C-band in corn and X-band in the cereals, were found to be advantageous since they are less influenced by soil moisture. In the cereals, the volume power estimates at C-band seem to provide more insight on the wet biomass dynamics than at X-band. In the corn, the non-uniform water distribution results in a saturation of the volume power at C-band while it increases at X- and L-band along the plant growth. Further, the scattering height information supports the interpretation of the power variations and allows the identification of the redistribution of the VWC in the corn or the bending of the heads in the barley.

As expected, it is not possible to resolve the incoherent volume power in terms of scattering and attenuation from the vegetation volume. Besides, the ground power is impacted by variation of soil and plant parameters due to the impact of attenuation and dihedral scattering.

In general, polarimetric differences are most pronounced at the co-polar channels supporting the identification of contributing scatterers and scattering mechanisms. However, polarimetry would be most beneficial towards parameter inversion by means of electromagnetic models since the incoherent polarimetric observation space is limited in this regard. Particularly the exploitation of the ground polarimetry might provide new opportunities for resolving the superposition of surface and dihedral scattering. However, in the case of the applied separation methodology the resulting ground polarimetry is too much impacted by residual volume scattering.

Concerning the implementation of TomoSAR techniques for crop monitoring, the required vertical Rayleigh resolution and the unambiguous height range that define both the maximum spatial baseline and the baseline sampling (i.e., the number of tracks required) depend on the application (i.e., the vegetation parameters to be estimated, the estimation accuracy required, the scattering scenario). The results in this paper show that the lower the frequency, the more the scattering scenario becomes characterized by volumetric scattering. A full TomoSAR characterization of such layers could require a larger number of tracks and high vertical Rayleigh resolutions, and it could still be limited nowadays to experimental areas and difficult to be realized with high temporal resolution. At high(er) frequencies, where the penetration into the vegetation volume reduces, a reduced number of acquisitions (even in a single-baseline interferometric configuration) may suffice. The problem is of course the increased impact of temporal decorrelation that constrains the temporal baselines of the acquisitions, making single-pass implementations crucial. A first step in the direction of a reduced parameter set was done with the analysis of the center of mass, and future work should also address the potential of estimating the coherent ground and volume signatures from polarimetric-interferometric SAR.

Acknowledgements

The authors would like to thank the team from the Ludwig-Maximilians-Universität in Munich for their help in the ground parameter collection. This work was supported by the Helmholtz Alliance Remote Sensing and Earth System Dynamics funded by the Initiative and Networking Fund of the Helmholtz Association.

4.6 References

- [1] H. McNairn and B. Brisco, “The Application of C-band Polarimetric SAR for Agriculture: A Review”, *Can. J. Remote Sen.*, vol. 30, no. 3, pp. 525-542, Jun. 2004.
- [2] S. C. Steele-Dunne, H. McNairn, A. Monsivais-Huertero, J. Judge, P. W. Liu, K. P. Papathanassiou, “Radar Remote Sensing of Agricultural Canopies: A Review”, *IEEE J. Sel. Top. Appl. Earth Obs. Remote Sens.*, vol. 10, no. 5, pp. 2249-2273, May 2017.

-
- [3] H. Skriver, "Crop Classification by Multitemporal C- and L-Band Single- and Dual-Polarization and Fully Polarimetric SAR", *IEEE Trans. Geosci. Remote Sens.*, vol. 50, no. 6, pp. 2138-2149, Jun. 2012.
- [4] L. Mascolo, J. M. Lopez-Sanchez, F. Vicente-Guijalba, F. Nunziata, M. Migliaccio, and G. Mazarella, "A Complete Procedure for Crop Phenology Estimation with PolSAR Data Based on the Complex Wishart Classifier", *IEEE Trans. Geosci. Remote Sens.*, vol. 54, no. 11, pp. 6505-6515, Nov. 2016.
- [5] J. D. Ballester-Berman, J. M. Lopez-Sanchez, and J. Fortuny-Guasch, "Retrieval of Biophysical Parameters of Agricultural Crops using Polarimetric SAR Interferometry", *IEEE Trans. Geosci. Remote Sens.*, vol. 43, no. 4, pp. 682-694, Apr. 2005.
- [6] J. M. Lopez-Sanchez, and J. D. Ballester-Berman, "Potentials of Polarimetric SAR Interferometry for Agriculture Monitoring", *Radio Sci.*, vol. 44, no. 2, pp. 141-177, Mar. 2009.
- [7] M. Pichierri, I. Hajnsek, and K. P. Papathanassiou, "A Multi-Baseline Pol-InSAR Inversion Scheme for Crop Parameter Estimation at Different Frequencies", *IEEE Trans. Geosci. Remote Sens.*, vol. 54, no. 8, pp. 4952-4970, Aug. 2016.
- [8] M. Pichierri, and I. Hajnsek, "Comparing Performances of Crop Height Inversion Schemes From Multifrequency Pol-InSAR Data," *IEEE J. Sel. Top. Appl. Earth Obs. Remote Sens.*, vol. 10, no. 5, pp. 1727-1741, May 2017.
- [9] F. T. Ulaby, and E. A. Wilson, "Microwave Attenuation Properties of Vegetation Canopies", *IEEE Trans. Geosci. Remote Sensing*, vol. GE-23, no. 5, pp. 746-753, Sept 1985.
- [10] T. Jackson and T. Schmugge, "Vegetation effects on the microwave emission of soils", *Remote Sensing of Environment*, vol. 36, no. 3, pp. 203-212, 1991.
- [11] H. Skriver, M. T. Svendsen, and A. G. Thomsen, "Multitemporal C- and L-band polarimetric signatures of crops", *IEEE Trans. Geosci. Remote Sens.*, vol. 37, no. 5, pp. 2413-2429, Sep. 1999.
- [12] S. Paloscia, "A summary of experimental results to assess the contribution of SAR for mapping vegetation biomass and soil moisture", *Can. Journal of Remote Sensing*, vol. 28, no. 2, pp. 246-261, Jun. 2002.
- [13] G. Wiseman, H. McNairn, S. Homayouni and J. Shang, "RADARSAT-2 Polarimetric SAR Response to Crop Biomass for Agricultural Production Monitoring", *IEEE J. Sel. Top. Appl. Earth Obs. Remote Sens.*, vol. 7, no. 11, pp. 4461-4471, Nov. 2014.
- [14] A. Reigber, and A. Moreira, "First Demonstration of Airborne SAR Tomography using Multibaseline L-band Data", *IEEE Trans. Geosci. Remote Sens.*, vol. 38, no. 5, pp. 2142-2152, Sep. 2000.

- [15] S. C. M. Brown, S. Quegan, K. Morrison, J. C. Bennett, and G. Cookmartin, “High-Resolution Measurements of Scattering in Wheat Canopies – Implications for Crop Parameter Retrieval,” *IEEE Trans. Geosci. Remote Sens.*, vol. 41, no. 7, pp. 1602-1610, Jul. 2003.
- [16] J. M. Lopez-Sanchez, J. Fortuny-Guasch, S. R. Cloude, and A. J. Sieber, “Indoor polarimetric radar measurements on vegetation samples at L, S, C and X band”, *J. Electromagn. Waves Appl.*, vol. 14, no.2, pp. 205-231, 2000.
- [17] J. M. Lopez-Sanchez, J. D. Ballester-Berman, and J. Fortuny-Guasch, “Indoor wide-band polarimetric measurements on maize plants: a study of the differential extinction coefficient,” *IEEE Trans. Geosci. Remote Sens.*, vol. 44, no. 4, pp. 758-767, Apr. 2006.
- [18] S. R. Cloude, “Dual-Baseline Coherence Tomography”, *IEEE Geosci. Remote Sens. Lett.*, vol. 4, no. 1, pp. 127-131, Jan. 2007.
- [19] H. Joerg, M. Pardini, I. Hajnsek, and K. P. Papathanassiou, “On the Separation of Ground and Volume Scattering Using Multibaseline SAR Data”, *IEEE Geosci. Remote Sens. Lett.*, vol. 14, no. 9, pp. 1570-1574, Jul. 2017.
- [20] H. Joerg, M. Pardini, I. Hajnsek, K. P. Papathanassiou, “3-D Scattering Characterization of Agricultural Crops at C-Band using SAR Tomography”, accepted for publication in *IEEE Trans. Geosci. Remote Sens.*, 2018.
- [21] U. Meier, et al., “The BBCH system to coding the phenological growth stages of plants – history and publications”, *Journal of Cultivated Plants*, vol. 61, no. 2, pp. 41-52, 2009.
- [22] C. Igathinathane, A. R. Womac, S. Sokhansanj, and L. O. Pordesimo, “Mass and moisture distribution in aboveground components of standing corn plants.”, *Transactions of the ASABE*, vol. 49, no. 1, pp. 97-106, 2006.
- [23] S. R. Cloude, *Polarisation: Applications in Remote Sensing*. Oxford, U.K.: Oxford Univ. Press, 2009.
- [24] H. Joerg, M. Pardini, I. Hajnsek and K. P. Papathanassiou, “First multi-frequency investigation of SAR tomography for vertical structure of agricultural crops”, in *Proc. EUSAR*, vol. 10, Jun. 2014.
- [25] A. Reigber, P. Prats, and J.J. Mallorqui, “Refined Estimation of Time-Varying Baseline Errors in Airborne SAR Interferometry”, *IEEE Geosci. Remote Sens. Lett.*, vol. 3, no. 1, pp. 145-149, Jan. 2006.
- [26] M. Pardini, and K. P. Papathanassiou, “A Two-Step Phase Calibration Method for Tomographic Applications with Airborne SAR Data”, in *Proc. EUSAR*, vol. 10, Jun. 2014.
- [27] F. Lombardini, and M. Pardini, “Experiments of Tomography-Based SAR Techniques with P-Band Polarimetric Data”, *Proc. PollnSAR*, Frascati, Italy, Jan. 2009.
- [28] O. Frey, and E. Meier, “3-D Time-Domain SAR Imaging of a Forest using Airborne Multibaseline Data at L- and P-Bands”, *IEEE Trans. Geosci. Remote Sens.*, vol. 49, no. 10, pp. 3660-3664, Oct. 2011.

-
- [29] L. Ferro-Famil, Y. Huang, and A. Reigber, “High-resolution SAR tomography using full rank polarimetric spectral estimators”, in *Proc. IEEE IGARSS*, pp. 5194-5197, Jul. 2012.
- [30] M. Pardini, and K. Papathanassiou, “On the Estimation of Ground and Volume Polarimetric Covariances in Forest Scenarios With SAR Tomography”, *IEEE Geosci. Remote Sens. Lett.*, vol. 14, no. 10, pp. 1860-1864, Oct. 2017.
- [31] S. Tebaldini, “Algebraic Synthesis of Forest Scenarios from Multibaseline PolInSAR Data”, *IEEE Trans. Geosci. Remote Sens.*, vol.47, no. 12, pp. 4132-4142, Dec. 2009.
- [32] B. Ottersten, P. Stoica, and R. Roy, “Covariance matching estimation techniques for array signal processing and applications”, *Digital Signal Processing*, vol. 8, no. 3, pp. 185-210, Jul. 1998.
- [33] D. H. Hoekman, and C. Varekamp, “Observation of tropical rain forest trees by airborne high-resolution interferometric radar,” *IEEE Trans. Geosci. Remote Sens.*, vol. 39, no. 3, pp. 584-594, Mar 2001.
- [34] M. Pichierri, I. Hajnsek, S. Zwieback, and B. Rabus, “On the potential of Polarimetric SAR Interferometry to characterize the biomass, moisture and structure of agricultural crops at L-, C- and X-Bands”, *Remote Sensing of Env.*, vol. 204, pp. 596-616, Jan. 2018.

Chapter 5

Conclusions

5.1 Main Findings

The application of tomographic SAR methodologies to agricultural scattering scenarios allows investigating the influence of changes of biophysical parameters over time on polarimetric SAR measurements separately for the ground and volume scattering component. The matrix filter approach for separating ground and volume from single polarimetric MB SAR data was selected based on the performance analysis in Chapter 2 [1]. Together with the tomographic analysis using a time series of polarimetric MB SAR data at C-band, the application of the matrix filter allowed for the first time a quantitative temporal analysis of ground and volume scattering contributions over the phenological cycle of corn, wheat and barley [2]. Based on these findings, the sensitivity of different frequencies to specific phenological transitions of the crop types under study was investigated using tomographic parameters [3]. In the following, the main findings and their added value in the context of SAR monitoring of agricultural crops are discussed for each Chapter separately.

Chapter 2 “On the Separation of Ground and Volume Scattering Using Multi-Baseline SAR Data” Simulated MB SAR data were used to compare two algorithms, based on an adaptive maximum likelihood method (AML) and a matrix filtering (MF) approach, for the estimation of MB volume coherences and ground and volume backscattering powers. The required a priori knowledge of the ground topography results to be a sufficient condition to enable a non-ambiguous separation for both algorithms. The main findings regarding the impact of vertical resolution, errors in the a priori knowledge of the ground topography and phase calibration errors on the estimation performance of the separation algorithms are the following:

- Volumes with heights in the order of the vertical Rayleigh resolution are a critical case. Nevertheless, the AML estimates the volume coherences and the ground power with high accuracy even for limited vertical resolution while the MF overestimates the volume coherences due to an overestimation of the ground power for volume dominated scenarios. Independently of the vertical resolution however, the uncertainties of the ground reflectivity estimates used by the AML leads to a worsening of the volume power estimate for ground dominated scenarios, which can partly be recovered by using a higher number of looks.
- The AML showed a higher sensitivity to errors in the a priori knowledge of the ground topography. To guarantee a RMSE of the estimated ground-to-volume power ratio below

20%, an unrealistic precision of the ground topography would be required. The MF is more robust in this respect and a topographic error of 30% of the vertical resolution is acceptable.

- Phase calibration residuals of the MB SAR data had a bigger impact on the performance of the AML as well. For an acceptable performance, i.e. an RMSE of the ground-to-volume power ratio below 20%, phase errors up to 10 degrees are tolerable for the MF.

Due to the very high sensitivity of the AML to small errors in the knowledge of the ground location and to residual MB phase miscalibration, the MF is a more reliable choice for the application to experimental MB SAR data. Its drawback is the overestimation of the volume coherences for limited resolution in volume dominated scenarios. For a ground-to-volume power ratio of -5 dB, the root-mean-square error for the ground power was found to increase from 10% (two height resolution units) up to 30% for only one height resolution unit while for the volume power it was always below 15%. Keeping this limitation of the ground power estimate for low vertical resolution in mind, the MF provides a tool to robustly quantify the ground and volume scattering components in agricultural vegetation even with a low number of looks.

Chapter 3 “3-D Scattering Characterization of Agricultural Crops at C-band using SAR Tomography” In this Chapter, airborne SAR Tomography at C-band was applied for the first time over agricultural crops. The three-dimensional scattering signature of agricultural crops was investigated at different polarizations using MB SAR acquisitions on different dates across the phenological cycle. The filtering approach analyzed in Chapter 2 was applied to separate ground and volume scattering components.

- The CROPEX 2014 campaign fills the gap of multi-temporal polarimetric MB SAR data. The acquisition design with up to 9 tracks per campaign date and large horizontal baselines facilitates a high vertical resolution up to 0.8 m. This facilitates the estimation of the vertical backscatter profiles at the different polarizations showing the distinctive three-dimensional scattering behavior of the different crop types which are impacted by changes of the soil and plant parameters over time. However, the vertical tomographic profiles are not sufficient to distinguish or quantify changes on the ground and in the volume for the low plant heights compared to the vertical resolution.
- After separation of ground and volume, the temporal variation of the separated powers and their ratio has been found to be sensitive to dielectric and geometric changes in the volume layer. In the corn, the plant growth and the redistribution of the water content within the plants [4,5] could be observed. The drying of the cereals could be identified and the bending of the heads in the barley causes differences between the polarimetric powers before the bending which assimilated afterwards. The ground power is the only observable reflecting soil moisture variations.
- Even though the variation of the center of mass reflected the soil and plant dynamics over time, it is important to mention that, before separation, it cannot resolve whether a change occurs on the ground or in the volume component. The complete understanding of the

resulting scattering characteristics is strongly driven by the analysis of the powers enabling to draw conclusions on the behavior of the center of mass a posteriori.

- The presence of anisotropic effects in the vegetation volume has been addressed by estimating the powers from the MB volume coherences fitted to a random volume model. In the corn, no differences compared to the results of the general, oriented volume hypothesis were detected. For wheat and barley, very small and probably not significant differences in the results under the oriented and the random volume assumption were observed on some acquisition dates.

Chapter 4 “Sensitivity of SAR Tomography to the Phenological Cycle of Agricultural Crops at X-, C- and L-band” The tomographic parameters as introduced in Chapter 2 and 3 are used to gain a better understanding of the sensitivity of X-, C- and L-band to specific phenological transitions related to dielectric and geometric changes in corn, barley and wheat.

The tomographic parameters at all frequencies are sensitive to changes in the vegetation volume with characteristics dependent on the crop type. The ability to separate in height is crucial for resolving the ambiguity of simultaneous changes in the soil and in the vegetation. The main findings are:

- In the cereals, the volume power estimates at C-band seem to provide more insight on wet biomass dynamics than X-band. In the corn, the non-uniform water distribution [4,5] results in a saturation of the volume power at C-band while it increases at X- and L-band along the plant growth, although the contributing scattering mechanisms are different. However, it is not possible to resolve the volume power with respect to backscattering and attenuation from the vegetation.
- The ground power is impacted by several factors, such as changes in attenuation, the amount of dihedral power and by soil moisture variations. The relative significance of each of them changes depending on the frequency. Ground power variations can be related to changes in attenuation particularly at higher frequencies, such as X- and C-band in corn and X-band in the cereals, since they are less influenced by soil moisture.
- The center of mass of the 3-D backscatter supports the interpretation of the power variations and allows the identification of the redistribution of the VWC in the corn or the bending of the heads in the barley.
- Polarimetric differences are most pronounced at the co-polar channels supporting the identification of contributing scatterers and scattering mechanisms.

Having in mind that spaceborne SAR sensors provide high potential regarding crop monitoring, the findings of this Chapter regarding the sensitivity of different frequencies to specific changes in the phenological cycle is of strong interest, particularly in view of current and future spaceborne SAR missions, like TanDEM-X [6], Radarsat-2 [7], Sentinel-1 [8] and Tandem-L [9].

5.2 Outlook

With the separation of scattering contributions in height, the application of tomographic SAR techniques allowed to resolve the ambiguity of changes located on the ground and in the vegetation volume of agricultural crops. The experimental results presented in Chapter 3 and 4 underline the added value of the distinct analysis of changes in the ground and volume powers at different polarizations along the phenological cycle. However, towards parameter inversion an incoherent polarimetric observation space, as given by the powers, is expected to be too limited. Coherent polarimetry would be most beneficial towards parameter inversion from electromagnetic models.

The separated ground component is of great interest towards soil moisture dynamics. The fact that it is influenced not only by direct surface scattering but also by the attenuation of the wave through the vegetation layer and by dihedral scattering makes it dependent on soil and plant parameters. The coherent polarimetric signature of the ground could provide new opportunities due to its relative character which makes it independent of attenuation. However, the ground polarimetry from the matrix filter is too impacted by residual volume scattering for limited vertical resolution. Separation methodologies based on the RVoG model exploit the full polarimetric space [10] and can therefore provide a more isolated ground signature even in cases with limited vertical resolution [11]. Chapter 3 concludes that anisotropic propagation effects for the crop types under study at C-band are negligible which would justify the application of the method in [10]. As outlined in [10], the polarimetry of the estimated ground component changes depending on the choice of interferometric volume coherences. Thus, a volume solution can be selected which yields a ground component where one polarimetric channel does not contribute to the scattering signature anymore, i.e. the entropy of the ground is low. For agricultural vegetation, this can give rise to an increased interpretation capability of the scattering mechanisms on the ground under agricultural vegetation.

First experimental results of the estimated ground entropy and mean alpha angle by using the separation in [11] are displayed in Figs. 1 and 2 for corn, wheat and barley fields. Compared to the entropy of the full polarimetric signal (shown in the introduction), the entropy of the separated ground component is reduced in all fields and rarely exceeds a value of 0.6, indicating the presence of only two scattering mechanisms on the ground. Further, the entropy is also reduced on fields with no or low vegetation cover across all frequencies, such as the corn fields on May 22. This suggests that such a separation indeed yields a ground component where one polarization does not contribute to the ground scattering and it can be supposed that depolarizing contributions, i.e. roughness effects, are cancelled. Due to the reduced entropy level, the mean alpha angle can be used to identify the kind of scattering mechanisms. Particularly in the corn at X- and C-band on the later dates, the higher values indicate a dominant dihedral component. This example illustrates the potential of estimating a ground component not influenced by soil roughness and represented by a mixture of surface and dihedral scattering. Even though the separation of surface and dihedral scattering is not straightforward due to the non-orthogonality of the two scattering mechanisms in nature [12], future research should be dedicated to the characterization and modelling of the scenario towards retrieving soil and trunk dielectrics.

Future research should further investigate also the potential of a reduced observation scenario by

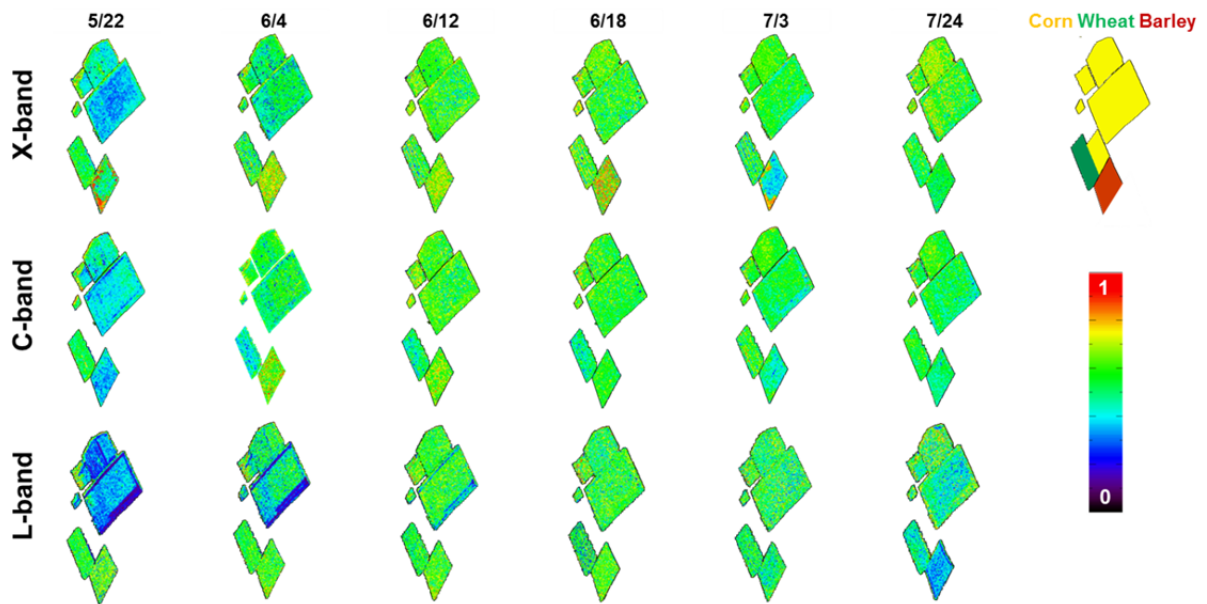


Fig. 1: Polarimetric entropy of the estimated ground component on different dates for X-, C- and L-band.

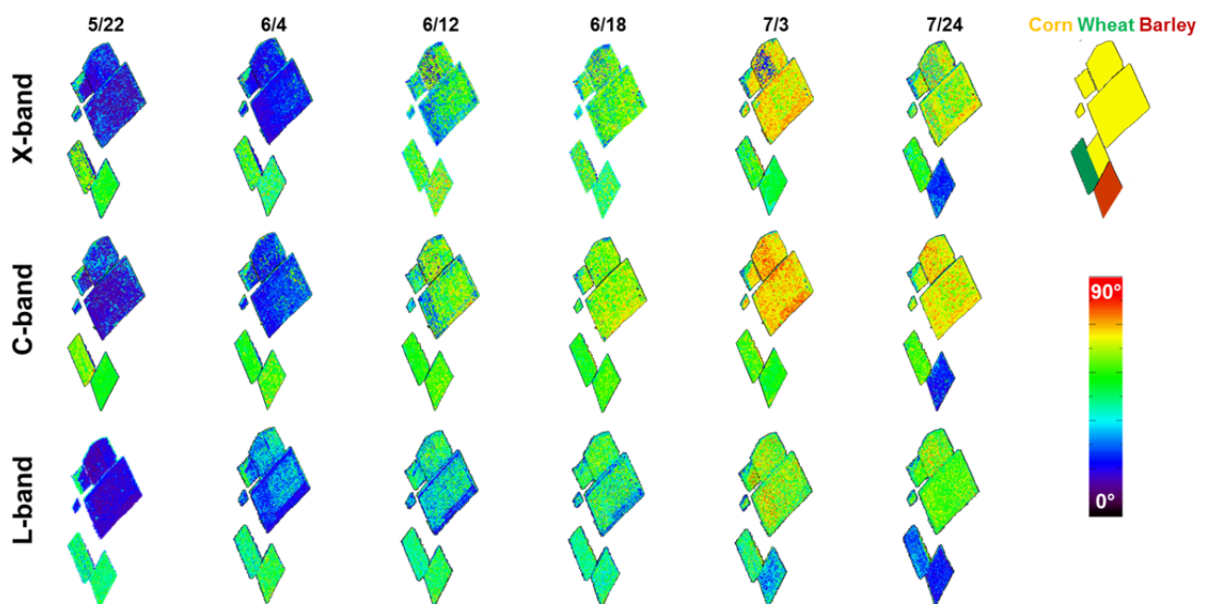


Fig. 2: Polarimetric mean alpha angle of the estimated ground component on different dates for X-, C- and L-band.

addressing the ground and volume separation provided from Pol-InSAR applied to a single or dual baseline configuration. A first step was done in this direction with the analysis of the center of mass regarding its sensitivity to phenological changes. Provided the same separation capability, the coherent ground and volume signatures from PolInSAR should be investigated towards their potential of inverting biophysical parameters.

5.3 References

- [1] H. Joerg, M. Pardini, I. Hajnsek, and K. P. Papathanassiou, “On the Separation of Ground and Volume Scattering Using Multibaseline SAR Data”, *IEEE Geosci. Remote Sens. Lett.*, vol. 14, no. 9, pp. 1570-1574, Jul. 2017.
- [2] H. Joerg, M. Pardini, I. Hajnsek, K. P. Papathanassiou, “3-D Scattering Characterization of Agricultural Crops at C-Band using SAR Tomography”, accepted for publication in *IEEE Trans. Geosci. Remote Sens.*, 2018.
- [3] H. Joerg, M. Pardini, I. Hajnsek, K. P. Papathanassiou, “Sensitivity of SAR Tomography to the Phenological Cycle of Agricultural Crops at X-, C- and L-band”, submitted to *IEEE J. Sel. Top. Appl. Earth Obs.*, 2017.
- [4] J. Casanova, M. Jang and J. Judge, “Transmission of Microwaves through a Dynamic Corn Canopy in Emission Models”, in *Proc. IEEE IGARSS*, pp. 2025-2027, Jul. 2006.
- [5] S. C. Steele-Dunne, H. McNairn, A. Monsivais-Huertero, J. Judge, P. W. Liu, K. P. Papathanassiou, “Radar Remote Sensing of Agricultural Canopies: A Review”, *IEEE J. Sel. Top. Appl. Earth Obs. Remote Sens.*, vol. 10, no. 5, pp. 2249-2273, May 2017.
- [6] G. Krieger, A. Moreira, H. Fiedler, I. Hajnsek, M. Werner, M. Younis, and M. Zink, “Tandem-X: A satellite formation for high-resolution SAR interferometry”, *IEEE Trans. Geosci. Remote Sens.*, vol. 45, no. 11, pp. 3317–3341, Nov 2007.
- [7] L. C. Morena, K V James, and J. Beck, “An introduction to the RADARSAT-2 mission”, *Canadian Journal of Remote Sensing*, vol. 30, no. 3, Jun 2004
- [8] R. Torres et al., “GMES Sentinel-1 mission”, *Remote Sensing of Env.*, vol. 120, pp. 9–24, May 2012.
- [9] A. Moreira, G. Krieger, I. Hajnsek, K. Papathanassiou, M. Younis, P. Lopez-Dekker, S. Huber, M. Villano, M. Pardini, M. Eineder, and F. De Zan, “Tandem-L: A highly innovative bistatic SAR mission for global observation of dynamic processes on the Earth's surface”, *IEEE Geosc. and Remote Sensing Magazine*, vol. 3, no. 2, pp. 8-23, 2015.
- [10] S. Tebaldini, “Algebraic Synthesis of Forest Scenarios from Multibaseline PolInSAR Data”, *IEEE Trans. Geosci. Remote Sens.*, vol.47, no. 12, pp. 4132-4142, Dec. 2009.
- [11] M. Pardini, and K. Papathanassiou, “On the Estimation of Ground and Volume Polarimetric Covariances in Forest Scenarios With SAR Tomography,” *IEEE Geosci. Remote Sens. Lett.*, vol. 14, no. 10, pp. 1860-1864, Oct. 2017.
- [12] S. R. Cloude, *Polarisation: Applications in Remote Sensing*. Oxford, U.K.: Oxford Univ. Press, 2009.

Curriculum Vitae – Hannah Joerg

Contact Information

Institution German Aerospace Center (DLR)
Microwave and Radar Institute
Address Muenchener Straße 20
82234 Wessling
Phone +49 (0)8153 28 3759
E-Mail hannah.joerg@dlr.de

Work Experience

- since 11/2016 **Research Scientist for Tandem-L**, *Microwaves and Radar Institute, German Aerospace Center (DLR), Oberpfaffenhofen (Germany)*
- Conceptual design of a mission exploitation platform for scientific users.
 - Participation in the development of the Science Service Segment and the User Requirements.
- since 03/2012 **PhD Candidate**, *Microwaves and Radar Institute, German Aerospace Center (DLR), Oberpfaffenhofen (Germany)*
- Planning and execution of a multi-temporal airborne SAR campaign and in-situ ground measurement collection over an agricultural test site.
 - Development of post-processing algorithms for multi-parametric SAR data using IDL.
 - Peer reviewer.
 - Supervision of three internship students.
- Line of research:
- Polarimetric, interferometric and tomographic SAR techniques.
 - Electromagnetic scattering of agricultural crops.

- Relating bio- and geophysical variables of agricultural crops to SAR observables.

05/2010 – 01/2011 **Working Student and Diploma Thesis Research**, *X-log Elektronik GmbH*, Munich (Germany)

- Research and Development for Avalanche Rescue Devices.
- Simulations and development of an optimization algorithm for the three-dimensional searching procedure.
- Patent: “Method and detector for searching a transmitter”.

01/2010 – 03/2010 **Internship**, *Danish Hydrological Insitute (DHI)*, Singapore (Singapore)
Study on extreme return analysis of multivariate sea-state

Graduate studies

since 06/2012 **PhD studies**, *ETH Zurich, Institute of Environmental Engineering*, Zurich (Switzerland)

- Topic: “Multi-Frequency Polarimetric SAR Tomography for the 3-D Characterization and Monitoring of Agricultural Crops” (expected graduation 12/2017)
- Research conducted at the Microwaves and Radar Institute, German Aerospace Center (DLR), Oberpfaffenhofen (Germany).
- Advisors: I. Hajsek, M. Pardini
- Examiners: L. Ferro-Famil, A. Moreira, H. Vereecken

06/2012 – 04/2017 **DLR Graduate Program**, *German Aerospace Center*, Germany.

- How to publish in peer reviewed journals.
- Effective scientific publications.
- Mastering the PhD study.
- The basics of project management.
- The basics of communication.
- Speed reading.
- Rhetoric and personality.
- Professional communication in scientific environments.

10/2006 – 01/2011 **Diploma studies in computational Mathematics (Dipl. Tech.-Math.)**, *Technische Universitaet Muenchen (TUM), Department of Mathematics*, Munich (Germany)

- Main focus on numerical mathematics and mathematical optimization.
- Minor subjects: electrical and mechanical engineering.

- Diploma thesis: “An Incremental Gauss-Newton-Algorithm for the Estimation of the Field Parameters of a Magnetic Dipole”.

08/2009 – 12/2009 **Guest student in the frame of the LAOTSE program**, *National University of Singapore (NUS), Department of Mathematics and Department of Engineering*, Singapore (Singapore)

Courses taken

04/2017 **Project Management**, *German Aerospace Center (DLR)*, Oberpfaffenhofen (Germany).

10/2015 **Python – Scientific Applications**, *German Aerospace Center (DLR)*, Oberpfaffenhofen (Germany).

06/2014 **Multistatic and Multi-Aperture SAR Systems: Introduction and Applications**, *Tutorial of the EUSAR 2014*, Berlin (Germany).

01/2013 **Advanced Course on Radar Polarimetry**, *European Space Agency (ESA)*, Frascati (Italy).

11/2012 **SAR Principles and Application**, *Carl-Cranz-Gesellschaft e.V. (CCG)*, Oberpfaffenhofen (Germany).

07/2012 **Vegetation Structure from Lidar and SAR**, *Tutorial of the IGARSS 2012*, Munich (Germany).

Awards

2017 **Young Scientist Best Paper Award** (1st Place) at the Kleinheubacher Tagung hosted by the German section of the International Union of Radio Science (U.R.S.I.).

Publications

Journals H. Joerg, M. Pardini, I. Hajnsek, K. P. Papathanassiou, “Sensitivity of SAR Tomography to the Phenological Cycle of Agricultural Crops at X-, C- and L-band“, *IEEE Journal of Selected Topics in Applied Earth Observations and Remote Sensing*, 2017. (submitted in November 2017).

H. Joerg, M. Pardini, I. Hajnsek, K. P. Papathanassiou, “3-D Scattering Characterization of Agricultural Crops at C-Band using SAR Tomography”,

accepted for publication in IEEE Transactions on Geoscience and Remote Sensing, 2018.

H. Joerg, M. Pardini, I. Hajnsek and K. P. Papathanassiou, "On the Separation of Ground and Volume Components for Natural Targets from Multi-Baseline SAR Data", IEEE Geoscience and Remote Sensing Letters, July 2017.

Conferences

H. Joerg, M. Pardini, I. Hajnsek, and K. P. Papathanassiou, "Fully Polarimetric Tomographic Time Series for Monitoring Phenological Changes of Agricultural Crops at Different Frequencies", ESA POLinSAR Workshop, Frascati, Italy, 2017.

A. Alonso-Gonzalez, H. Joerg, K. Papathanassiou and I. Hajnsek, "Multi-Frequency PolSAR Change Analysis for Agricultural Monitoring," ESA POLinSAR Workshop, Frascati, Italy, 2017.

A. Alonso-González, H. Joerg, K. Papathanassiou and I. Hajnsek, "Dual-polarimetric agricultural change analysis of long baseline TanDEM-X time series data," IEEE International Geoscience and Remote Sensing Symposium (IGARSS), Beijing, China, 2016.

O. Ponce, H. Joerg, R. Scheiber, P. Prats, I. Hajnsek and A. Reigber, "First study on holographic SAR tomography over agricultural crops at C-/X-band," IEEE International Geoscience and Remote Sensing Symposium (IGARSS), Beijing, China, 2016.

H. Joerg, M. Pardini, K. P. Papathanassiou and I. Hajnsek, "Analysis of Orientation Effects of Crop Vegetation Volumes by Means of SAR Tomography at Different Frequencies," 11th European Conference on Synthetic Aperture Radar (EUSAR), Hamburg, Germany, 2016.

A. Alonso-Gonzalez, H. Joerg, K. Papathanassiou and I. Hajnsek, "Change Analysis and Interpretation in Polarimetric Time Series over Agricultural Fields at C-band," 11th European Conference on Synthetic Aperture Radar (EUSAR), Hamburg, Germany, 2016.

H. Joerg, M. Picchierri, M. Pardini, K. Papathanassiou and I. Irena, "Agricultural Crop Structure by Means of Multi-Baseline Pol-InSAR and SAR Tomography," ESA Workshop on Retrieval of Bio- & Geophysical Parameters from SAR Data, Harwell, UK, 2015.

H. Joerg, M. Pardini and I. Hajnsek, "Spatial and Temporal Characterization of Agricultural Crop Volumes by Means of Polarimetric SAR Tomography at C-band," IEEE International Geoscience and Remote Sensing Symposium (IGARSS), Milan, 2015.

H. Joerg, M. Pardini, I. Hajnsek, and K. P. Papathanassiou, "Application of SAR Tomography on Agricultural Vegetation for Scattering Characterisation," ESA POLinSAR Workshop, Frascati, Italy, 2015.

H. Joerg, M. Pardini, I. Hajnsek and K. P. Papathanassiou, "First multi-frequency investigation of SAR tomography for vertical structure of agricultural crops," 10th European Conference on Synthetic Aperture Radar (EUSAR), Berlin, Germany, 2014.

H. Joerg, T. Jagdhuber, F. Kugler, I.Hajnsek und Jagdhuber, "Interpretation of Single-Pass Pol-InSAR Vegetation Signatures at X-Band: Dual- vs. Quad-Pol Case," ESA POLinSAR Workshop, Frascati, Italy, 2013.

Patents

R. Matzner, F. Greimel, H. Jörg. 2016. "Method and detector for searching a transmitter". U.S. Patent US9310460 B2, filed September 26 2012, and issued April 12 2016.

R. Matzner, F. Greimel, H. Jörg. 2013. "Verfahren und Suchgerät zum Suchen eines Sendegeräts". EU Patent EP2573583 A1, filed October 14 2011, and issued March 27 2013.

Invited Talks

2017 8th Water Research Horizon Conference of the Water Research Alliance.

Organizational Activities and Committees

Since 2015 Young Professionals' Speaker of the German Chapter of the IEEE Geoscience and Remote Sensing Society.

2016 Member of the organizational and technical program committee of the 2016 IEEE Young Professionals Conference on Remote Sensing.

2013-2015 PhD speaker of the Microwaves and Radar Institute, German Aerospace Center (DLR).

Membership

since 2012 Student Member of the IEEE Geoscience and Remote Sensing Society.
